

# Real fermion modes, impurity entropy, and nontrivial fixed points in the phase diagram of junctions of interacting quantum wires and topological superconductors

Domenico Giuliano<sup>a,b,\*</sup>, Ian Affleck<sup>c</sup>

<sup>a</sup>*Dipartimento di Fisica, Università della Calabria, Arcavacata di Rende I-87036, Cosenza, Italy*

<sup>b</sup>*INFN, Gruppo collegato di Cosenza, Arcavacata di Rende I-87036, Cosenza, Italy*

<sup>c</sup>*Department of Physics and Astronomy and Stewart Blusson Quantum Matter Institute, University of British Columbia, Vancouver, B.C., Canada, V6T, 1Z1*

---

## Abstract

We discuss how to extend the impurity entropy to systems with boundary interactions depending on zero-mode real fermion operators (Majorana modes as well as Klein factors). As specific applications of our method, we consider a junction between  $N$  interacting quantum wires and a topological superconductor, as well as a Y-junction of three spinless interacting quantum wires. In addition we find a remarkable correspondence between the  $N = 2$  topological superconductor junction and the Y-junction. On one hand, this allows us to determine the range of the system parameters in which a stable phase of the  $N = 2$  junction is realized as a nontrivial, finite-coupling fixed point corresponding to the  $M$ -fixed point in the phase diagram of the Y-junction. On the other hand, it enables us to show the occurrence of a novel “planar” finite-coupling fixed point in the phase diagram of the Y-junction. Eventually, we discuss how to set the system’s parameters to realize the correspondence.

*Keywords:*

Quantum wires, Fermions in reduced dimensions, Electron states and collective excitations in multilayers, quantum wells, mesoscopic, and nanoscale systems

*PACS:* 73.21.Hb, 71.10.Pm, 73.21.-b

---

## 1. Introduction

Recently, considerable interest has arisen in junctions involving interacting quantum wires (QW’s), both in the case of spinless [1, 2, 3, 4, 5, 6], and of spinful wires [7, 8, 9, 10]. This is mainly due to the fact that Landau’s Fermi liquid paradigm typically breaks down in one-dimensional interacting electronic systems, whose low-energy, long-wavelength properties are rather described by means of the Tomonaga-Luttinger liquid (TLL) framework [11, 12]. Within

---

\*Corresponding author

*Email addresses:* domenico.giuliano@fis.unical.it (Domenico Giuliano), iaffleck@phas.ubc.ca (Ian Affleck)

the TLL-approach, tunneling processes at a junction are described in terms of nonlinear vertex operators of the bosonic fields, with nonuniversal scaling dimensions continuously depending on the “bulk” interaction parameters [13, 14]. This opens the way to a plethora of nonperturbative features in the phase diagram of those systems, including the remarkable emergence of intermediate, finite-coupling fixed points (FCFP’s), either describing phase transitions between different phases (repulsive fixed points), or novel, nontrivial phases of the junction (attractive fixed points), thus generalizing to multi-wire junctions the Kane-Fisher FCFP emerging at a junction between two spinful QW’s [15].

In this context, the prediction that localized Majorana modes (MM’s) can appear at a junction between a normal QW and a topological superconductor (TS) [16] has opened additional brand-new scenarios, as the direct coupling between a quantum wire and a localized MM can potentially give rise to relevant boundary interactions, typically not allowed at junctions between normal wires [17]. As a result, it has been possible to predict the emergence of novel FCFP’s in the phase diagram of junctions between more-than-one interacting QW and TS’s [18, 19]. Moreover, due to ubiquity of the TLL-formalism, which successfully describes (junctions of) quantum spin chains [20, 21, 22, 23], Josephson junction networks [24, 25, 26, 27], as well as topological, Kondo-like systems [28, 29, 30, 31], novel FCFP’s have been predicted to emerge in the phase diagram of those systems, as well. Besides their theoretical interest, FCFP’s have been argued to correspond to “decoherence-frustrated” phases, in which competing frustration effects can operate to reduce the unavoidable decoherence in the boundary quantum degrees of freedom coupled to the “bath” of bulk modes [32, 33], thus making the junction, regarded as a localized quantum impurity, a good candidate to work as a frustration-protected quantum bit [24]. For this reason, it becomes of importance to search for FCFP’s in the phase diagram of pertinently designed junctions of quantum wires.

An effective means to study the phase diagram of junctions of QW’s is given by a cooperative combination of perturbative renormalization group (RG) approach [34, 15, 35] and of the delayed evaluation of boundary conditions (DEBC) technique [2, 7]. In particular, as extensively discussed in e.g. Ref. [2], DEBC method is based on constructing the boundary operators allowed by symmetries at a certain fixed point: the emergence of (at least one) relevant operator is, therefore, evidence of the instability of that fixed point against some other one. In addition, as pointed out, for instance, in Ref. [2], for a junction of normal QW’s and in Refs. [18, 19] for junctions between interacting QW’s and TS’s, those methods are efficiently complemented by using the zero-temperature impurity entropy (IE) to characterize the fixed points of the junction. The IE was originally introduced as a mean to characterize and classify, at zero temperature, quantum impurity systems that are critical in the bulk at the fixed points of their boundary phase diagram [35, 36]. Later on, it has been shown to correspond to the impurity contribution to the groundstate entanglement entropy, which is particularly suitable for characterizing the phases of 1+1-dimensional models via the Density Matrix Renormalization Group (DMRG) technique [37]. The exponentiated IE  $g$  yields the groundstate degeneracy of the system at a certain fixed point. In general,  $g$  corresponds to the specific value of the “ $g$ -function”, which always decreases along renormalization group trajectories (“ $g$ -theorem”); therefore, if two boundary fixed points are characterized by groundstate degeneracies  $g_1$  and  $g_2$ , with  $g_1 > g_2$ , provided there is the possibility of connecting the two of them with a renormalization group trajectory, this will always flow from  $g_1$

to  $g_2$ . [35, 36, 38, 39, 40].

Technically, to compute  $g$  one first constructs the partition function over a strip of length  $\ell$  for the model at a boundary critical point. Letting  $\mathcal{A}$  label the conformally invariant boundary conditions (CIBC's) characterizing a specific boundary critical point, one computes the partition function on the strips,  $\mathcal{Z}_{AA}$ , by assuming type  $\mathcal{A}$ -CIBC's at both boundaries. Specifically, one gets  $\mathcal{Z}_{AA} = \sum_n \exp\left[-\frac{x_{AA}^n \beta u}{\ell}\right]$ , where the sum is taken over energy eigenstates of the whole system,  $u$  is a velocity scale determined by the (critical) bulk of the system,  $\beta$  is the inverse temperature, and  $x_{AA}^n$  are dimensionless numbers typical of the system. The  $g$ -function is derived by sending  $\ell \rightarrow \infty$  at finite  $\beta$ . In this limit, one obtains  $\mathcal{Z}_{AA} \rightarrow g_A^2 e^{\frac{\pi c}{6\beta u}}$ , with the dimensionless number  $c$  being the conformal anomaly of the bulk critical theory. From the last result,  $g_A$  can be readily extracted [41].

In this paper we employ a combined use of perturbative RG approach, DEBC-method and calculation of the  $g$ -function to study junctions of interacting QW's and TS's and to spell out the correspondence between this sort of junctions and the Y-junction of three interacting quantum wires (Y3J) studied in Ref. [2] in the bulk  $\mathbf{Z}_3$ -symmetric version and later on discussed in Ref. [42] in the general case in which the  $\mathbf{Z}_3$  symmetry is broken. In doing so, we have necessarily to take into account the emergence of real fermionic modes at our junctions. These are primarily provided by the localized MM's  $\{\gamma_j\}$  emerging at the interface between a topological superconductor and a normal system [16, 43, 44]. In addition, real fermionic operators also appear as Klein factors (KF's),  $\{\Gamma_j\}$ , which have to be introduced when employing the bosonization approach to interacting one dimensional fermionic systems, to recover the correct (anti)commutation relations between fermionic fields for different wires, as well as between the fermionic field for each wire and the  $\gamma_j$ 's. In many cases, KF's play no role, as the relevant multi-point correlation functions of the fermionic fields either contain an equal number of creation and annihilation operators of fermions of the same kind (see, for instance, Ref. [45] and reference therein), or, at most, the net effect of KF's can be an extra minus sign which can be equally well accounted for by, for instance, redefining the zero-mode operators of the bosonic fields [46]. On the other hand, they are definitely essential to recover the correct phase diagram of e.g. a junction of three interacting QW's [2], as well as to correctly account for the hybridization between MM's and normal electronic modes in a conductor [47, 48], at junctions between normal wires and TS's [17, 18, 49], and in the remarkable "topological" realization of the Kondo effect, in which MM's determine an effective impurity spin coupled to electronic modes by the normal contacts [50]. Thus, it is by now evident that they must be properly accounted for in applying the  $g$ -theorem to junctions of interacting quantum wires.

Besides generalizing the results of Refs. [18, 2] respectively to a multiwire junction of interacting QW's and a TS's and to a non  $\mathbf{Z}_3$ -symmetric Y3J, we unveil the remarkable correspondence between the two models. In doing so, we prove how, extending the range of system's parameters with respect to the case discussed in Ref. [18], it is possible for a FCFP to correspond to the stable phase of the system. Remarkably, this completely reverses the scenario found within the range of parameters discussed in Ref. [18], where we proved that it is necessary to fine-tune the boundary couplings to the MM, to drive the RG flow towards the FCFP, which was unstable against more "trivial" fixed points. Apart being interesting per se, this result appears also of relevance for engineering stable phases with frustrated decoherence, potentially amenable for applications

to quantum computation. An important point to stress about the correspondence is that it holds despite the obvious observation that the Y3J has three KF's, while the  $N = 2$  junction has just two KF's and one MM. In fact, as we discuss in the following, while one of the three fields of the Y3J decouples from the boundary interaction, its KF gets “left behind” and it plays the role of the MM. Therefore, the correspondence works perfectly well when considering a single junction in both systems. Remarkably, it also yields the right result when computing  $g$  at the fixed points of the two model. In this case, as we discuss in detail below, one has to resort to a two-boundary version of the corresponding model Hamiltonian. Thus, one cannot ignore the intrinsic difference between MM's, which can be assumed to be basically local in real space, and KF's, which on the contrary are global, as one naturally associates them with the whole extent of a QW in real space. Despite this, the correspondence works fine and allows for recovering a number of nontrivial results about the phase diagram of one model from what is known about the phase diagram of the other.

The paper is organized as follows:

- In section 2 we introduce our procedure for computing the  $g$ -function in boundary models with real fermionic modes emerging in the boundary interaction Hamiltonian. To illustrate our procedure, here we apply it to a single interacting spinless quantum wire connected to two  $p$ -wave superconductors, by discussing in detail the subtleties in counting the degrees of freedom associated with the real fermionic modes and how to deal with them;
- In section 3 we discuss the main features of the phase diagram and compute the impurity entropy at the fixed points of a junction between two quantum wires and a topological superconductor and of the asymmetric Y junction of three spinless interacting quantum wires. In both cases, we mostly review known results [18, 2, 42] which, nevertheless, are important for the sake of the presentation of the following results;
- In section 4 we discuss in detail the correspondence between a junction with two quantum wires and a topological superconductor and the asymmetric Y3J. In particular, we show how the results derived in Ref. [18] for the former system can shed light on the phase diagram of the Y3J in the case of asymmetric bulk, as well as boundary interaction and, conversely, how the results of Refs. [2, 42] for the Y3J allow for extending the analysis of the phase diagram of the junction with two quantum wires and a topological superconductor to windows of values of the system's parameters which were not encompassed in the derivation of Ref. [18];
- In section 5, as a further application of our method for computing the  $g$ -function in boundary models with real fermion modes emerging at the boundary interaction, we generalize the results of Ref. [18] by discussing the fixed points in the phase diagram, and the corresponding calculation of the  $g$ -function, in a junction between  $N$  quantum wires and a topological superconductor.
- In section 6 we provide our conclusions and discuss possible further developments of our work.
- In the various appendices, we provide mathematical details of our derivation.

TLL	Tomonaga-Luttinger liquid
FCFP	Finite-coupling fixed point
MM	Majorana mode
TS	Topological superconductor
IE	Impurity entropy
CIBC	Conformally invariant boundary condition
RG	Renormalization group
KF	Klein factor
QW	Quantum wire
Y3J	Y-junction of three interacting quantum wires

Table 1: Glossary of most commonly used abbreviations

To help following the various abbreviations, we list in table 1 the meaning of the ones we use most commonly throughout the paper.

## 2. Impurity entropy in a boundary model with real fermionic modes in the boundary interaction

When bosonizing more than one species of fermion operators in one dimension, real fermionic Klein factors must be introduced, to properly account for the anticommutation relations between operators corresponding to different species of fermions. Typically, KF's appear in boundary Hamiltonians describing junctions of one-dimensional quantum wires (which is appropriate, at points where different wires contact each other) and, in many cases, they strongly affect the boundary dynamics of the junction [45]. For instance, only by properly accounting for KF's in the boundary Hamiltonian, does one prove the emergence of a FCFP in the Y3J discussed in Refs. [1, 2], or in its spinful version [7]. In addition to KF's, real fermion operators emerge as MM's at junctions between QW's and TS's [16]. The combined effect of KF's and MM's can eventually lead to the "Majorana-Klein" hybridization and, eventually, to a remarkable topological version of the Kondo effect [50, 28, 30], also discussed in its multi-channel realization [51, 31, 29], as well as to novel phases corresponding to FCFP's in the phase diagram of junctions between QW's and TS's [18, 19]. Thus, despite their definition as a mathematical means for properly doing bosonization, KF's affect the boundary dynamics of a junction exactly as "physical" MM's do and, accordingly, they must be properly accounted for, when computing the IE of the junction. To demonstrate this point, in this section we compute the IE in a paradigmatic system given by a single spinless interacting wire connected to two TS's at its endpoints. This enables us to show how, in order to find results for the  $g$ -function consistent with the expected phase diagram of this systems, one has to count the degrees of freedom associated with real fermions at the system boundaries. In doing so, we face an additional subtlety, which was originally put forward in Ref. [52], which is strictly related to how to count real, zero-mode fermionic degrees of freedom.

In general, two real fermionic modes, say  $\gamma_a$  and  $\gamma_b$ , can be combined together into a complex (Dirac) fermionic mode  $a = \frac{1}{2}(\gamma_a + i\gamma_b)$ , which leads to a single fermion energy level, which can be either empty, or full, eventually resulting in an additional degeneracy factor of 2 in the

partition function. In a boundary theory, the procedure for computing the partition function (and, eventually extracting the  $g$ -function from the result) consists in making up a two-boundary version of the model Hamiltonian by mirroring the boundary interaction describing the junction at the other boundary of a finite-size ( $\ell$ ) version of the system (see Ref. [53] for details of the procedure). While this procedure unavoidably leads to a doubling of the MM's emerging at the interfaces (so they always contribute an even number of real fermionic modes) [17, 18, 49, 19], when introducing KF's through bosonization of the normal wires, the final total number of real fermionic modes can either be even, or odd. When it is odd, one has to face an ambiguity about how to count the left-over real fermion, which is strictly related to the need to account for fermion parity conservation in the presence of real fermion operators [52]. To overcome such a difficulty, we introduce an additional decoupled "auxiliary" fermionic wire which, in bosonization language, is characterized by its own Luttinger parameter  $\bar{K}$  and by its Klein factor  $\bar{\Gamma}$ .  $\bar{\Gamma}$  enters the total counting of degrees of freedom related to real fermions, by pairing with the real mode that is left over after all the other "physical" ones have paired into Dirac complex modes. Of course, we expect this to affect the actual value of the  $g$  function. Yet, as for any definition of entropy, what matters in the  $g$ -theorem is the entropy *difference* between two different fixed points or, which is the same, the ratio between the corresponding values of  $g$ . In fact, we expect our procedure to provide the correct result for the ratio and, to ground our speculation, in the following we provide a number of different examples of physical interest where we show that this is, in fact, the case.

To illustrate our procedure, here we apply it to compute the  $g$ -function in a single interacting spinless quantum wire connected to two  $p$ -wave superconductors in their topological phase [16] at its endpoints. At low energies, the superconducting leads can be traded for two MM's  $\gamma_L, \gamma_R$ , respectively residing at the left-hand side and at the right-hand side of the QW. In addition, the interacting QW is effectively described by resorting to the bosonization approach, which we review in Appendix A, in terms of the bosonic fields  $\phi(x), \theta(x)$ , whose dynamics is encoded in the Luttinger liquid Hamiltonian in Eq. (A.10). In particular, when expressing the chiral fermion operators  $\psi_R(x), \psi_L(x)$  in terms of  $\phi(x)$  and  $\theta(x)$ , one sets

$$\psi_R(x) = \Gamma e^{i\sqrt{\pi}[\phi(x)+\theta(x)]} \quad , \quad \psi_L(x) = \Gamma e^{i\sqrt{\pi}[\phi(x)-\theta(x)]} \quad , \quad (1)$$

with the KF  $\Gamma$  such that  $\{\Gamma, \gamma_L\} = \{\Gamma, \gamma_R\} = 0$ . Together with the MM's, the KF forms a set of three real fermionic zero-mode operators. This is the case in which, as we discuss above, to consistently count for the corresponding degrees of freedom, we introduce a second wire, described again by a Luttinger liquid Hamiltonian such as the one in Eq. (A.10), with bosonic fields  $\bar{\phi}(x), \bar{\theta}(x)$ , with parameters  $\bar{u}, \bar{K}$  and, more importantly, requiring the introduction of a second KF,  $\bar{\Gamma}$ . The second wire is fully decoupled from the rest of the system. Therefore, for any values of the boundary couplings,  $\bar{\theta}(x)$  is pinned at both  $x = 0$  and  $x = \ell$  and, accordingly,  $\partial_x \bar{\phi}(x = 0) = \partial_x \bar{\phi}(x = \ell) = 0$  (type  $N$  CIBC's). Therefore,  $\bar{\phi}(x), \bar{\theta}(x)$  are decomposed in normal modes according to Eqs. (A.11), with velocity and Luttinger parameters  $\bar{u}, \bar{K}$ . The calculation of the factor that the auxiliary QW contribute the total partition function,  $\bar{\mathcal{Z}}$ , is, therefore, a straightforward exercise in elementary algebra: the result is

$$\bar{\mathcal{Z}} = \frac{1}{\eta(\bar{q})} \sum_m \bar{q}^{\frac{m^2}{2\bar{K}}} \quad , \quad (2)$$

with  $\bar{q} = e^{-\frac{\beta\pi\bar{u}}{\ell}}$  (see [Appendix C](#) for the definition of the Dedekind function  $\eta(q)$ ). At the disconnected fixed point of the phase diagram the QW is fully decoupled from the TS's. Therefore,  $\phi(x), \theta(x)$  take the expansion in normal modes in Eqs. (A.11), as well, and they will accordingly contribute the total partition function by a factor analogous to  $\hat{\mathcal{Z}}$  in Eq. (2). In addition, we have to account for the (4) real fermionic zero mode operators. As at the disconnected fixed point they are fully decoupled from each other, as well as from the dynamical degrees of freedom of the bulk, according to the above argument, we expect them to contribute to the partition function a factor equal to 2 elevated to the total number of real fermions divided by 2 (that is, 4). As a result, the total partition function at the disconnected fixed point is given by

$$\hat{\mathcal{Z}}_{\text{Disc}} = \frac{4}{\eta(q)\eta(\bar{q})} \sum_{m,m'} q^{\frac{m^2}{2K}} \bar{q}^{\frac{(m')^2}{2K}} , \quad (3)$$

with  $q = e^{-\frac{\beta\pi u}{\ell}}$ . Using the standard asymptotic expansions of the Dedekind function and of the elliptic functions in the  $\ell \rightarrow \infty$  ( $q \rightarrow 1$ )-limit, one eventually finds that

$$\hat{\mathcal{Z}}_{\text{Disc}} \rightarrow_{\ell \rightarrow \infty} e^{[\pi\ell/(6u)] + [\pi\ell/(6\bar{u})]} [4\sqrt{K\bar{K}}] , \quad (4)$$

which implies, for the  $g$ -function at the disconnected fixed point

$$g_{\text{Disc}} = 2[K\bar{K}]^{\frac{1}{4}} . \quad (5)$$

Turning on the (two)-boundary coupling to the MM, taking into account the type  $N$  CIBC's at the disconnected fixed point, the two-boundary Hamiltonian  $H_b$  takes the form

$$H_b = -2it\gamma_L\Gamma \cos[\sqrt{\pi}\phi(0)] - 2it\gamma_R\Gamma \cos[\sqrt{\pi}\phi(\ell)] . \quad (6)$$

When  $K > 1/2$ ,  $H_b$  is a relevant operator, which drives the system toward a fixed point in which  $\phi(x)$  is pinned both at  $x = 0$  and at  $x = \ell$ , as  $\phi(0) = \sqrt{\pi}\nu_0$ ,  $\phi(\ell) = \sqrt{\pi}\nu_\ell$ , with integer  $\nu_0, \nu_\ell$ . Accordingly,  $\phi(x)$  and  $\theta(x)$  take the mode expansion in Eqs. (A.12) and, in addition, taking into account the boundary conditions, one gets  $H_b = -2it\{(-1)^{\nu_0}\gamma_L + (-1)^{\nu_\ell}\gamma_R\}\Gamma$ . A mode expansion such as the one in Eqs. (A.12) implies a corresponding contribution to the total partition function such as the one in Eq. (2), except for switching  $K$  with  $K^{-1}$ . In addition, minimizing  $H_b$  locks together the real fermions  $\Gamma$  and  $\tilde{\gamma} = \frac{1}{\sqrt{2}}\gamma_L + (-1)^{\nu_0-\nu_\ell}\frac{1}{\sqrt{2}}\gamma_R$  by the condition that physical states are annihilated by the complex fermionic operator  $a = \frac{1}{2}(\tilde{\gamma} + i\Gamma)$ . This condition leaves unpaired the real fermion operator  $\eta = -\frac{1}{\sqrt{2}}\gamma_L + (-1)^{\nu_0-\nu_\ell}\frac{1}{\sqrt{2}}\gamma_R$  which, together with  $\bar{\Gamma}$ , determines an additional degeneracy factor of 2. Therefore, the partition function and the  $g$ -function at the corresponding fixed point are given by

$$\mathcal{Z}_A = \frac{2}{\eta(q)\eta(\bar{q})} \sum_{m,m'} q^{\frac{Km^2}{2}} \bar{q}^{\frac{(m')^2}{2K}} \rightarrow_{\ell \rightarrow \infty} e^{[\pi\ell/(6u)] + [\pi\ell/(6\bar{u})]} \left[ 2\sqrt{\frac{\bar{K}}{K}} \right] . \quad (7)$$

From Eq.(7) we eventually extract the corresponding value of the  $g$ -function,  $g_A = \sqrt{2}\left[\frac{\bar{K}}{K}\right]^{\frac{1}{4}}$ . The derivation of Eq. (7) is a first example of implementation of the Majorana-Klein hybridization

[50] in computing the  $g$ -function at the  $A$  fixed point. Indeed, the real-fermion zero-mode operator we combined together with  $\bar{\Gamma}$  to obtain the degeneracy factor of 2 originates from a linear combination of  $\gamma_L$  and  $\gamma_R$ , with coefficients determined by the boundary conditions. In addition, we note that, introducing the auxiliary wire on one hand allowed us to perform the calculations in an unambiguous way, on the other hand gave us back  $g_{\text{Disc}}$  and  $g_A$  up to an over-all arbitrary, multiplicative factor. To get rid of the factor, we normalize  $g_A$  to  $g_{\text{Disc}}$  by considering the ratio

$$\rho_A = \frac{g_A}{g_{\text{Disc}}} = \frac{1}{\sqrt{2K}} \quad , \quad (8)$$

which, on one hand shows that the ratio is independent of the (arbitrary) parameter  $\bar{K}$ , as it must be, on the other hand that, consistently with the  $g$ -theorem, the renormalization group trajectories are expected to flow from the disconnected to the  $A$  fixed point when  $K > 1/2$ .

Later on in the paper, we generalize the results of this section to a junction between a generic number  $N$  of QW's and a topological superconductor. In this case, the relevant Luttinger parameters are  $K_\rho = K/\sqrt{1 + \frac{(N-1)UK}{\pi u}}$  and  $K_\sigma = K/\sqrt{1 - \frac{UK}{\pi u}}$ , with  $u, K$  being the Luttinger parameter of each QW and  $U$  being the inter-wire interaction strength. (See [Appendix A](#) for a detailed derivation and discussion of the Luttinger parameters for the  $N$ -wire junction.)

### 3. Review of the phase diagram of the 2-wire junction with a topological superconductor for $\frac{1}{2} < K_\sigma < 1$ and of the Y-junction of interacting quantum wires

To complement the calculation of the  $g$ -function and to pave the way to the derivation of the correspondence between the  $N=2$ -wire junction with a TS and the Y3J, here we review known results about the phase diagram of the two systems. In doing so, we also compute the  $g$ -function at the various fixed points of the (generically asymmetric) Y3J, and demonstrate the consistency between our results and what is known about the phase diagram of that system [42]. We now begin by briefly reviewing the phase diagram of the  $N = 2$ -wire junction with a TS, which we extensively analyzed and discussed in Ref. [18] in the regime  $K_\sigma < 1$ .

#### 3.1. Phase diagram of the 2-wire junction with a topological superconductor for $K_\sigma < 1$

We refer to section 5 for an extensive derivation, from the microscopic Hamiltonian, of the Luttinger liquid description of a generic junction between  $N$ -QW's and a TS and for the analysis of the corresponding phase diagram. Here, we just review the main features of the phase diagram in the case  $N = 2$  starting from the effective Luttinger liquid Hamiltonian,  $H_{2,B} = H_{2,\text{Bulk}} + H_{b,B,2}^{(1)}$ , with the bulk Hamiltonian

$$H_{2,\text{Bulk}} = \frac{u_\rho}{2} \int_0^\ell dx \{K_\rho (\partial_x \phi_\rho(x))^2 + K_\rho^{-1} (\partial_x \theta_\rho(x))^2\} + \frac{u_\sigma}{2} \int_0^\ell dx \{K_\sigma (\partial_x \phi_\sigma(x))^2 + K_\sigma^{-1} (\partial_x \theta_\sigma(x))^2\} \quad , \quad (9)$$

with the plasmon velocities and the Luttinger parameters defined in terms of the microscopic system parameters as per Eqs. (A.9) for  $N = 2$ , and  $\phi_\rho(x) = \frac{1}{\sqrt{2}}[\phi_1(x) + \phi_2(x)]$ ,  $\phi_\sigma(x) = \frac{1}{\sqrt{2}}[\phi_1(x) - \phi_2(x)]$ ,  $\phi_1(x), \phi_2(x)$  being the fields in the two wires, and analogous formulas for  $\theta_\rho(x), \theta_\sigma(x)$  in terms of  $\theta_1(x), \theta_2(x)$ . By construction,  $H_{2,\text{Bulk}}$  in Eq. (9) corresponds to the symmetric version of

the model Hamiltonian of Ref. [18], in which the Luttinger parameters of the two QW's are equal to each other,  $K_1 = K_2 = K$ ,  $u_1 = u_2 = u$ , and  $\phi_\rho(x), \theta_\rho(x)$  ( $\phi_\sigma(x), \theta_\sigma(x)$ ) simply correspond to the symmetric (asymmetric) linear combinations of  $\phi_1(x), \phi_2(x)$  and  $\theta_1(x), \theta_2(x)$ . Accordingly, the chiral fermionic fields in the QW's are bosonized as (see [Appendix A](#) for details)

$$\begin{aligned}\psi_{R,a}(x) &= \Gamma_a e^{i\sqrt{\pi}[\phi_a(x)+\theta_a(x)]} \\ \psi_{L,a}(x) &= \Gamma_a e^{i\sqrt{\pi}[\phi_a(x)-\theta_a(x)]} \quad ,\end{aligned}\tag{10}$$

with  $a = 1, 2$  and  $\Gamma_1, \Gamma_2$  fermionic KF's. Having stated this, the phase diagram for  $K_\sigma < 1$  is readily recovered from the analysis of Ref. [18].

The simplest fixed point corresponds to setting all the boundary couplings  $t_a = 0$ . This is the disconnected fixed point, which, in a sample defined over a segment of length  $\ell$ , corresponds to pinning  $\theta_1(x), \theta_2(x)$  at both boundaries  $x = 0, \ell$ . The corresponding value of the  $g$ -function can be computed as done in Ref. [18], yielding, as a special case of the general formula we derive in section 5, the result

$$g_{\text{Disc}} = 2[K_\rho K_\sigma]^{\frac{1}{4}} \quad ,\tag{11}$$

with the factor 2 stemming from the fourfold degeneracy due to the two MM's in the two-boundary version of the model and to the KF's associated to the two QW's. (Note that, differently from what was done in Ref. [18], here we do not count the additional degeneracy associated with the MM's at the outer boundaries of the superconducting lead, as they contribute to the  $g$ -function just an overall factor of 2, which drops from the physically meaningful ratios between  $g$  computed at two different fixed points). At the disconnected fixed point, the boundary Hamiltonian describing the coupling of the QW's to the MM is presented in bosonic coordinates as

$$H_{b,B,2}^{(1)} = -2it_1\gamma_L\Gamma_1 \cos\left[\sqrt{\frac{\pi}{2}}(\phi_\rho(0) + \phi_\sigma(0))\right] - 2it_2\gamma_L\Gamma_2 \cos\left[\sqrt{\frac{\pi}{2}}(\phi_\rho(0) - \phi_\sigma(0))\right] \quad .\tag{12}$$

The scaling dimension of  $H_{b,B,2}^{(1)}$ ,  $d_b$ , can be readily derived using the transformation in Eqs. (A.6). The result is  $d_b = \frac{1}{4K_\rho} + \frac{1}{4K_\sigma}$ . For  $1/2 < K < 1$  and for  $U > 0$ , we find  $\frac{1}{2} < d_b < 1$ , which implies that  $H_{b,B,2}^{(1)}$  always corresponds to a relevant boundary interaction. In addition, other boundary interactions, though not present in the original (“bare”) Hamiltonian, can be generated from the RG. The first one corresponds to boundary normal intra-wire backscattering, described by operators of the form  $\psi_{R,a}^\dagger(0)\psi_{L,a}(0) + \text{h.c.}$ , which are not effective, due to Dirichlet boundary conditions on  $\theta_a(x)$  at  $x = 0$ . Then, one has inter-wire normal backscattering, corresponding to operators of the form  $V_{\text{Normal,(1,2)}} = \psi_{R,1}^\dagger(0)\psi_{L,2}(0) + \text{h.c.} \propto \Gamma_1\Gamma_2 \cos[\sqrt{2\pi}\phi_\sigma(0)]$ , with corresponding scaling dimension  $d_{\text{Normal,(1,2)}} = K_\sigma^{-1}$ . Finally, one has inter-channel pairing, corresponding to operators of the form  $V_{\text{Pair,(1,2)}} = \psi_{R,1}(0)\psi_{L,2}(0) + \text{h.c.} \propto \Gamma_1\Gamma_2 \cos[\sqrt{2\pi}\phi_\rho(0)]$ , with scaling dimension  $d_{\text{Pair,(1,2)}} = K_\rho^{-1}$ . Thus, as long as  $1/2 < K_\rho, K_\sigma < 1$ , no relevant operators are allowed at the disconnected fixed point but the boundary coupling to the MM,  $H_{b,B,2}^{(1)}$ .

The relevance of the operators in  $H_{b,B,2}^{(1)}$  implies that, as soon as (at least one of) the  $t_a$ 's are  $\neq 0$ , the corresponding operator(s) trigger an RG flow away from the disconnected fixed point. In

Ref. [18] it is shown that, for  $K_\sigma < 1$ , the junction either flow towards a fixed point with type  $A(N)$  boundary conditions in channel-1(2) (the  $A \otimes N$  fixed point), or towards the complementary,  $N \otimes A$  fixed point. In both cases, a straightforward implementation of our method yields, for the  $g$  function

$$g_{A \otimes N} = g_{N \otimes A} = \frac{\sqrt{2K}}{(K_\rho K_\sigma)^{\frac{1}{4}}} \Rightarrow \rho_{1,1} = \frac{g_{A \otimes N}}{g_{\text{Disc}}} = \frac{1}{\sqrt{2K}} \left[ 1 - \left( \frac{KU}{\pi u} \right)^2 \right]^{\frac{1}{4}}. \quad (13)$$

The result in Eq. (13) corresponds to the symmetric limit of the junction discussed in Ref. [18]. Note that it also fixes an error in that reference, though without affecting the final result. The important point is the over-all factor  $\sqrt{2}$ , which ensures that  $\rho_{1,1} < 1$  as long as  $1/2 < K$ . It actually comes from the correct counting of the degrees of freedom associated with zero-mode real fermion operators. In particular, for the RG flow towards the  $A \otimes N$  ( $N \otimes A$ ) fixed point to occur, the bare couplings must be such that  $t_1 > t_2$  ( $t_1 < t_2$ ). In this case, the RG makes the running coupling corresponding to the larger bare coupling constant flow all the way to  $\infty$ . Let us assume this is  $t_1$ . Accordingly, to recover the  $A \otimes N$  fixed point, one considers the two-boundary version of  $H_{b,B,2}^{(1)}$ , in which  $t_1 \rightarrow \infty$ . In fact, this implies “locking” two of the four real fermions (2 KF’s plus 2 MM’s) into a linear combination annihilating the physical states, leaving the other two decoupled from the boundary interaction, with a total degeneracy factor of 2 in the total partition function and, therefore, a factor  $\sqrt{2}$  in  $g_{A \otimes N}$  [18]. The set of allowed boundary operators at the  $A \otimes N$  fixed point includes the same operators we listed at the disconnected fixed point, though realized differently, and with different scaling dimensions, due to the change in the boundary conditions for the bosonic fields [18]. In particular, normal intra-channel 1 backscattering corresponds to an operator  $V_{\text{Intra},1} \propto \cos[2\sqrt{\pi}\theta_1(0)]$ , with scaling dimension  $d_{\text{Intra},1} = d_b^{-1}$ . At the same time, inter-channel normal backscattering and inter-channel pairing are described by boundary operators that are linear combinations of  $V_{a,(1,2)}$  and of  $V_{b,(1,2)}$ , respectively given by

$$\begin{aligned} V_{a,(1,2)} &= \Gamma_1 \Gamma_2 e^{i\sqrt{\pi}[\theta_1(0) - \phi_2(0)]} \\ V_{b,(1,2)} &= \Gamma_1 \Gamma_2 e^{i\sqrt{\pi}[\theta_1(0) + \phi_2(0)]}, \end{aligned} \quad (14)$$

together with their Hermitean conjugates. The operators in Eqs. (14) have the same scaling dimension,  $d_{a,(1,2)} = d_{b,(1,2)}$ , which is consistent with the result in Eq. (D.26) of Ref. [18]. As a result, one obtains  $d_{a,(1,2)} = d_{b,(1,2)} = \frac{1+K_\rho K_\sigma}{K_\rho + K_\sigma}$ . For  $N = 2$ , one obtains  $K_\rho = K / \sqrt{1 + \frac{UK}{\pi u}}$ , which is always  $< 1$  for  $1/2 < K < 1$  and  $U > 0$ . Thus, one obtains that  $\frac{1+K_\rho K_\sigma}{K_\rho + K_\sigma} > 1$ , as long as  $K_\sigma < 1$ . Therefore, we conclude that both inter-channel normal backscattering and inter-channel pairing are described by irrelevant operators. Finally, an additional boundary operator arises from the residual boundary coupling of channel 2 to the MM. This corresponds to the term  $\propto t_2$  in Eq. (12). Despite the fact that it appears to correspond to a relevant operator, due to the hybridization between  $\gamma_L$  and  $\Gamma_1$  in the state that sets in at the  $A \otimes N$  fixed point, it becomes effective only to order  $t_2^2$ , corresponding to an operator  $V_{2,\text{Res}} \propto \cos[2\sqrt{\pi}\phi_2(0)]$ , with scaling dimension  $d_{2,\text{Res}} = \frac{4}{K_\rho + K_\sigma} > 1$ . This eventually proves that, for  $K_\sigma < 1$ , the stable phase of the  $N = 2$  junction either corresponds to the  $A \otimes N$ , or to the  $N \otimes A$  fixed point.

An additional possibility is provided by the  $A \otimes A$  fixed point of Ref. [18], with type  $A$  boundary conditions in both channels. The  $g$ -function at the  $A \otimes A$  fixed point can be readily derived either from the analysis of Ref. [18] (up to an over-all  $\sqrt{2}$ , as discussed above), or from the general result of section 5, taken for  $N = 2$  and for  $N_a = 2, N_n = 0$ . As a result, one obtains

$$g_{A \otimes A} = \frac{2}{[K_\rho K_\sigma]^{\frac{1}{4}}} \Rightarrow \begin{cases} \rho_{A \otimes A} = \frac{g_{A \otimes A}}{g_{\text{Disc}}} = \frac{1}{\sqrt{K_\rho K_\sigma}} \\ \hat{\rho}_{A \otimes A} = \frac{g_{A \otimes A}}{g_{A \otimes N}} = \sqrt{\frac{2}{K}} \end{cases} . \quad (15)$$

From Eqs. (15) one readily checks that, as long as  $K_\sigma < 1$ , one obtains  $\rho_{A \otimes A} < 1$ , as well as  $\hat{\rho}_{A \otimes A} < 1$ , which implies that the  $A \otimes A$  fixed point is unstable to both the  $N \otimes N$ , as well as to the  $A \otimes N$  fixed point. This is consistent with the DEBC results about the set of allowed boundary operators at the  $A \otimes A$  fixed point. Indeed, implementing type  $A$  boundary conditions at  $x = 0$  for both  $\phi_1(x)$  and  $\phi_2(x)$ , we see that the boundary operators describing inter-channel normal backscattering, as well as inter-channel pairing, are in general expressed as linear combinations of the operators  $V_{a,(1,2)}, V_{b,(1,2)}$ , respectively given by

$$\begin{aligned} V_{a,(1,2)} &= \Gamma_1 \Gamma_2 e^{i \sqrt{2\pi} \theta_\sigma(0)} \\ V_{b,(1,2)} &= \Gamma_1 \Gamma_2 e^{i \sqrt{2\pi} \theta_\rho(0)} \end{aligned} , \quad (16)$$

together with their Hermitean conjugates. Their scaling dimensions are accordingly given by  $d_{a,(1,2)} = K_\sigma, d_{b,(1,2)} = K_\rho$ . Thus, we see that, for  $K_\sigma < 1$ , they both correspond to relevant boundary interactions. Other boundary interaction terms are determined by the operators  $\tilde{V}_{\text{Res},1}, \tilde{V}_{\text{Res},2}$  describing the residual coupling to the MM which, as discussed in detail in Appendix B, in this case can be effective to first-order in the boundary interaction strengths, different from what happens at the  $A \otimes N$  fixed point. In particular, on applying the bosonization procedure to the operators derived in Appendix B, one obtains

$$\begin{aligned} \tilde{V}_{\text{Res},1} &\propto e^{i \sqrt{\frac{\pi}{2}} [\theta_\rho(0) + \theta_\sigma(0)]} \\ \tilde{V}_{\text{Res},2} &\propto e^{i \sqrt{\frac{\pi}{2}} [\theta_\rho(0) - \theta_\sigma(0)]} \end{aligned} . \quad (17)$$

The corresponding scaling dimensions are readily derived to be equal to each other and given by  $d_{\text{Res},1} = d_{\text{Res},2} = \frac{K_\rho + K_\sigma}{4}$ . Given the definition of  $K_\rho$  and  $K_\sigma$  in section 2, we see that they are both relevant, as long as  $K_\sigma < 1$ . Incidentally, we note that the other allowed boundary operators, corresponding to intra-channel boundary backscattering processes, are realized as  $V_{\text{Intra},1(2)} \propto \cos[2 \sqrt{\pi} \theta_{1(2)}(0)] = \cos[\sqrt{2\pi}(\theta_\rho(0) \pm \theta_\sigma(0))]$ . Accordingly, they have the same scaling dimension,  $d_{\text{Intra},1} = d_{\text{Intra},2} = K_\rho + K_\sigma$  and, therefore, they are both irrelevant, for  $1/2 < K$  and  $U > 0$ .

The conclusion that, for  $K_\sigma < 1$ , there are two equivalent stable fixed points in the phase diagram of the  $N = 2$  junction (the  $A \otimes N$  and the  $N \otimes A$  fixed points discussed above) implies that there must be a phase transition between the two of them. In Ref. [18], the phase transition has been identified at a FCFP in the phase diagram of the junction, which is attractive along the line in parameter space corresponding, in the symmetric case, to  $t_1 = t_2$ , and otherwise repulsive. To show this, an effective means is to resort to the perturbative RG approach within the  $\epsilon$ -expansion method.

Basically, one assumes that the junction parameters are such that  $d_b = 1 - \epsilon$ , with  $0 < \epsilon \ll 1$ , and accordingly derives the RG equations to the first nonlinear order in the boundary couplings, so as to recover nontrivial zeroes for the  $\beta$ -functions corresponding to the FCFP. For the details of the systematic derivation of the corresponding RG equations we refer to Ref. [18] in the specific case  $N = 2$ , as well as to Appendix D.1 for the generalization of the procedure to a generic  $N$ , while here we just quote the final result. Specifically, as extensively discussed in Appendix D.1, one introduces the dimensionless running couplings  $\bar{t}_a = t_a \tau_0^\epsilon$ , with the cutoff  $\tau_0 \propto D_0^{-1}$ ,  $D_0$  being a high-energy (band) cut-off for the system. Therefore, letting the scale run from  $D_0$  down to the scale parameter  $D < D_0$ , one obtains that the corresponding RG trajectories of the running couplings are determined by the differential equations

$$\begin{aligned} \frac{d\bar{t}_1}{dl} &= \epsilon \bar{t}_1 - \mathcal{F} \left( \frac{1}{2K_\rho} - \frac{1}{2K_\sigma} \right) \bar{t}_1 \bar{t}_2^2 \\ \frac{d\bar{t}_2}{dl} &= \epsilon \bar{t}_2 - \mathcal{F} \left( \frac{1}{2K_\rho} - \frac{1}{2K_\sigma} \right) \bar{t}_2 \bar{t}_1^2 \end{aligned} \quad , \quad (18)$$

with  $l = \ln(D_0/D)$ ,  $D$  being the running energy scale, and the function  $\mathcal{F}(v)$  defined in Eq. (D.7). In general, for small initial values of the  $\bar{t}_i$ 's, Eq. (18) implies a growth of the  $\bar{t}_a$  along the RG trajectories. Along the symmetric line  $t_1 = t_2$  in parameter space, this takes the system to the FCFP discussed in Ref. [18], which corresponds to the nontrivial zeroes of the right-hand sides of Eqs. (18) at  $\bar{t}_1 = \bar{t}_2 = t_* = \sqrt{\epsilon / \mathcal{F} \left( \frac{1}{2K_\rho} - \frac{1}{2K_\sigma} \right)}$ . Alternatively, if the initial condition lies off the symmetric line, the RG trajectories flow towards either the  $A \otimes N$ , or the  $N \otimes A$ , fixed point, according to whether, at  $D = D_0$ , one has  $t_1 > t_2$ , or  $t_1 < t_2$ . While an exact description of the FCFP is still missing, within the  $\epsilon$ -expansion method it is possible to estimate the corresponding value of the  $g$  function to leading order in the  $\epsilon$ , obtaining [18]

$$g_{FCFP} = g_{N \otimes N} \left\{ 1 - \frac{2\pi\epsilon^2}{\mathcal{F} \left( \frac{1}{2K_\rho} - \frac{1}{2K_\sigma} \right)} \right\} \quad , \quad (19)$$

which implies  $\frac{g_{FCFP}}{g_{N \otimes N}} < 1$ , consistently with the RG flow from the disconnected fixed point to the FCFP, for  $\epsilon > 0$ .

### 3.2. Phase diagram of the Y-junction of three spinless interacting normal wires

The Y3J has been introduced and extensively discussed in Ref. [2] in the fully  $\mathbf{Z}_3$ -symmetric case (bulk and boundary interaction). Later on, in Ref. [42], the effects of relaxing the bulk  $\mathbf{Z}_3$ -symmetry have been considered. Here, we consider the most general situation in which the  $\mathbf{Z}_3$  symmetry between the QW's can be broken by the boundary interaction, or by the bulk Hamiltonian [42], or both. Accordingly, we use as bulk Hamiltonian of the (asymmetric) Y3J,  $H_{\text{Bulk}}$ , given by

$$H_{\text{Bulk}} = \sum_{a=1,2} \frac{u}{2} \int_0^\ell dx [K(\partial_x \phi_a(x))^2 + K^{-1}(\partial_x \theta_a(x))^2] + \frac{u}{2} \int_0^\ell dx [K_3(\partial_x \phi_3(x))^2 + K_3^{-1}(\partial_x \theta_3(x))^2], \quad (20)$$

with  $K, K_3$  Luttinger parameters of the QW's and the velocity  $u$  set equal in all three channels to avoid unnecessary formal complications.

In the absence of a boundary interaction, the  $g$ -function for the Y3J can be readily computed following the recipe of section 2 for  $N = 3$ . In particular, since  $N$  is odd, we add an auxiliary disconnected wire, with parameters  $\bar{u}$  and  $\bar{K}$  and Klein factor  $\bar{\Gamma}$ , so to recover a total even number of KF's. Taking into account that, for a generic  $K_3$ , the  $g$ -function at the disconnected fixed point,  $g_{\text{Disc}}(K, K_3)$ , is given by

$$g_{\text{Disc}}(K, K_3) = 2[K_3 K^2 \bar{K}]^{\frac{1}{4}}, \quad (21)$$

with the factor 2 due to the four real fermions that determine a total degeneracy of 4. Keeping all the  $\theta_a(0)$  pinned and turning on a (non  $\mathbf{Z}_3$ -symmetric) boundary interaction, one may readily present the corresponding boundary Hamiltonian  $H_b$  by implementing the transformation matrix  $\mathbf{M}_N$  in Eq. (A.6) with  $N = 3$  to resort to the center of mass- and to the relative-field basis, that is, by setting

$$\begin{bmatrix} \Phi(x) \\ \varphi_1(x) \\ \varphi_2(x) \end{bmatrix} = \begin{bmatrix} \frac{1}{\sqrt{3}} & \frac{1}{\sqrt{3}} & \frac{1}{\sqrt{3}} \\ \frac{1}{\sqrt{2}} & -\frac{1}{\sqrt{2}} & 0 \\ \frac{1}{\sqrt{6}} & \frac{1}{\sqrt{6}} & -\frac{2}{\sqrt{6}} \end{bmatrix} \begin{bmatrix} \phi_1(x) \\ \phi_2(x) \\ \phi_3(x) \end{bmatrix}, \quad \begin{bmatrix} \Theta(x) \\ \vartheta_1(x) \\ \vartheta_2(x) \end{bmatrix} = \begin{bmatrix} \frac{1}{\sqrt{3}} & \frac{1}{\sqrt{3}} & \frac{1}{\sqrt{3}} \\ \frac{1}{\sqrt{2}} & -\frac{1}{\sqrt{2}} & 0 \\ \frac{1}{\sqrt{6}} & \frac{1}{\sqrt{6}} & -\frac{2}{\sqrt{6}} \end{bmatrix} \begin{bmatrix} \theta_1(x) \\ \theta_2(x) \\ \theta_3(x) \end{bmatrix}. \quad (22)$$

As a result, one obtains

$$\begin{aligned} H_b = & \{t_{2,1}\Gamma_2\Gamma_1 e^{-i[\sqrt{2\pi}\varphi_1(0)]} + t_{3,2}\Gamma_3\Gamma_2 e^{-i[\sqrt{2\pi}(-\frac{1}{2}\varphi_1(0) + \frac{\sqrt{3}}{2}\varphi_2(0))]} \\ & + t_{1,3}\Gamma_1\Gamma_3 e^{-i[\sqrt{2\pi}(-\frac{1}{2}\varphi_1(0) - \frac{\sqrt{3}}{2}\varphi_2(0))]} \} + \text{h.c.} \equiv \sum_{a=1}^3 t_{a+1,a} V_{a,a+1} + \text{h.c.}, \quad (23) \end{aligned}$$

with  $t_{a+1,a}$ ,  $a = 1, 2, 3$  being the boundary interaction strengths (assuming the convention  $a + 1 \equiv 1$  for  $a = 3$ ) and the  $\{\Gamma_a\}$ 's being the three KF's required to bosonize the fermionic fields of the three wires, which shows that  $H_b$  only depends on the relative fields  $\varphi_1(x), \varphi_2(x)$ . Therefore, in constructing other boundary fixed points, we only act on the boundary conditions on  $\varphi_1(x), \varphi_2(x)$ , which are type  $N$  at the disconnected fixed point but, in general, can change at other fixed points [2, 42]. Incidentally, we note that the right-hand side of Eq. (23) is the leading boundary operator allowed at the disconnected fixed point. It is a linear combination of the operators  $V_{a,a+1}$  (plus their Hermitean conjugates), with scaling dimensions respectively given by  $d_{V_{1,2}} = \frac{1}{K}$ ,  $d_{V_{2,3}} = d_{V_{3,1}} = \frac{1}{2K} + \frac{1}{2K_3}$ . So, a necessary condition for the disconnected fixed point not to be stable is that either one of the scaling dimensions above (or both) become  $< 1$ .

A first, alternative, fixed point is recovered by assuming type  $A$  boundary conditions for both  $\varphi_1(x)$  and  $\varphi_2(x)$ . This corresponds to the  $D_P$  fixed point of Refs. [2, 42]. To stabilize  $D_P$ , we introduce a two-boundary pairing potential  $V_P$ , given by

$$\begin{aligned} V_P = & -\Delta \sum_{a=1}^3 \{ \psi_{R,a}(0) \psi_{L,a}(0) \psi_{L,a+1}^\dagger(0) \psi_{R,a+1}^\dagger(0) \} - \Delta \sum_{a=1}^3 \{ \psi_{R,a}(\ell) \psi_{L,a}(\ell) \psi_{L,a+1}^\dagger(\ell) \psi_{R,a+1}^\dagger(\ell) \} + \text{h.c.} \\ = & -\Delta \sum_{a=1}^3 e^{2i\sqrt{\pi}[\phi_a(0) - \phi_{a+1}(0)]} - \Delta \sum_{a=1}^3 e^{2i\sqrt{\pi}[\phi_a(\ell) - \phi_{a+1}(\ell)]} + \text{h.c.}, \quad (24) \end{aligned}$$

and eventually send  $\Delta \rightarrow \infty$ . Sending  $\Delta \rightarrow \infty$ , one pins  $\varphi_1(x)$  and  $\varphi_2(x)$  at both boundaries. Taking this into account, one determines the corresponding spectrum of the zero-mode operators and, repeating the calculation of the  $g$ -function at the  $D_P$  fixed point, one obtains

$$g_{D_P}(K, K_3) = \frac{2\sqrt{2K+K_3}\bar{K}^{\frac{1}{4}}}{(K_3K^2)^{\frac{1}{4}}}, \quad (25)$$

which yields the ratio

$$\rho_{D_P}(K, K_3) = \frac{g_{D_P}(K, K_3)}{g_{\text{Disc}}(K, K_3)} = \frac{1}{K} \sqrt{\frac{2K+K_3}{K_3}}. \quad (26)$$

An important comment about Eq. (26) is that, despite the fact that, for  $K = K_3$ , neither  $g_{\text{Disc}}(K, K_3)$ , nor  $g_{D_P}(K, K_3)$ , are equal to the values derived in Ref. [2], the ratio between the two of them is the same as one would get by using the results obtained there. This is due to the fact that, in our derivation, we count the degrees of freedom associated with the real KF's, including the auxiliary one and, in addition, do not restrict our derivation to the sector involving the relative fields only. Nevertheless, the ratio between the two of them is consistent with Ref. [2]. Clearly, this further enforces our intuition that, despite the arbitrary aspects of our procedure, the ratios between values of the  $g$ -function at different fixed points do always give back the right, physical result.

The leading dimension boundary interaction at the disconnected fixed point is  $H_b$  in Eq. (23). It is a linear combination of operators with scaling dimensions  $d_{V_{1,2}} = \frac{1}{K}$ ,  $d_{V_{2,3}} = d_{V_{3,1}} = \frac{1}{2K} \left( \frac{K_3+K}{K_3} \right)$ . At variance, at the  $D_P$  fixed point, the leading dimension boundary operators are given by [2, 42]

$$\begin{aligned} T_{1,2} &= \Gamma_1 \Gamma_2 e^{-i\sqrt{\pi}[\theta_1(0)+\theta_2(0)]} \\ T_{2,3} &= \Gamma_2 \Gamma_3 e^{-i\sqrt{\pi}[\theta_2(0)+\theta_3(0)]} \\ T_{3,1} &= \Gamma_3 \Gamma_1 e^{-i\sqrt{\pi}[\theta_3(0)+\theta_1(0)]}, \end{aligned} \quad (27)$$

together with their Hermitean conjugates. To derive the corresponding scaling dimensions, one has to resort to the center of mass- and relative field basis by using Eqs.(22) and to take into account that  $\Theta(0)$  is always pinned, as  $\Phi(0)$  never appears in the boundary interaction [2]. As a result, one obtains [42]  $d_{T_{1,2}} = \frac{KK_3}{2K+K_3}$  and  $d_{T_{2,3}} = d_{T_{3,1}} = \frac{K(K_3+K)}{2(K_3+2K)}$ . From the scaling dimensions of the boundary operators we see that there is a  $K_3/K$ -dependent window of values of  $K$  in which neither the disconnected, nor the  $D_P$  fixed point, is stable. Specifically, this happens for  $1 < K < 3$  for  $K = K_3$  [2] and, more generically, for  $K > K_{\min} = \max\left\{1, \frac{2K_3}{K+K_3}\right\}$  and  $K < K_{\max} = \left(\frac{2K+K_3}{K_3}\right)$  for a generic  $K_3$  [42]. The absence of time-reversal breaking in  $H_b$  in Eq. (23) rules out the possibility of stabilizing the ‘‘chiral’’  $\chi_{\pm}$  fixed points: thus, one concludes that, for  $K_{\min} < K < K_{\max}$ , the stable phase of the system either corresponds to one of the asymmetric  $A_a$ -points emerging in the Y3J when the  $\mathbf{Z}_3$ -symmetry between the channels is broken, or to a generically asymmetric version of the  $M$ -FCFP found in the  $\mathbf{Z}_3$ -symmetric Y3J in the time-reversal symmetric case [2].

The symmetries of the bulk Hamiltonian in Eq. (20) naturally lead to two different types of asymmetric fixed points: the  $A_3$  fixed point corresponds to QW-3 disconnected from the junction, while the two-wire junction between QW's -1 and -2 is ‘‘healed’’ (which is a natural consequence

of having  $K > 1$ , once QW-3 is disconnected from the junction [15]), and the (equivalent, up to swapping QW-1 and QW-2 with each other)  $A_1$  and  $A_2$  fixed points, in which respectively QW-1 and QW-2 are disconnected from the junction. Mathematically, disconnecting QW- $a$  corresponds to imposing type  $N$  (type  $A$ ) boundary conditions on  $\phi_a(x)$  ( $\theta_a(x)$ ), as well as type  $A$  (type  $N$ ) boundary conditions on  $\phi_{a+1}(x) - \phi_{a+2}(x)$  ( $\theta_{a+1}(x) - \theta_{a+2}(x)$ ). Accordingly, the calculation of the corresponding value of the  $g$ -function can be readily carried out, providing the result

$$\begin{aligned} g_{A_3}(K, K_3) &= 2[K_3 \bar{K}]^{\frac{1}{4}} \\ g_{A_1}(K, K_3) &= g_{A_2}(K, K_3) = 2[K_3 \bar{K}]^{\frac{1}{4}} \left[ \frac{1}{2} + \frac{K}{2K_3} \right]^{\frac{1}{2}} . \end{aligned} \quad (28)$$

yielding the ratios

$$\begin{aligned} \rho_{A_3}(K, K_3) &= \frac{g_{A_3}(K, K_3)}{g_{\text{Disc}}(K, K_3)} = K^{-\frac{1}{2}} \\ \rho_{A_1}(K, K_3) &= \rho_{A_2}(K, K_3) = \frac{g_{A_1}(K, K_3)}{g_{D_p}(K, K_3)} = K^{-\frac{1}{2}} \sqrt{\frac{K + K_3}{2K_3}} . \end{aligned} \quad (29)$$

It is useful to also compute the ratios with  $g_{D_p}(K, K_3)$ . The result is

$$\begin{aligned} \tilde{\rho}_{A_3}(K, K_3) &= \frac{g_{A_3}(K, K_3)}{g_{D_p}(K, K_3)} = K^{\frac{1}{2}} \sqrt{\frac{K_3}{2K + K_3}} \\ \tilde{\rho}_{A_1}(K, K_3) &= \tilde{\rho}_{A_2}(K, K_3) = \frac{g_{A_1}(K, K_3)}{g_{D_p}(K, K_3)} = K^{\frac{1}{2}} \sqrt{\frac{2K + K_3}{2(K + K_3)}} . \end{aligned} \quad (30)$$

An effective mean to infer the stability of the  $A_a$  fixed points against the disconnected and the  $D_p$  fixed point consists in using Eqs. (29,30) in combination of the DEBC analysis of the corresponding allowed boundary operators. To construct the leading boundary perturbation at the  $A_a$  fixed point, one considers the operators  $T_{a,a+1}$ ,  $\tilde{T}_{a,a+1}$ , respectively given by [42]

$$\begin{aligned} T_{a,a+1} &= \Gamma_a \Gamma_{a+1} e^{-i \sqrt{\pi}[\phi_a(0) - \phi_{a+1}(0)] - i \sqrt{\pi}[\theta_a(0) + \theta_{a+1}(0)]} \\ \tilde{T}_{a,a+1} &= \Gamma_a \Gamma_{a+1} e^{-i \sqrt{\pi}[\phi_a(0) - \phi_{a+1}(0)] + i \sqrt{\pi}[\theta_a(0) + \theta_{a+1}(0)]} , \end{aligned} \quad (31)$$

together with their Hermitean conjugates.  $T_{a,a+1}$  and  $\tilde{T}_{a,a+1}$  respectively correspond to the boundary operators bilinear in the  $\{\psi_{R,a}, \psi_{L,a}\}$ 's given by  $\psi_{R,a}^\dagger(0) \psi_{L,a+1}(0)$  and  $\psi_{L,a}^\dagger(0) \psi_{R,a+1}(0)$ . Once the appropriate CIBC's are implemented, they only depend on the linear combinations of the  $\phi_a(0)$ 's and of the  $\theta_a(0)$ 's that are not pinned at the corresponding fixed point. In particular, the CIBC's corresponding to the  $A_a$  fixed point are recovered by pinning the arguments of both  $T_{a+1,a+2}$  and  $\tilde{T}_{a+1,a+2}$ . The  $T_{a,a+1}$ ,  $\tilde{T}_{a,a+1}$ -operators are the only operators that may become relevant at the  $A_a$  fixed point, with scaling dimension  $d_{A_3} = \frac{2K+K_3+K_3K^2}{4K_3K}$ , and  $d_{A_1} = d_{A_2} = \frac{2K+K_3+K_3K^2}{2(K+K_3)K}$  [42]. As a result, from Eqs. (29,30) one finds that, in order for the  $A_3$  fixed point to be stable with respect to both the disconnected and the  $D_p$  fixed point, the condition  $1 < K < 1 + \frac{2K}{K_3}$  has to be satisfied. In

addition, there must be no relevant boundary operators allowed at  $A_3$  in order for it to correspond to the actual stable fixed point of the Y3J. This leads to the additional condition  $d_{A_3} > 1$ , that is,  $K_3 < 2K/(4K - 1 - K^2)$ . In particular, for  $1 < K < 3$ , the last condition implies  $K_3 < K$ , which yields  $g_{A_3}(K, K_3)/g_{A_1}(K, K_3) = \rho_{A_3}(K, K_3)/\rho_{A_1}(K, K_3) = \sqrt{\frac{2K_3}{K+K_3}} < 1$ , thus showing that  $A_3$  is stable against both  $A_1$  and  $A_2$ , as well. This is ultimately consistent with the results plotted in Fig.5 of Ref. [42], as well as with the observation that, a small enough  $K_3/K$  eventually makes the interaction in wire-3 to be effectively repulsive, thus triggering the disconnection of this wire from the junction, in agreement with the known results about junctions of Luttinger liquids [34, 15, 2]. Conversely, in order for either  $A_1$ , or  $A_2$ , to be stable against the disconnected, as well as the  $D_P$  fixed point, the condition  $\frac{K+K_3}{2K_3} < K < \frac{2(K+K_3)}{2K+K_3}$  has to be met. In addition, the condition  $d_{A_1} > 1$  implies  $K_3 > \frac{2K}{K-1}$ . In particular, the above conditions yield  $g_{A_3}(K, K_3)/g_{A_1}(K, K_3) = \sqrt{\frac{2K_3}{K+K_3}}$ , which shows that having  $K_3 < K$  ( $K_3 > K$ ) is a necessary condition to make  $A_3$  ( $A_1$ ) stable against  $A_1$  ( $A_3$ ).

Finally, we note that there are regions in parameter space in which, though one has that one of the conditions  $\rho_{A_3}(K, K_3) < 1$ , or  $\rho_{A_1}(K, K_3) < 1$  is met, none of the above fixed points is stable. This happens for  $\frac{2K}{4K-1-K^2} < K_3 < K$ , as well as for  $K < K_3 < \frac{2K}{K-1}$ . In this case, based on the well-grounded results of Ref. [2] about the  $\mathbf{Z}_3$ -symmetric Y3J, we expect that the stable phase of the system corresponds to a (possibly non- $\mathbf{Z}_3$ -symmetric) FCFP, which generalize the  $M$ -FCFP of Ref. [2]. In the  $\mathbf{Z}_3$ -symmetric case  $K = K_3$ , the emergence of the  $M$ -FCFP can be inferred from the perturbative RG equations in Eqs. (D.22) of Appendix D.2, given by

$$\begin{aligned} \frac{d\bar{t}_{2,1}}{dl} &= \epsilon\{\bar{t}_{2,1} - \bar{t}_{2,1}[b(\bar{t}_{2,1})^2 + c((\bar{t}_{3,2})^2 + (\bar{t}_{1,3})^2)]\} \equiv \beta_1[\bar{t}_{2,1}, \bar{t}_{3,2}, \bar{t}_{1,3}] \\ \frac{d\bar{t}_{3,2}}{dl} &= \epsilon\{\bar{t}_{3,2} - \bar{t}_{3,2}[b(\bar{t}_{3,2})^2 + c((\bar{t}_{1,3})^2 + (\bar{t}_{2,1})^2)]\} \equiv \beta_2[\bar{t}_{2,1}, \bar{t}_{3,2}, \bar{t}_{1,3}] \\ \frac{d\bar{t}_{1,3}}{dl} &= \epsilon\{\bar{t}_{1,3} - \bar{t}_{1,3}[b(\bar{t}_{1,3})^2 + c((\bar{t}_{2,1})^2 + (\bar{t}_{3,2})^2)]\} \equiv \beta_3[\bar{t}_{2,1}, \bar{t}_{3,2}, \bar{t}_{1,3}] \quad , \end{aligned} \quad (32)$$

with  $0 < \epsilon (= 1 - K^{-1}) \ll 1$ , and the parameters  $b$  and  $c$  estimated in Appendix D.2 to be  $b \approx 26.32$ ,  $c \approx 16.45$ . An important point about the  $\beta$ -functions in Eqs. (32) is that they are over-all  $\propto \epsilon$ . As a result, the  $M$ -FCFP is found to lie at  $\bar{t}_{2,1} = \bar{t}_{3,2} = \bar{t}_{1,3} = t_* = 1/\sqrt{b+2c}$ , independent of  $\epsilon$ . On one hand, this result points in the right direction. Indeed, analytical [2], as well as numerical [53], results for the conductance tensor at the  $M$ -FCFP ultimately show that it has to be finite, as  $\epsilon \rightarrow 0$ . Had we found an  $M$ -FCFP at  $t_*$  going to zero as  $\epsilon \rightarrow 0$ , we would unavoidably get a conductance tensor going to zero as  $\epsilon \rightarrow 0$ , as well, which would be incorrect [2, 53]. On the other hand, since there is no ‘‘small parameter’’, such as  $\epsilon$ , that can be used to control the coupling strengths at the FCFP’s, one cannot really expect Eqs. (32) to be reliable to make quantitative predictions on e.g. the conductance tensor at the FCFP, or on the  $g$ -function (at variance with what happens for the junction between  $N$  QW’s and a TS). Yet, besides the emergence of the  $M$ -FCFP itself, other remarkable conclusions can be derived from Eqs. (32), such as that the RG-trajectories always point towards the  $\mathbf{Z}_3$ -symmetric  $M$ -FCFP, that is, any asymmetry in the boundary couplings is an irrelevant perturbation of the RG flow trajectories. In fact, this is a remarkable feature that, in the  $\mathbf{Z}_3$ -symmetric case, the Y3J shares with the topological Kondo effect, in which the magnetic

impurity is realized in terms of localized MM's [28]. In the general case  $K_3 \neq K$ , we rather refer to the corresponding generalization of Eqs. (32) that we provide in Eqs. (D.23) of Appendix D.2. In particular, looking for nontrivial zeroes of the  $\hat{\beta}_a$ -functions of Eqs. (D.23), we see that the predicted values of the running couplings corresponding to the  $M$ -FCFP are either characterized by an “easy plane” asymmetry for  $K_3 > K$  (which implies  $\bar{t}_{2,1,*} < \bar{t}_{3,2,*} = \bar{t}_{1,3,*}$ ), or by an “easy axis” asymmetry in the complementary case,  $K_3 < K$  (which implies  $\bar{t}_{2,1,*} > \bar{t}_{3,2,*} = \bar{t}_{1,3,*}$ ). In both cases, the flow towards the  $M$ -FCFP always requires the relevance of all the  $V_{a,a+1}$ -operators entering  $H_b$ , as we discuss in detail in section 4, when spelling out the correspondence between the  $N = 2$  junction and the Y3J.

#### 4. Correspondence between an $N = 2$ junction with a topological superconductor and a Y-junction of three spinless quantum wires

In this section we discuss in detail the various aspects of the correspondence between a junction with 2 QW's and a topological superconductor and the (generically asymmetric) Y3J. For the purpose of this work, the correspondence is of the utmost importance for several reasons. First of all, it works as a sort of “model duality”, allowing for recovering results about the phase diagram of one of the two systems from the known (and controlled) features of the phase diagram of the other, in the various regions of the system parameters. Moreover, the correspondence is useful in computing the  $g$ -function of one model from known results on the other one. About this point, it is worth stressing that, as in our work we attribute physical meaning only to the ratio between the  $g$ -function at different fixed points of the phase diagram, contributions from modes not entering the correspondence factorize and cancel, when computing the ratios, which enforces the reliability of the correspondence to computing the IE. Finally, as the correspondence requires defining MM's in the  $N = 2$  junction in terms of KF's in the Y3J, and vice versa, it provides also strong evidence for the fact that both real fermionic modes have to be taken into account, and considered on the same footing, when computing the  $g$ -function, which is one of the main points we make here.

For clarity, in the following we split the presentation of the correspondence in two sub-sections. In sub-section 4.1, we explicitly construct the mapping from the  $N = 2$  junction to the Y3J. This allows us to use known results about the phase diagram of the  $N = 2$  junction [18] to unveil specific features in the phase diagram of the Y3J, such as emergence of “planar” FCFP's (that is, with one of the boundary coupling strengths set to 0). In sub-section 4.2, we derive the mapping from the Y3J to the  $N = 2$  junction. Reversing the direction of the correspondence allows us to employ the known results about the phase diagram of the non- $\mathbf{Z}_3$ -symmetric Y3J to derive the phase diagram of the  $N = 2$  junction for  $K_\sigma > 1$ , a range of values of the system's parameters which was not discussed in Ref. [18].

##### 4.1. From the $N = 2$ junction with a topological superconductor to the Y-junction

We now consider the asymmetric Y3J with  $K$  and  $K_3$  set so that  $V_{1,2}$ , defined in Eq. (23), becomes irrelevant, while  $V_{2,3}, V_{3,1}$  both stay relevant, that is, so that  $d_{V_{1,2}} = \frac{1}{K} > 1$ , while  $d_{V_{2,3}} = d_{V_{3,1}} = \frac{1}{2K} + \frac{1}{2K_3} < 1$  (which amounts to choosing  $r$  so that  $r^{-1} < 2K - 1$ ). For the asymmetric Y3J, the boundary coupling flow is determined by the perturbative RG Eqs. (D.23). Since  $V_{1,2}$  is irrelevant,  $\bar{t}_{2,1}$  expected to renormalize to 0 for  $D_0/D \rightarrow \infty$  and, as a result, one may recover

the phase diagram of the Y3J in this regime by restricting the analysis to the plane  $\bar{t}_{2,1} = 0$  in parameter space. Setting  $\bar{t}_{2,1} = 0$  in the second- and in the third ones of Eqs. (D.23), we obtain the system of two coupled RG equations given by

$$\begin{aligned}\frac{d\bar{t}_{3,2}}{d\ln(D_0/D)} &= \left(1 - \frac{1}{2K} - \frac{1}{2rK}\right)\bar{t}_{3,2} - \mathcal{B}\left[\frac{1}{2K} + \frac{1}{2rK}\right](\bar{t}_{3,2})^3 - C\left[\frac{1}{K}, \frac{1}{rK}\right]\bar{t}_{3,2}(\bar{t}_{1,3})^2 \\ \frac{d\bar{t}_{1,3}}{d\ln(D_0/D)} &= \left(1 - \frac{1}{2K} - \frac{1}{2rK}\right)\bar{t}_{1,3} - \mathcal{B}\left[\frac{1}{2K} + \frac{1}{2rK}\right](\bar{t}_{1,3})^3 - C\left[\frac{1}{K}, \frac{1}{rK}\right]\bar{t}_{1,3}(\bar{t}_{3,2})^2\end{aligned}\quad (33)$$

Remarkably, Eqs. (33) can now be consistently dealt with within the  $\epsilon$ -expansion method, by setting  $\frac{1}{2K} + \frac{1}{2rK} = 1 - \epsilon$ , with  $0 < \epsilon \ll 1$ . Expanding to linear order in  $\epsilon$  and neglecting subleading contributions (in  $\epsilon$ ) to nonlinear terms in the  $\hat{\beta}$ -functions, according to Eqs. (33) and to the definition of the function  $\mathcal{B}$  in Eq. (D.21), which implies that terms  $\propto \mathcal{B}$  at the right-hand side of Eqs. (33) are all  $\propto \epsilon$ , we trade Eqs. (33) for the system

$$\begin{aligned}\frac{d\bar{t}_{3,2}}{d\ln(D_0/D)} &= \epsilon\bar{t}_{3,2} - \mathcal{F}\left(2 - \frac{1}{K}\right)\bar{t}_{3,2}(\bar{t}_{1,3})^2 \\ \frac{d\bar{t}_{1,3}}{d\ln(D_0/D)} &= \epsilon\bar{t}_{1,3} - \mathcal{F}\left(2 - \frac{1}{K}\right)\bar{t}_{1,3}(\bar{t}_{3,2})^2\end{aligned}\quad (34)$$

where  $\mathcal{F}$  is defined in Eq. (D.7). Apparently, Eqs. (34) correspond to the perturbative RG equations of an  $N = 2$  junction with  $\frac{1}{4K_p} + \frac{1}{4K_r} = 1 - \epsilon$  and  $\frac{1}{2K_p} - \frac{1}{2K_r} = 2 - \frac{1}{K}$ . The correspondence is clearly not accidental. Indeed, on performing the canonical transformations

$$\begin{aligned}\bar{\phi}_{1,2}(x) &= \sqrt{K}\phi_{1,2}(x) \quad , \quad \bar{\theta}_{1,2}(x) = \theta_{1,2}(x)/\sqrt{K} \\ \bar{\phi}_3(x) &= \sqrt{K_3}\phi_3(x) \quad , \quad \bar{\theta}_3(x) = \theta_3(x)/\sqrt{K_3}\end{aligned}\quad (35)$$

followed by the rotation

$$\begin{bmatrix} \hat{\phi}_\sigma(x) \\ \hat{\phi}_\rho(x) \\ \hat{\phi}_\chi(x) \end{bmatrix} = \begin{bmatrix} -\frac{1}{\sqrt{2}} & \frac{1}{\sqrt{2}} & 0 \\ \frac{1/\sqrt{K}}{\sqrt{2/K+4/K_3}} & \frac{1/\sqrt{K}}{\sqrt{2/K+4/K_3}} & \frac{-2/\sqrt{K_3}}{\sqrt{2/K+4/K_3}} \\ \frac{1/\sqrt{K_3}}{\sqrt{1/K+2/K_3}} & \frac{1/\sqrt{K_3}}{\sqrt{1/K+2/K_3}} & \frac{1/\sqrt{K}}{\sqrt{1/K+2/K_3}} \end{bmatrix} \begin{bmatrix} \bar{\phi}_1(x) \\ \bar{\phi}_2(x) \\ \bar{\phi}_3(x) \end{bmatrix}\quad (36)$$

and analogous rotation from  $\{\bar{\theta}_1(x), \bar{\theta}_2(x), \bar{\theta}_3(x)\}$  to  $\{\hat{\theta}_\sigma(x), \hat{\theta}_\rho(x), \hat{\theta}_\chi(x)\}$ , one obtains, for the bulk Hamiltonian

$$H_{\text{Bulk}} = \frac{u}{2} \sum_{a=r,c,\chi} \int_0^\ell dx \{(\partial_x \hat{\phi}_a(x))^2 + (\partial_x \hat{\theta}_a(x))^2\}\quad (37)$$

Once  $\bar{t}_{2,1}$  is set to 0 in the boundary Hamiltonian (which corresponds to dropping the term  $\propto V_{1,2}$  in Eq.(23)),  $H_b$  becomes

$$\begin{aligned}
H_b = & t_{3,2}\Gamma_2\Gamma_3 \exp \left\{ -i \sqrt{\frac{\pi}{2}} \left[ \frac{1}{\sqrt{K}} \hat{\phi}_\sigma(0) + \sqrt{\frac{1}{K} + \frac{2}{K_3}} \hat{\phi}_\rho(0) \right] \right\} \\
& + t_{1,3}\Gamma_3\Gamma_1 \exp \left\{ -i \sqrt{\frac{\pi}{2}} \left[ \frac{1}{\sqrt{K}} \hat{\phi}_\sigma(0) - \sqrt{\frac{1}{K} + \frac{2}{K_3}} \hat{\phi}_\rho(0) \right] \right\} + \text{h.c.} \quad . \quad (38)
\end{aligned}$$

Apparently,  $\hat{\phi}_\chi(x), \hat{\theta}_\chi(x)$  fully decouple from  $H_b$  in Eq. (38). Moreover, shifting  $\hat{\phi}_\rho(x)$  by a constant, so that  $\sqrt{\frac{\pi}{2}} \sqrt{\frac{1}{K} + \frac{2}{K_3}} \hat{\phi}_\rho(0) \rightarrow \sqrt{\frac{\pi}{2}} \sqrt{\frac{1}{K} + \frac{2}{K_3}} \hat{\phi}_\rho(0) + \frac{\pi}{2}$ , one obtains

$$\begin{aligned}
H_b \rightarrow & -2it_{3,2}\Gamma_2\Gamma_3 \cos \left\{ \sqrt{\frac{\pi}{2}} \left[ \frac{1}{\sqrt{K}} \hat{\phi}_\sigma(0) + \sqrt{\frac{1}{K} + \frac{2}{K_3}} \hat{\phi}_\rho(0) \right] \right\} \\
& + 2it_{1,3}\Gamma_3\Gamma_1 \cos \left\{ \sqrt{\frac{\pi}{2}} \left[ \frac{1}{\sqrt{K}} \hat{\phi}_\sigma(0) - \sqrt{\frac{1}{K} + \frac{2}{K_3}} \hat{\phi}_\rho(0) \right] \right\} \quad . \quad (39)
\end{aligned}$$

Finally, performing the reverse canonical rescaling given by

$$\begin{aligned}
\phi_\rho(x) = & \sqrt{\frac{1}{K} + \frac{2}{K_3}} \hat{\phi}_\rho(x) \quad , \quad \phi_\sigma(x) = \frac{1}{\sqrt{K}} \hat{\phi}_\sigma(x) \\
\theta_\rho(x) = & \hat{\theta}_\rho(x) / \left[ \sqrt{\frac{1}{K} + \frac{2}{K_3}} \right] \quad , \quad \theta_\sigma(x) = \sqrt{K} \hat{\theta}_\sigma(x) \quad , \quad (40)
\end{aligned}$$

and setting  $\Gamma_3 \rightarrow \gamma_L$ , we recover the Hamiltonian for the  $N = 2$  junction with a topological superconductor, with Luttinger parameters given by

$$\begin{aligned}
K_\rho = & \frac{KK_3}{(K_3 + 2K)} \\
K_\sigma = & K (< 1) \quad . \quad (41)
\end{aligned}$$

Besides the mapping procedure involving  $H_b$ , to further ground the correspondence we now extend it to all the allowed boundary operators in the Y3J and in the  $N = 2$  junction, at each fixed point in the boundary phase diagram of the two systems that we discuss in section 3.

Starting with the disconnected fixed point, due to the condition  $K < 1$ , the only relevant allowed boundary operators are  $V_{2,3}$  and  $V_{3,1}$  entering  $H_b$  in Eq.(38). Consistently with their scaling dimensions, these are identified with the operators at the second and third line of the table in appendix A.a of Ref. [42]. Another operator, which is irrelevant due to our choice of the system parameter, is the boundary operator  $V_{1,2}$  of the asymmetric Y3J, with scaling dimension  $1/K$ . Referring to the table in appendix A.a of Ref. [42], it apparently corresponds to any of the operators listed at the first line, taken at the disconnected fixed point. According to the analysis of section 3.1, its counterpart in the  $N = 2$  junction is the normal boundary backscattering operator  $V_{\text{Normal},(1,2)}$ , with scaling dimension  $1/K_\sigma = 1/K$ . Additional boundary operators can potentially appear in the Y3J, which are quartic in the fermionic fields of the Y3J such as, for instance (in the notation of Ref. [42])  $T = T_{31}^{LR} T_{32}^{RL}$ . Quartic operators do not appear in the table in appendix

A.a of Ref. [42], which only contains quadratic operators: to make them relevant a strong, bulk inter-channel attractive interaction is required, which we exclude here, as we only focus on repulsive, inter-channel bulk interactions. Yet, to complete the correspondence with the  $N = 2$  junction, we see that  $T$  is the second boundary operator that must be identified with the boundary pairing operator of the  $N = 2$  junction,  $V_{\text{Pair},(1,2)}$ , with scaling dimension  $1/K_\rho$ .

Moving to the  $A \otimes N$  and to the  $N \otimes A$  fixed points of the  $N = 2$  junction [18], based on the analysis of section 3, we naturally identify them with respectively the  $A_1$ - and the  $A_2$ -asymmetric fixed point of the Y3J. To further corroborate our identification, we now show that it is realized as a one-to-one correspondence between boundary operators in the two systems. Here, we only discuss the correspondence between the  $A \otimes N$  and the  $A_1$  fixed point. The complementary one can be readily recovered by symmetry. At the  $A \otimes N$  fixed point of the  $N = 2$  junction, the first pair of allowed boundary operators corresponds to boundary inter-channel backscattering/pairing between channels 1 and 2. The corresponding operators are realized as a linear combination of  $V_{a,(1,2)}$ ,  $V_{b,(1,2)}$ , respectively given by

$$\begin{aligned} V_{a,(1,2)} &= \Gamma_1 \Gamma_2 e^{i\sqrt{\pi}[\phi_2(0) - \theta_1(0)]} = \Gamma_1 \Gamma_2 e^{i\sqrt{\frac{\pi}{2}}[\phi_\rho(0) - \phi_\sigma(0) - \theta_\rho(0) - \theta_\sigma(0)]} \\ V_{b,(1,2)} &= \Gamma_1 \Gamma_2 e^{i\sqrt{\pi}[\phi_2(0) + \theta_1(0)]} = \Gamma_1 \Gamma_2 e^{i\sqrt{\frac{\pi}{2}}[\phi_\rho(0) - \phi_\sigma(0) + \theta_\rho(0) + \theta_\sigma(0)]} \quad , \end{aligned} \quad (42)$$

plus their Hermitean conjugates. (Note that, due to the boundary conditions at the  $A \otimes N$  fixed point,  $V_{a,(1,2)}$  and  $V_{b,(1,2)}$  do no more correspond respectively to normal boundary scattering and to boundary pairing, as they instead do at the disconnected fixed point – see the discussion after Eq.(12) in sub-section 3.1. Instead, as we state above, normal boundary scattering and boundary pairing operators are realized as linear combinations of the two of them.) Inverting the transformations above to get back to the fields of the Y3J, it is not difficult to check that the operators in Eqs. (42) respectively correspond to the  $T_{21}^{RL}$ - and to the  $T_{21}^{RR}$ -operators at the  $A_1$  fixed point of the asymmetric Y3J, plus their Hermitean conjugates (see appendix A.d of Ref. [42]). This is further confirmed by the observation that, using the results of section 3 for the  $N = 2$  junction, the scaling dimension of the operators in Eqs. (42) are the same and are given by  $d_{a,(1,2)} = d_{b,(1,2)} = \frac{1+K_\sigma K_\rho}{K_\sigma + K_\rho} = \frac{2K+K_3+K_3 K^2}{2(K+K_3)K}$ , which is the correct result for the  $T_{21}^{RL}$ - and for the  $T_{21}^{RR}$ -operators at the  $A_1$  fixed point of the Y3J [42].

A second class of boundary operators at the  $A \otimes N$  fixed point corresponds to intra-channel 1 normal backscattering processes, that is, to the operator

$$V_{\text{Intra},1} \propto \cos[\sqrt{2\pi}(\theta_\rho(0) + \theta_\sigma(0))] \quad . \quad (43)$$

Considering that  $\hat{\phi}_\chi(x)$ ,  $\hat{\theta}_\chi(x)$  are fully decoupled from  $H_b$ , it is natural to assume that, throughout the whole phase diagram of the system,  $\hat{\theta}_\chi(x)$  is pinned at  $x = 0$ . As a result, going again backwards along the sequence of transformations discussed above, we express  $V_{\text{Intra},1}$  in terms of the fields of the Y3J at  $x = 0$  as

$$V_{\text{Intra},1} \propto \cos[2\sqrt{\pi}\theta_2(0)] \quad . \quad (44)$$

The right hand side of Eq. (44) corresponds to the  $T_{22}^{RL}$ -operator at the second line of the table at appendix A.d of Ref. [42] (plus its Hermitean conjugate), as witnessed by the perfect agreement

between the scaling dimension of that operator and the result of section 3 for the dimension of  $V_{\text{Intra},1}$ ,  $d_{\text{Intra},1} = \frac{2K_3}{K+K_3}$ .

Finally, in the  $N = 2$  junction one has the residual coupling of channel-2 to the MM. When properly accounting for the ‘‘Schrödinger cat’’ nature of the state formed out of the hybridization between the MM and the KF  $\Gamma_1$ , one obtains, as corresponding boundary operator,  $V_{2,\text{Res}}$  given by [18]

$$V_{2,\text{Res}} \propto \cos[\sqrt{2\pi}(\phi_\rho(0) - \phi_\sigma(0))] \quad . \quad (45)$$

Again, just as for the other operators listed above, one can readily check that the right-hand side of Eq. (45) corresponds to the operator  $T_{21}^{RL}[T_{12}^{RL}]^\dagger$  at the third line of the table in appendix A.d of Ref. [42] (plus its Hermitean conjugate), consistent with the result for the scaling dimension of  $V_{2,\text{Res}}$  we derived in section 3,  $d_{2,\text{Res}} = \frac{4}{K_\rho + K_\sigma} = \frac{2(2K+K_3)}{K(K+K_3)}$ .

The  $A \otimes A$  fixed point of the  $N = 2$  junction corresponds to pinning both  $\phi_\rho(x)$  and  $\phi_\sigma(x)$  at  $x = 0$ . Accordingly, one naturally identifies it with the  $D_P$  fixed point of the Y3J. To double-check the identification between the two fixed point, we note that the leading boundary operators at the  $A \otimes A$  fixed point of the  $N = 2$  junction corresponds to the  $V_{b,(1,2)}$  operator at the second line of Eq. (16), as well as  $\tilde{V}_{\text{Res},1}$  and  $\tilde{V}_{\text{Res},2}$  in Eqs. (17). Following the correspondence between the parameters of the  $N = 2$  junction and the ones of the Y3J, one finds that the corresponding scaling dimensions are given by

$$\begin{aligned} d_{b,(1,2)} &= K_\rho = K \left[ \frac{K_3}{2K + K_3} \right] \\ d_{\text{Res},1} = d_{\text{Res},2} &= \frac{K_\rho + K_\sigma}{4} = K \left[ \frac{K + K_3}{2(2K + K_3)} \right] \quad . \end{aligned} \quad (46)$$

A comparison of the results in Eqs. (46) with the table at appendix A.b of Ref. [42] again supports the identification of  $A \otimes A$  with the  $D_P$  fixed point in the Y3J. (Note that, according to Eqs. (46),  $A \otimes A$  becomes a stable fixed point as soon as the conditions  $d_{b,(1,2)} > 1$  and  $d_{\text{Res},1} > 1$  are both satisfied. This may clearly happen only for  $K_\sigma > 1$ , without contradicting the conclusions of Ref. [18] and of section 3.1, which were reached under the assumption that  $K_\sigma < 1$ ).

In view of the perfect correspondence of the  $N = 2$  junction and the asymmetric Y3J with  $K < 1$ ,  $2K > 1 + K/K_3$ , one naturally concludes that an analog of the FCFP found in the  $N = 2$  junction along the symmetric line  $\bar{t}_2 = \bar{t}_3$  exists in the phase diagram of the Y3J, as well. In particular, we infer that, for  $K < 1$ ,  $2K > 1 + K/K_3$  the stable fixed point of the Y3J is either the  $A_1$  or the  $A_2$  asymmetric fixed point of Ref. [42], depending on whether, at the reference scale,  $\bar{t}_{3,2} > \bar{t}_{1,3}$ , or  $\bar{t}_{3,2} < \bar{t}_{1,3}$ , or the FCFP of the  $N = 2$  junction located, according to the analysis of Ref. [18], at  $\bar{t}_{3,2,*} = \bar{t}_{1,3,*} = \epsilon/\mathcal{F}(2 - K^{-1})$ .

Before concluding this sub-section, two remarks are in order. First of all, we would like to stress that the condition  $K < 1$ , which we have assumed at the start of the discussion here, has the mere effect of making  $V_{1,2}$  irrelevant, thus allowing for dropping terms  $\propto \bar{t}_1$  from the following discussion. In fact, this condition can be relaxed and one can extend all the conclusions we derive here to the case  $K > 1$ , as well, but only provided  $\bar{t}_1$  is fine-tuned to 0 from the very beginning, and remains =0 along the RG trajectories. Secondly, we would like to emphasize that, in order to

make the mapping effective, we identified one of the three KF's, specifically  $\Gamma_3$ , with the MM  $\gamma_L$  emerging at the  $N = 2$  junction with a topological superconductor. This points out, once more, that, to make a comprehensive discussion of the physics of real fermions at junctions of one-dimensional interacting electronic systems and/or topological superconductors, KF's and MM's have to be considered altogether as actual degrees of freedom, despite the apparent conventional definition of the former ones as a mere mathematical means to properly follow the bosonization procedure.

#### 4.2. From the Y-junction to the $N = 2$ junction with a topological superconductor

In the previous section we used the known results about the  $N = 2$  junction [18] to infer the emergence of a planar FCFP in the phase diagram of the asymmetric Y3J for  $K < 1$ ,  $\frac{1}{2K} + \frac{1}{2K_3} < 1$ . Nevertheless, the identification of  $K$  with the Luttinger parameter  $K_\sigma$  of the  $N = 2$  junction makes it impossible to directly extend the correspondence to the case  $K > 1$ . In fact, the analysis of Ref. [18] is limited to the regime  $K_\sigma < 1$ . For  $K_\sigma > 1$ , two key things happen. First, the identification of the argument  $\nu$  of the  $\mathcal{F}$ -function in the perturbative RG Eqs. (34) with  $2 - K^{-1}$  implies that  $\nu > 1$  for  $K > 1$ . For  $\nu > 1$ ,  $\mathcal{F}(\nu) < 0$ , with the corresponding disappearance of the FCFP along the diagonal in the  $\bar{t}_{3,2} - \bar{t}_{1,3}$ -plane. Second, DEBC method shows the emergence of a relevant operator at the  $A \otimes N$ , as well as at the  $N \otimes A$ , fixed point, given by the inter-channel normal backscattering operator,  $V_{\text{Normal,(1,2)}}$ , which implies that, unless one fine-tunes to 0 the coupling strength in front of  $V_{\text{Normal,(1,2)}}$ , neither  $A \otimes N$ , nor  $N \otimes A$ , are stable fixed points anymore. To figure out what the phase diagram of the  $N = 2$  junction looks like for  $K_\sigma > 1$ , in this section we reformulate the correspondence with the Y3J, but this time to retrieve informations about the  $N = 2$  junction from what is known about the phase diagram of the asymmetric Y3J.

To begin with, we refer to the disconnected fixed point. There, as stated above, for  $K_\sigma > 1$ , the leading boundary operators for the  $N = 2$  junction are the couplings of the two wires to the MM,  $V_{b,1(2)}$ , and the inter-channel normal backscattering operator,  $V_{\text{Normal,(1,2)}}$ , given by

$$\begin{aligned} V_{b,1} &= 2it_1 \gamma_L \Gamma_1 \cos[\sqrt{\pi}\phi_1(0)] \\ V_{b,2} &= 2it_2 \gamma_L \Gamma_1 \cos[\sqrt{\pi}\phi_2(0)] \\ V_{\text{Normal,(1,2)}} &= v_{1,2} \Gamma_1 \Gamma_2 e^{i\sqrt{\pi}[\phi_1(0) - \phi_2(0)]} + \text{h.c.} \quad , \end{aligned} \quad (47)$$

of scaling dimensions respectively given by  $d_{b,1} = d_{b,2} = \frac{1}{4K_\rho} + \frac{1}{4K_\sigma}$ ,  $d_{\text{Normal,(1,2)}} = \frac{1}{K_\sigma}$ . At a given  $U$ , the condition  $K_\sigma > 1$  is recovered by setting  $\frac{1}{2} < K < K_*(U)$ , with

$$K_*(U) = -\frac{U}{2\pi u} + \sqrt{1 + \left(\frac{U}{2\pi u}\right)^2} \leq 1 \quad . \quad (48)$$

Thus, we conclude that, for  $\frac{1}{2} < K < K_*(U)$ , the disconnected fixed point is unstable, with three allowed independent relevant boundary operators.

Moving to the  $A \otimes N$  fixed point (and/or to the complementary  $N \otimes A$  fixed point), we see that, referring to the operators  $V_{a,(1,2)}$ ,  $V_{b,(1,2)}$ , their scaling dimension can be rewritten as

$$d_{a,(1,2)} = d_{b,(1,2)} = \frac{1 + K_\sigma K_\rho}{K_\sigma + K_\rho} = 1 + \frac{(1 - K_\sigma)(1 - K_\rho)}{K_\sigma + K_\rho} \quad , \quad (49)$$

which is clearly  $< 1$  for  $K_\sigma > 1, K_\rho < 1$ . Therefore, we conclude that both inter-channel normal boundary backscattering, as well as boundary pairing, provide relevant perturbations at the  $A \otimes N$  fixed point, as soon as  $K_\sigma > 1$ .

Finally, we readily see that the  $A \otimes A$  fixed point is not stable either, as a relevant boundary perturbation is provided by the operator  $V_{b,(1,2)}$  of Eq. (16), with scaling dimension  $K_\rho < 1$ . To get some insight on the phase diagram of the  $N = 2$  junction for  $K_\sigma > 1$ , we now employ the correspondence with the Y3J. In order to do so, we start by assuming, for the time being, that  $V_{b,1}, V_{b,2}$  and  $V_{\text{Normal},(1,2)}$  all have the same scaling dimension, that is,  $d_b = d_{\text{Normal},(1,2)}$ . At  $N = 2$ , this condition requires

$$\frac{1}{4K_\rho} = \frac{3}{4K_\sigma} \Rightarrow \frac{KU}{\pi u} = \frac{4}{5} . \quad (50)$$

Let  $\hat{K}(U)$  be the value of  $K$  that satisfies Eq. (50) at given  $U$ . We obtain  $\frac{\hat{K}(U)U}{\pi u} = \frac{4}{5}$  and, in addition, due to the assumption of a repulsive intra-wire interaction, which implies  $\frac{1}{2} < \hat{K}_2(U) < 1$ , we also get  $\frac{1}{\sqrt{5}} < d_b < \frac{2}{\sqrt{5}}$ . At  $K = \hat{K}(U)$ , one obtains  $K_\rho = \hat{K}(U) \left[ \frac{\sqrt{5}}{3} \right]$  and  $K_\sigma = \hat{K}(U) \sqrt{5}$ , that is,  $K_\rho = K_\sigma/3$ , and  $u_\rho = u_\sigma \frac{K_\sigma}{K_\rho} = 3u_\sigma$ . Accordingly,  $H_{2,\text{Bulk}}$  now takes the form

$$H_{2,\text{Bulk}} = \frac{u_\sigma}{2} \int_0^\ell dx \left\{ K_\sigma [(\partial_x \phi_\rho(x))^2 + (\partial_x \phi_\sigma(x))^2] + K_\sigma^{-1} [9(\partial_x \theta_\rho(x))^2 + (\partial_x \theta_\sigma(x))^2] \right\} . \quad (51)$$

In deriving the boundary phase diagram one has to work on the semi-infinite system. Thus, the upper integration bound ( $\ell$ ) in the integrals at the right-hand side of Eq. (51) must be sent to  $\infty$ . Taking this into account, we now perform the canonical transformation

$$\begin{aligned} \Phi(x) &= \phi_\rho(x)/\sqrt{3} \quad , \quad \Theta(x) = \sqrt{3}\theta_\rho(x) \\ \varphi(x) &= \phi_\sigma(x) \quad , \quad \vartheta(x) = \theta_\sigma(x) \quad , \end{aligned} \quad (52)$$

followed by a rescaling by  $\sqrt{3}$  of the  $x$  coordinate in the integrals involving the center-of-mass fields. As a result, Eq. (51) becomes

$$H_{2,\text{Bulk}} = \frac{u_\sigma}{2} \int_0^\ell dx \left\{ K_\sigma [(\partial_x \Phi(x))^2 + (\partial_x \varphi(x))^2] + K_\sigma^{-1} [(\partial_x \Theta(x))^2 + (\partial_x \vartheta(x))^2] \right\} , \quad (53)$$

while, upon also redefining the field  $\Phi(x)$  according to  $\sqrt{3}\Phi(x) \rightarrow \sqrt{3}\Phi(x) + \sqrt{\frac{\pi}{2}}$ , the most general boundary interaction at the disconnected fixed point,  $\hat{H}_b$ , can be written as a linear combination of  $V_{b,1}, V_{b,2}$  and  $V_{\text{Normal},(1,2)}$  as

$$\begin{aligned} \hat{H}_b \rightarrow & -2it_1\gamma_L\Gamma_1 \sin \left[ \sqrt{\frac{\pi}{2}} (-\varphi(0) - \sqrt{3}\Phi(0)) \right] - 2it_2\Gamma_2\gamma_L \sin \left[ \sqrt{\frac{\pi}{2}} (-\varphi(0) + \sqrt{3}\Phi(0)) \right] \\ & - 2iv_{1,2}\Gamma_1\Gamma_2 \sin[ \sqrt{2\pi}\varphi(0) ] . \end{aligned} \quad (54)$$

The right-hand side of Eq. (54) corresponds to the boundary Hamiltonian of a Y3J with relative fields  $\varphi(x), \Phi(x)$ , boundary couplings  $t_1, t_2, v_{1,2}$  and Luttinger parameters  $K = K_3 = K_\sigma$ . In section

3.2, we argue that, as soon as all three of the boundary couplings are  $\neq 0$ , for  $1 < K_\sigma < 3$  (as is the case here), the system flows towards the  $\mathbf{Z}_3$ -symmetric  $M$ -FCFP of the symmetric Y3J [2]. Thus, we conclude that, for  $K_\sigma > 1$ , as soon as  $v_{1,2} \neq 0$ , the stable fixed point of the  $N = 2$  junction is realized outside of the  $t_1 - t_2$ -plane. It sets in at a finite value of the three boundary couplings  $\bar{t}_1 = \bar{t}_2 = v_{1,2} = t_*$ , with  $t_*$  corresponding to the  $M$ -FCFP of the  $\mathbf{Z}_3$ -symmetric Y3J with Luttinger parameter  $K = K_\sigma$ . The  $M$ -FCFP is the endpoint of RG flow lines that, were  $v_{1,2} = 0$ , would instead end up at the  $A \otimes A$  fixed point of the  $N = 2$  junction.

To complete our derivation, we now discuss the phase diagram of the  $N = 2$  junction when  $K_\rho = \lambda K_\sigma / 3$ , with  $\lambda \neq 1$ , and  $K_\sigma > 1$ . In this case, going backwards along the mapping we derived in section 4.1, we see that the  $N = 2$  junction maps onto the (bulk) asymmetric Y3J we review in section 3.2, with  $K = K_\sigma$  and  $K_3 = \left(\frac{2\lambda}{3-\lambda}\right)K$ . Accordingly, one obtains for the scaling dimensions  $d_{b,1} = d_{b,2} = \frac{1}{4K_\sigma} \left(1 + \frac{3}{\lambda}\right)$ . This implies  $d_{b,1} > (<)d_{\text{Normal},(1,2)}$  depending on whether  $\lambda < 1$  ( $\lambda > 1$ ). Apparently, the difference between  $d_{b,1(2)}$  and  $d_{\text{Normal},(1,2)}$  could, in principle, trigger RG trajectories either towards an  $A_a$ -asymmetric fixed point, or towards an asymmetric version of the  $M$ -FCFP. As a function of  $\lambda$  and of  $K_\sigma$ , one obtains for the scaling dimensions of the relevant boundary operators at the  $A_3$  and at the  $A_1, A_2$  fixed points of the corresponding Y3J the expressions

$$\begin{aligned} d_{A_3}(\lambda, K_\sigma) &= \frac{3 + \lambda K_\sigma^2}{4\lambda K_\sigma} \\ d_{A_1}(\lambda, K_\sigma) &= d_{A_2}(\lambda, K_\sigma) = \frac{3 + \lambda K_\sigma^2}{(3 + \lambda)K_\sigma} \end{aligned} \quad (55)$$

Given the assumption  $K_\sigma > 1$ , based on the discussion of sections 3.1,3.2, in the following, referring to the fixed points of the Y3J, we assume that the stable fixed point has to be identified with  $A_3$  if  $d_{A_3}(\lambda, K_\sigma) > 1, d_{A_1}(\lambda, K_\sigma) < 1$ , with either one of  $A_1$ , or  $A_2$  (or with a planar FCFP) if  $d_{A_3}(\lambda, K_\sigma) < 1, d_{A_1}(\lambda, K_\sigma) > 1$ , with the  $D_P$  fixed point if  $d_{A_3}(\lambda, K_\sigma) > 1, d_{A_1}(\lambda, K_\sigma) > 1$  and, finally, with the  $M$ -FCFP if  $d_{A_3}(\lambda, K_\sigma) < 1, d_{A_1}(\lambda, K_\sigma) < 1$ . Eventually, from the correspondence rules of section 4.1, we make the appropriate identifications with the fixed points of the  $N = 2$  junction. A straightforward algebraic derivation leads us to conclude that, depending on whether  $\lambda > 1$ , or  $\lambda < 1$ , there is the possibility of stabilizing either the  $A_3$ , or the  $A_1, A_2$  fixed points. In particular, without considering additional constraints on the various parameters, one would obtain

- $\lambda > 1$ :

In this case, for  $K_\sigma < \frac{3}{4} + \frac{9}{4\lambda^2}$  the stable fixed point corresponds to the  $M$ -FCFP of the Y3J. For  $\frac{3}{4} + \frac{9}{4\lambda^2} < K_\sigma < 6 - \frac{3}{\lambda}$  the stable fixed point would correspond to either the  $A_1$  or the  $A_2$  fixed point and, for  $K_\sigma > 6 - \frac{3}{\lambda}$ , to the  $D_P$  fixed point. However, these last two possibilities are ruled out by the observation that, by definition, one has  $K_\sigma = \frac{3}{\lambda}K_\rho < \frac{3}{\lambda}$ . Therefore, one obtains that  $\frac{3}{4} + \frac{9}{4\lambda^2} < K_\sigma \Rightarrow \frac{1}{3} < \lambda < 1$ , against the initial assumption. As a result, for  $\lambda > 1$  only the  $M$ -FCFP of the Y3J corresponds to a stable fixed point of the  $N = 2$  junction.

- $\lambda < 1$ :

In this case, the  $M$ -FCFP of the Y3J corresponds to the stable phase of the system for  $K_\sigma < 6 - \frac{3}{\lambda}$ . For  $6 - \frac{3}{\lambda} < K_\sigma < \frac{3}{4} + \frac{9}{4\lambda^2}$  the stable fixed point corresponds to the  $A_3$  fixed

point. For  $K_\sigma > \frac{3}{4} + \frac{9}{4\lambda^2}$ ,  $D_P$  would become the stable fixed point. Again, we rule out this last possibility, due to the observation that, by definition,  $K_\sigma^{-2} + K_\rho^{-2} = 2(K_j)^{-2}$  where, to avoid confusion, we here use  $K_j$  to mean the Luttinger parameter of each QW in the  $N = 2$  junction in the absence of bulk, inter-wire interaction. At this stage, we are assuming, just as in Ref. [18],  $\frac{1}{2} < K_j < 1$  (later on we discuss an extension of our analysis to  $K_j > 1$  in the absence of inter-wire interaction). As a result, we find the condition  $\frac{9}{4\lambda^2} = \frac{K_\sigma^2}{2K_\rho^2} - \frac{1}{4} < 2K_\sigma^2 - \frac{1}{4}$ .

Taking this into account, we see that  $K_\sigma > \frac{3}{4} + \frac{9}{4\lambda^2} \Rightarrow 2\left(K_\sigma - \frac{1}{2}\right)^2 < 0$ , clearly impossible. Therefore, the only allowed phase transition happens for  $6 - \frac{3}{\lambda} = K_\sigma$ , where the stable fixed point of the system changes from the  $M$ -FCFP of the Y3J (for  $K_\sigma < 6 - \frac{3}{\lambda}$ ) to the  $A_3$  fixed point (for  $K_\sigma > 6 - \frac{3}{\lambda}$ ).

In terms of the parameters of the  $N = 2$  junction, such a fixed point corresponding to setting  $\bar{v}_{1,2} \rightarrow \infty$ , and  $\bar{t}_1 = \bar{t}_2 = 0$ . Accordingly, we see that it corresponds to the perfect healing of the junction between wires-1 and -2, with the MM decoupled from the two wires. To double-check its stability, we resort to DEBC-approach, by imposing type  $N$  boundary conditions on  $\Phi(x)$ ,  $\vartheta(x)$  at  $x = 0$  and, accordingly, type  $A$  boundary conditions on  $\varphi(x)$ ,  $\Theta(x)$ . In this case, the leading boundary perturbation is indeed realized as a linear combination of the  $V_{b,1}$  and  $V_{b,2}$ -operators in Eqs. (47), that is, by the hybridization between the normal wires and the MM, which now take the form

$$\begin{aligned} V_{b,1} &\rightarrow it_1\gamma_L\Gamma_1 e^{i\frac{\sqrt{x}}{2}[\sqrt{3}\Phi(0)\pm\vartheta(0)]} + \text{h.c.} \\ V_{b,2} &\rightarrow it_2\gamma_L\Gamma_2 e^{i\frac{\sqrt{x}}{2}[\sqrt{3}\Phi(0)\pm\vartheta(0)]} + \text{h.c.} \end{aligned} \quad , \quad (56)$$

both with scaling dimension  $d_b = \frac{3+\lambda K_\sigma^2}{4\lambda K_\sigma} > 1$ . Therefore, we conclude that, as soon as  $K_\sigma > 6 - \frac{3}{\lambda}$ , the system is attracted towards the  $A_3$ -like fixed point, in which the MM is ‘‘pushed out’’ of the quantum wires, which hybridize with each other to an effectively uniform wire, out of which lies the decoupled MM.

In conclusion, we have shown that the condition  $K_\sigma > 1$  is enough to reverse the phase diagram of the junction between two quantum wires and a topological superconductor, with respect to the result derived in Ref. [18] for  $K_\sigma < 1$ . Specifically, at  $K_\sigma > 1$ , the FCFP corresponds to the true stable phase of the system and is eventually identified with the (in general non- $\mathbf{Z}_3$ -symmetric)  $M$ -FCFP of the Y3J. Further increasing  $K_\sigma$  with respect to  $K_\rho$  may eventually trigger an additional phase transition towards a phase corresponding to the perfect healing of the junction between wires-1 and -2, with the MM decoupled from the two wires. To evidence the new phases we find in the  $N = 2$  junction by means of the correspondence with the Y3J, in Fig. 1 we draw the phase diagram of the  $N = 2$  junction for  $K_\rho < 1$  by including, in addition to what we found in Ref. [18] for  $K_\sigma < 1$ , the phases emerging when the parameter  $K_\sigma$  is  $> 1$ .

Before concluding this sub-section, it is worth remarking how the correspondence between the  $N = 2$  junction and the Y3J also allows for inferring the phase diagram of the former system in the case of zero inter-wire bulk interaction ( $U = 0$ ), and attractive intra-wire interaction ( $K > 1$ ). To do so, we first of all note that  $U = 0$  implies  $K_\rho = K_\sigma = K$ . From Eqs.(41), one sees that this condition is recovered in the  $\frac{K_3}{K} \rightarrow \infty$  limit, which yields  $K_\rho = K_\sigma = K$ . Accordingly,

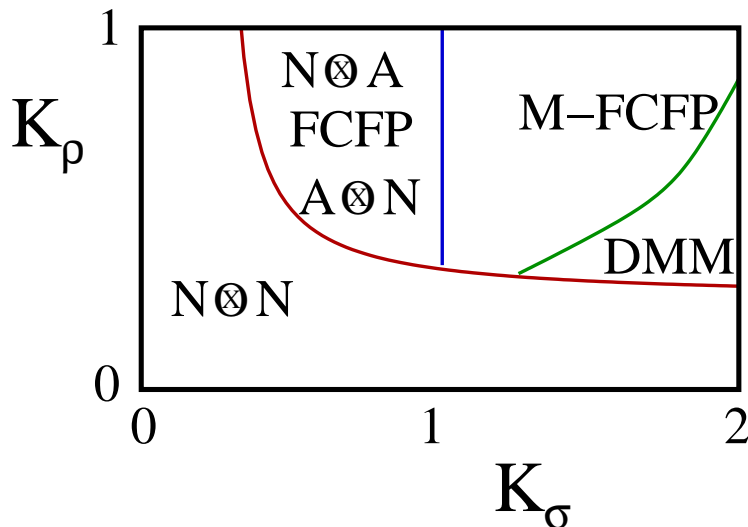


Figure 1: Sketch of the phase diagram of the  $N = 2$  junction for  $K_\rho < 1$ . The red curve corresponds to  $\frac{1}{4K_\rho} + \frac{1}{4K_\sigma} = 1$ : it separates the phase corresponding to the disconnected fixed point ( $\frac{1}{4K_\rho} + \frac{1}{4K_\sigma} < 1$ ) from the other, “nontrivial” phases. For  $K_\sigma < 1$ , the phase of the junction corresponds to either the  $A \otimes N$ , or to the  $N \otimes A$ , fixed point, according to whether the initial boundary coupling  $t_1$  is larger, or smaller, than  $t_2$ . In the symmetric case  $t_1 = t_2$ , the system’s phase corresponds to the FCFP of Ref. [18]. When  $K_\sigma$  becomes  $> 1$ , a phase that maps onto a (generically non- $\mathbf{Z}_3$  symmetric) deformation of the M-FCFP of the Y3J opens till, after crossing the green line, corresponding to the curve  $K_\sigma(1 + K_\rho^{-1}) = 6$ , an additional phase opens (DMM), corresponding to the MM fully decoupled from the junction with the other two wires.

one sees that, at the disconnected fixed point, the leading boundary operator is again provided by a generic linear combination of  $V_{2,3}$  and of  $V_{3,1}$  in Eq. (23) (plus their Hermitean conjugates), all with scaling dimensions  $d_{V_{2,3}} = d_{V_{3,1}} = \frac{1}{2K}$ . Thus, we recover the expected result that the disconnected fixed point is unstable for  $K > 1/2$  [18]. At the  $A \otimes N$  fixed point, the most general allowed boundary interaction contains  $V_{a,(1,2)}$  and  $V_{b,(1,2)}$  in Eqs. (42), both with scaling dimension  $d_{a,(1,2)} = d_{b,(1,2)} = \frac{1+K^2}{2K}$ , of the intra-channel 1 normal backscattering operator in Eq. (44), with scaling dimension  $d_{\text{Intra},1} = 2K$ , and the operator  $V_{2,\text{Res}}$  in Eq. (45) describing the residual coupling to channel 2, with scaling dimension  $d_{2,\text{Res}} = \frac{2}{K}$ . Among all those operators, the only one that can become relevant for  $K > 1$  is  $V_{2,\text{Res}}$ , whose scaling dimension becomes  $< 1$  as  $K > 2$ . Finally, at the  $A \otimes A$  fixed point, the leading boundary interaction is provided by a linear combination of  $\tilde{V}_{\text{Res},1}$  and  $\tilde{V}_{\text{Res},2}$  in Eqs. (17), with corresponding scaling dimension  $d_{\text{Res}} = \frac{K}{2}$ . Putting the above results all together, one therefore infers that, for  $U = 0$ ,  $K > 1$ , the stable fixed point of the  $N = 2$  junction either corresponds to  $A \otimes N$ , or to  $N \otimes A$ , for  $K < 2$ , depending on the initial values of the boundary coupling strengths. For  $K > 2$ ,  $A \otimes A$  becomes the stable fixed point of the junction. Moreover, consistently with the discussion of sub-section 3.1, as well as with the results of Ref. [18], one expects  $A \otimes N$  and  $N \otimes A$  to be separated by some intermediate phase(s). Whether this corresponds to just a FCFP, as it happens for  $K < 1$  [18], or to more than one FCFP’s, or even to a continuous line of fixed points, cannot be firmly stated with our method in this range of values of system’s parameters and, very likely, to discriminate among the various possible options will require resorting to a nonperturbative, numerical approach to the problem.

$N = 2$ junction	Y3J
Disconnected fixed point ( $N \otimes N$ )	Disconnected fixed point
$A \otimes N$ fixed point	$A_1$ fixed point
$N \otimes A$ fixed point	$A_2$ fixed point
FCFP at $\bar{t}_1 = \bar{t}_2 = t_* = \left[ \epsilon / \mathcal{F} \left( \frac{1}{2K_\rho} - \frac{1}{2K_\sigma} \right) \right]^{\frac{1}{2}}$	“Planar” FCFP at $\bar{t}_{1,2} = 0$
$A \otimes A$ fixed point	$D_p$ fixed point
“Off-planar” FCFP	(Non $\mathbf{Z}_3$ -symmetric) M-FCFP
Disconnected MM fixed point	$A_3$ fixed point

Table 2: Table of correspondence between phases (fixed points) of the  $N = 2$  junction and of the Y3J. The fixed points inferred in each one of the systems by means of the correspondence with the other one are highlighted in red. The fixed points already known in both systems are highlighted in blue (see Ref.[18] for the  $N = 2$  junction, Refs.[2, 7] for the Y3J).

To summarize the correspondence between phases of the  $N = 2$  junction and of the Y3J, in table 2 we provide a synoptic view of corresponding fixed points in the two models, using a different color (red, instead than blue) to highlight phases that in either model are predicted by means of the correspondence with the other.

To complement the results of the previous sub-sections, we now briefly discuss how the correspondence between the  $N = 2$  junction and the Y3J has to be implemented in computing the  $g$ -function at corresponding fixed points of the two models.

#### 4.3. Calculation of the $g$ -function at corresponding fixed points

The simplest fixed point in both the  $N = 2$  junction and in the Y3J is the disconnected one, in which all the boundary interaction strengths are set to 0. As from Eqs. (11,21), at the disconnected fixed point, one obtains  $g_{\text{Disc}} = 2[K_\rho K_\sigma]^{\frac{1}{4}}$  in the  $N = 2$  junction, and  $g_{\text{Disc}} = 2[K_3 K^2 \bar{K}]^{\frac{1}{4}}$  in the Y3J. On comparing the two results, the first observation is that, to recover the over-all factor of 2 in the case of the Y3J, one has to include in the calculation the auxiliary KF  $\bar{\Gamma}$ , as well. Besides that, the two results are apparently not related to each other via the correspondence between the Luttinger parameters in the two models in Eqs. (41). This is due to the fact that the Y3J  $g$ -function receives contributions from overall degrees of freedom not entering the correspondence with the  $N = 2$  junction, that is, the auxiliary field and the center of mass field  $\phi_\chi(x)$ . On recomputing  $g_{\text{Disc}}$  in the Y3J by dropping those contributions, one eventually obtains the asymmetric version of the result of Ref. [2], that is

$$g_{\text{Disc}} = 2 \left[ \frac{K^2 K_3}{2K + K_3} \right]^{\frac{1}{4}}, \quad (57)$$

that is, exactly the result one obtains when inserting Eqs. (41) into the formula for  $g_{\text{Disc}}$  in the  $N = 2$  junction. Having stated the correspondence between the  $g$ -function at the disconnected fixed points, in the following we consider the  $g$ -function at alternative fixed points always normalized to  $g_{\text{Disc}}$ , in both models.

The  $A \otimes A$  fixed point in the  $N = 2$  junction corresponds to the  $D_P$  fixed point of the Y3J. Here, despite the counting of the real fermionic degrees of freedom working differently in the two models, the results for the  $g$ -function are again consistent with each other. While in [Appendix B](#) we discuss in detail the derivation of the corresponding degeneracy factor in the  $N = 2$  junction, it is worth recalling how one recovers it in the Y3J. Setting for simplicity  $t_{2,1} = 0$ , when mirroring  $H_b$  in Eq. (39), one obtains its two-boundary version,  $H_b^{(2)}$ , given by

$$H_b^{(2)} = -2it_{3,2}\Gamma_2\Gamma_3 \cos \left\{ \sqrt{\frac{\pi}{2}} [\phi_\sigma(0) + \phi_\rho(0)] \right\} - 2it_{1,3}\Gamma_1\Gamma_3 \cos \left\{ \sqrt{\frac{\pi}{2}} [\phi_\sigma(0) - \phi_\rho(0)] \right\} \\ - 2it_{3,2}\Gamma_2\Gamma_3 \cos \left\{ \sqrt{\frac{\pi}{2}} [\phi_\sigma(\ell) + \phi_\rho(\ell)] \right\} - 2it_{1,3}\Gamma_1\Gamma_3 \cos \left\{ \sqrt{\frac{\pi}{2}} [\phi_\sigma(\ell) - \phi_\rho(\ell)] \right\} . \quad (58)$$

This is the two-boundary Hamiltonian for the  $N = 2$  junction, except that now one has  $\gamma_L = \gamma_R = \Gamma_3$ . When discussing the degeneracy factor due to the zero-mode real fermion operators, in [Appendix B](#) we separately consider this case, concluding that, when both  $\phi_\rho(0)$  and  $\phi_\sigma(0)$  are properly pinned, one recovers a total number of three real-fermion zero modes which, put together with  $\bar{\Gamma}$ , provide the degeneracy factor of 4 (2) to the total partition function (to the  $g$ -function). Once the correct degeneracy factors have been taken into account, in the  $N = 2$  junction one obtains that  $\rho_{A \otimes A} = g_{A \otimes A} / g_{N \otimes N} = [K_\rho K_\sigma]^{-\frac{1}{4}}$ , which, using Eqs. (41), one readily shows to be the same as the result of Eq. (26) for the Y3J.

When computing the  $g$ -function at the  $A \otimes N$  fixed point of the  $N = 2$  junction, we have to pertinently modify the result in Eq. (13), due to the identity  $u_\sigma = u_\rho = u$ , which is a direct consequence of the mapping from the Y3J. In this case, implementing the approach of Ref. [18], one readily derives, using Eqs. (29), the identity

$$g_{A \otimes N} = \left[ \frac{1}{4K_\rho} + \frac{1}{4K_\sigma} \right]^{\frac{1}{2}} g_{\text{Disc}} = \left[ \frac{1}{2K} + \frac{1}{2K_3} \right]^{\frac{1}{2}} g_{\text{Disc}} , \quad (59)$$

which shows that, once normalized to the  $g$ -function at the disconnected fixed point,  $\frac{g_{A \otimes N}}{g_{\text{Disc}}}$  in the  $N = 2$  junction is equal to  $\frac{g_{A1}}{g_{\text{Disc}}}$  in the Y3J, as expected from the correspondence between the two models (note the apparent difference between the right-hand side of Eq. (59) for  $g_{A \otimes N}$  and the result in Eq. (13). This is due to the condition  $u_\rho = u_\sigma = u$  which naturally arises from the mapping and, in this case, takes the place of the formulas one generally derives from Eqs. (A.9) of [Appendix A](#).)

Before concluding this section, a comment is in order about the correspondence between real fermion operators in the  $N = 2$  junction and in the Y3J. On one hand, we see that it is rather straightforward in the single-boundary version of the models, as, in that case, one simply uses the observation that the center of mass field of the Y3J decouples from the junction dynamics and, therefore, the ‘‘left-over’’ KF can be formally mapped onto the MM in the  $N = 2$  junction. On the other hand, the correspondence is not anymore straight when resorting to the two-boundary version of the model Hamiltonian to compute  $g$ . In this case, the different nature of the MM’s, which are local in real space, and of the KF’s, which are global along the full extent of a QW, results, for instance, in that, while in the  $N = 2$  junction one has a TSS at each end of the system

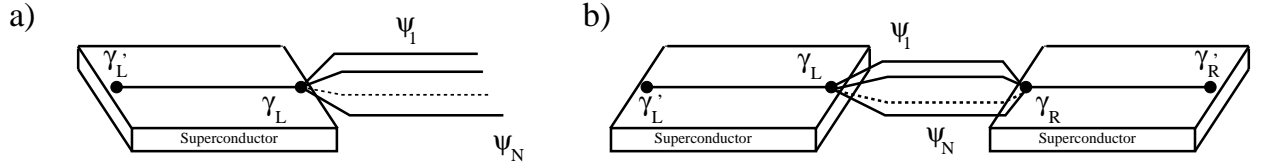


Figure 2: **a)**: Sketch of the junction between  $N$  interacting quantum wires and one topological superconductor. The one-dimensional topological superconductor is realized by depositing a semiconducting nanowire on top of a bulk,  $s$ -wave topological superconductor and applying a magnetic field (see Refs. [43, 44] for details).  $\psi_a$  denotes the field of electrons in wire- $a$ ,  $\gamma_L$  is the Majorana mode emerging at the interface between the quantum wires and the topological superconductor,  $\gamma'_L$  is the second Majorana mode expected to emerge at the opposite side of the topological superconductor [16]; **b)**: Two-boundary version of the device sketched in **a)**:  $\gamma_R, \gamma'_R$  now denote the Majorana modes at the endpoints of the topological superconductor connected to the right endpoint of the normal wires.

and, therefore, two MM's, in the Y3J one still has only the KF associated to the center of mass field. Remarkably, as we discuss above, this mismatch can be fixed by adding the auxiliary KF  $\bar{\Gamma}$  to the count of the degrees of freedom of the Y3J, though without the possibility of rigorously extending the Hamiltonian mapping to the two-boundary systems, as well. Yet, the very fact that the results are the same in the two models, apparently further supports the extension of the actual correspondence between the  $N = 2$  junction and the Y3J also to the  $g$ -function at corresponding fixed points, which can be eventually regarded as a double check of the results about the mapping of the phase diagram of one system to the other.

## 5. Phase diagram and impurity entropy of a junction between $N$ quantum wires and a topological superconductor

As a further example of application of our method for computing the  $g$ -function, in this section we discuss the fixed points in the phase diagram, and the corresponding calculation of the IE, in a junction between  $N$  QW's and a topological superconductor. For the sake of simplicity, in the following we make the symmetric assumption that the Luttinger parameters  $u, K$  are the same for each QW. In this respect, this is a symmetric multiwire generalization of the junction discussed, for  $K_\sigma < 1, N = 2$  and (partially) for  $N = 3$ , in Ref. [18]. (An error occurred there in the final numerical estimate of the  $g$ -function, which we amend here; it did not affect the final conclusions.) Referring to the TLL-model Hamiltonian for the junction in Eq. (A.5) of Appendix A, in the following, we assume that both intra-wire and inter-wire bulk interactions are repulsive, which implies  $K < 1, U > 0$ . In addition, we assume that  $1/2 < K$ , which is a necessary condition to assure the relevance of the boundary coupling to the MM [17, 18]. In Fig.2 we provide a sketch of the junction between  $N$  interacting QW's and a TS in the single-boundary version (which we use to discuss the phase diagram) and in the two-boundary version (which we use to compute the  $g$ -function). We now provide a discussion of the phase diagram, which basically generalizes the analysis of Ref. [18] to a generic  $N$ .

### 5.1. Phase diagram of the $N$ -wire junction with a topological superconductor

The simplest fixed point in the phase diagram corresponds to having all the wires disconnected from the TS. This implies type  $N$  boundary conditions at  $x = 0$  for all the channels. When turning

on nonzero couplings to the TS,  $\{t_a\}$ , taking into account the boundary conditions, one may write the bosonized boundary Hamiltonian at the disconnected fixed point,  $H_{b,B,N}^{(1)}$ , in the form

$$H_{b,B,N}^{(1)} = 2i \sum_{a=1}^N t_a \gamma_L \Gamma_a \cos[\sqrt{\pi} \phi_a(0)] \quad . \quad (60)$$

The scaling dimension of  $H_{b,B,N}^{(1)}$ ,  $d_b$ , can be readily derived using the transformation in Eqs. (A.6). The result is  $d_b = \frac{1}{2NK_\rho} + \frac{N-1}{2NK_\sigma}$ . For  $1/2 < K < 1$  and for  $U > 0$ , we find  $\frac{1}{2} < d_b < 1 \forall N$ , which implies that  $H_{b,B,N}^{(1)}$  always corresponds to a relevant boundary interaction for the range of parameters considered. Thus, having nonzero  $t_a$ 's paves the way to the opening of new phases, corresponding to additional fixed points in the phase diagram of the junction. To discuss them and especially their stability under RG flow, one has to first identify the corresponding CIBC's, and then to employ them to construct, within the spirit of DEBC approach, all the allowed boundary operators at a given fixed point and eventually to check whether any of them corresponds to a relevant perturbation. This can be readily done within the imaginary-time framework, in which we describe the wires using the Euclidean action  $S_{\text{Eff}}$  only depending on the fields at  $x = 0$ . To derive  $S_{\text{Eff}}$ , one has to integrate over the bulk fields everywhere in real space, except at  $x = 0$ . Doing so, due to the duality between the  $\phi$ - and the  $\theta$ -fields on the semi-infinite line,  $S_{\text{Eff}}$  can be either expressed in terms of the fields  $\phi_a(\tau) = \phi_a(x = 0, \tau)$ , or of the fields  $\theta_a(\tau) = \theta_a(x = 0, \tau)$  [2], as

$$\begin{aligned} S_{\text{Eff}}[\{\phi_a\}] &= \frac{1}{2\pi} \int d\Omega |\Omega| \vec{\phi}^\dagger(\Omega) [\mathbf{M}_N]^T \mathbf{K}_N \mathbf{M}_N \vec{\phi}(\Omega) \\ S_{\text{Eff}}[\{\theta_a\}] &= \frac{1}{2\pi} \int d\Omega |\Omega| \vec{\theta}^\dagger(\Omega) [\mathbf{M}_N]^T \mathbf{K}_N^{-1} \mathbf{M}_N \vec{\theta}(\Omega) \quad , \end{aligned} \quad (61)$$

with  $\vec{\phi}(\Omega) = \int d\tau e^{i\Omega\tau} [\phi_1(\tau), \phi_2(\tau), \dots, \phi_N(\tau)]^T$ ,  $\vec{\theta}(\Omega) = \int d\tau e^{i\Omega\tau} [\theta_1(\tau), \theta_2(\tau), \dots, \theta_N(\tau)]^T$ , the matrix  $\mathbf{M}_N$  defined in Eq.(A.7) of Appendix A, and the matrix  $\mathbf{K}_N$  given by

$$\mathbf{K}_N = \begin{bmatrix} K_\rho & 0 & \dots & 0 \\ 0 & K_\sigma & \dots & 0 \\ \vdots & \vdots & \ddots & \vdots \\ 0 & 0 & \dots & K_\sigma \end{bmatrix} \quad . \quad (62)$$

Eqs. (61) are true in general. The specific choice of either one of the actions in Eqs. (61) depends on the boundary conditions on the various fields.

At the disconnected fixed point, all the  $\theta$ -fields obey Dirichlet boundary conditions at  $x = 0$ . Therefore, we must use  $S_{\text{Eff}}[\{\phi_a\}]$  in Eq. (61), with all the  $\phi$ 's different from 0. A straightforward calculation allows us to derive the scaling dimension of  $H_{b,B,N}^{(1)}$ , which is simply given by  $\frac{1}{2} \{ [[\mathbf{M}_N]^T \mathbf{K}_N \mathbf{M}_N]^{-1} \}_{1,1} = d_b$ , where we have used the identity  $[[\mathbf{M}_N]^T \mathbf{K}_N \mathbf{M}_N]^{-1} = [\mathbf{M}_N]^T \mathbf{K}_N^{-1} \mathbf{M}_N$ . In addition, while normal intra-wire backscattering plays no role, due to Dirichlet boundary conditions on  $\theta_a(0)$ , inter-wire backscattering and inter-wire pairing between channels  $a$  and  $b$  respectively correspond to the operators  $V_{\text{Normal},(a,b)}$  and  $V_{\text{Pair},(a,b)}$ , given by

$$\begin{aligned}
V_{\text{Normal},(a,b)} &= \Gamma_a \Gamma_b e^{-i\sqrt{\pi}[\phi_a(0) - \phi_b(0)]} \\
V_{\text{Pair},(a,b)} &= \Gamma_a \Gamma_b e^{-i\sqrt{\pi}[\phi_a(0) + \phi_b(0)]} \quad , \quad (63)
\end{aligned}$$

plus their Hermitean conjugates. Their scaling dimensions are respectively given by (assuming  $a \neq b$ )

$$\begin{aligned}
d_{\text{Normal},(a,b)} &= \{[[\mathbf{M}_N]^T \mathbf{K}_N^{-1} \mathbf{M}_N]_{a,a} - [[\mathbf{M}_N]^T \mathbf{K}_N^{-1} \mathbf{M}_N]_{a,b}\} = K_\sigma^{-1} \\
d_{\text{Pair},(a,b)} &= \{[[\mathbf{M}_N]^T \mathbf{K}_N^{-1} \mathbf{M}_N]_{a,a} + [[\mathbf{M}_N]^T \mathbf{K}_N^{-1} \mathbf{M}_N]_{a,b}\} = K_\sigma^{-1} + \frac{2}{N} (K_\rho^{-1} - K_\sigma^{-1}) \quad . \quad (64)
\end{aligned}$$

Given the assumption that  $K_\sigma < 1$  (which we relaxed, when discussing the correspondence with the Y3J in section 4), we conclude that both  $d_{\text{Normal},(a,b)}$  and  $d_{\text{Pair},(a,b)}$  are  $> 1$  and, accordingly,  $H_{b,B,N}^{(1)}$  provides the only relevant perturbation at the disconnected fixed point.

To move away from the disconnected fixed point, in analogy to our derivation of Ref. [18], we employ the perturbative RG approach within  $\epsilon$ -expansion method, which we briefly review in in Appendix D.1. The corresponding RG equations for the running couplings are given by

$$\frac{d\bar{t}_a}{dl} = \epsilon \bar{t}_a - \mathcal{F}(\nu) \bar{t}_a \left[ \sum_{b \neq a} \bar{t}_b^2 \right] \quad , \quad (65)$$

with  $l = -\ln(D/D_0)$ ,  $D$  being the running energy scale,  $D_0$  the high-energy (band) cutoff  $\sim \tau_0^{-1}$ , and the function  $\mathcal{F}(\nu)$  defined in Eq. (D.7), with  $\nu = \frac{1}{NK_\rho} - \frac{1}{NK_\sigma}$ . In general, Eq. (65) implies a growth of the  $\bar{t}_a$  along the RG trajectories. This may either take the system to some FCFP, which generalizes the one discussed in Ref. [18] for  $N = 2, 3$ , or to pinning  $N_a$   $\phi_a(0)$ 's, leaving the corresponding  $\theta_a(0)$  unpinned. Because of the symmetry between the channels, in the following we assume always that such a fixed point corresponds to pinning the first  $N_a$   $\phi_a(x)$ 's at  $x = 0$ , leaving the remaining  $N_n$  unpinned (so that, for instance, the disconnected fixed point corresponds to  $N_a = 0, N_n = N$ ).

Let us consider the  $N_a = 1, N_n = N - 1$  fixed point. From Eq. (60), we see that this is recovered by sending  $\bar{t}_1 \rightarrow \infty$  and minimizing the corresponding contribution to  $H_{b,B,N}^{(1)}$ . Accordingly, besides pinning  $\phi_1(0)$ , this also requires ‘‘locking’’ the system into a state either annihilated by the Dirac fermion  $a_1 = \frac{1}{2}[\gamma_L + i\Gamma_1]$ , or by  $a_1^\dagger$ , depending on the value at which  $\phi_1(0)$  is pinned. Taking this into account, we may list the various allowed boundary operators at that fixed point. First of all, the intra-channel normal backscattering operator in channel-1 is realized as  $V_{\text{Intra},1} \sim V_a \cos[2\sqrt{\pi}\theta_1(0)]$ . To derive the corresponding scaling dimension,  $d_{\text{Intra},1}$ , in Eq. (61) we set to 0 all the  $\theta_a$ 's but  $\theta_1$ . As a result, we eventually find

$$d_{\text{Intra},1} = 2\{[[\mathbf{M}_N]^T \mathbf{K}_N^{-1} \mathbf{M}_N]_{1,1}\}^{-1} = \frac{2}{\left[\frac{1}{NK_\rho} + \frac{N-1}{NK_\sigma}\right]} = [d_{b,\text{Disc}}]^{-1} \quad , \quad (66)$$

which implies  $d_{\text{Intra},1} = [d_{b,\text{Disc}}]^{-1}$ . Switching to boundary inter-channel normal backscattering/pairing operators, we have to separately consider whether those processes involve channel-1, or not. In the latter case, assuming that both  $a$  and  $b \neq 1$ , the corresponding boundary operators are again linear combinations of the ones in Eqs. (63), with the corresponding scaling dimensions

in Eqs. (64) proving their irrelevance. At variance, when e.g.  $a = 1$ , the analog of the operators in Eqs. (63) are given by linear combinations of the operators

$$\begin{aligned} V_{a,(1,b)} &= \Gamma_1 \Gamma_b e^{-i \sqrt{\pi}[\theta_1(0) - \phi_b(0)]} \\ V_{b,(1,b)} &= \Gamma_1 \Gamma_b e^{-i \sqrt{\pi}[\theta_1(0) + \phi_b(0)]} \quad , \end{aligned} \quad (67)$$

plus their Hermitean conjugates. To compute the corresponding scaling dimensions, we have to account for the Dirichlet boundary conditions on  $\phi_1(0)$ . To do so, we get rid of the corresponding field in the Euclidean action, by employing the “reduced” action  $S_{\text{Eff,(1)}}[\{\phi_b\}]$ , given by

$$S_{\text{Eff,(1)}}[\{\phi_b\}] = \frac{1}{2\pi} \int d\Omega |\Omega| \tilde{\phi}^\dagger(\Omega) \tilde{\mathcal{K}}_N \tilde{\phi}(\Omega) \quad , \quad (68)$$

with  $\tilde{\phi}(\Omega) = \int d\tau e^{i\Omega\tau} [\phi_2(\tau), \dots, \phi_N(\tau)]^T$  and  $\tilde{\mathcal{K}}_N = \frac{K_\rho + (N-1)K_\sigma}{N} \mathbf{I}_{N-1} + \frac{K_\rho - K_\sigma}{N} \tilde{I}_{N-1}$ , and  $\mathbf{I}_N$  being the  $N$ -dimensional identity matrix and  $\tilde{I}_N$  being the  $N$ -dimensional square matrix with all the entries equal to 1 but the ones at the diagonal, which are equal to 0. Accordingly, we find

$$d_{a,(1,b)} = d_{b,(1,b)} = \frac{1}{2} \{ \{ [\mathbf{M}_N]^T \mathbf{K}_N^{-1} \mathbf{M}_N \}_{1,1} \}^{-1} + \{ [\tilde{\mathcal{K}}_N]^{-1} \}_{b,b} \quad . \quad (69)$$

By mathematical recursion, one may show that

$$\tilde{\mathcal{K}}_N^{-1} = \left[ \frac{(N-2)K_\rho + 2K_\sigma}{(N-1)K_\rho K_\sigma + K_\sigma^2} \right] \mathbf{I}_{N-1} - \left[ \frac{K_\rho - K_\sigma}{(N-1)K_\rho K_\sigma + K_\sigma^2} \right] \tilde{I}_{N-1} \quad , \quad (70)$$

which eventually leads to the final result

$$d_{\text{Normal,(1,b)}} = d_{\text{Pair,(1,b)}} = \frac{1}{4} \left\{ \frac{1}{d_{b,\text{Disc}}} + 2 \frac{(N-2)K_\rho + 2K_\sigma}{(N-1)K_\rho K_\sigma + K_\sigma^2} \right\} \quad . \quad (71)$$

For  $1/2 < K_\rho, K_\sigma < 1$  and for  $U > 0$  one obtains  $d_{\text{Inter,(1,b)}} > 1$ , thus showing the irrelevance of the corresponding operators. Finally, we consider the residual coupling to the MM. In this case, as discussed at length in Refs. [17, 18], though the residual coupling between, say, channel-2 and the Majorana mode seems to provide a relevant perturbation, in fact, it does not, due to the condition that the physical states must either be annihilated by  $a_1$ , or by  $a_1^\dagger$  defined above. This makes an operator such as  $2i\bar{t}_2\gamma\Gamma_2 \cos[\sqrt{\pi}\phi_2(0)]$  become effective only to second order in  $\bar{t}_2$ , where it effectively behaves like an operator  $V_{2,\text{Res}} \propto \cos[2\sqrt{\pi}\phi_2(0)]$ , with scaling dimension  $d_{\text{Res,2}} = 4\{[\tilde{\mathcal{K}}_N]^{-1}\}_{2,2} = 2\frac{(N-2)K_\rho + 2K_\sigma}{(N-1)K_\rho K_\sigma + K_\sigma^2} > 1$  for  $1/2 < K < 1$  and for  $U > 0$ . Accordingly, this is an irrelevant operator, which leads us to conclude that, as long as  $K_\sigma < 1$ , the stable phase of the  $N$ -wire junction with a topological superconductor always corresponds to a  $N_a = 1, N_n = N - 1$  fixed point.

While our above analysis can in principle be readily extended to any  $N_a \geq 2$ , in the following we limit ourselves to the case  $N_a = 2$  to show how, in this case, at least two relevant boundary operators emerge at the corresponding fixed point. Eventually, this leads to the conclusion that the corresponding fixed point is not stable, consistently with the result of Ref. [18] for  $N = 2$ . The instability of fixed points with an  $N_a \geq 3$  can eventually be inferred by means of similar arguments.

Assuming  $N_a = 2$ , the key operators correspond to normal boundary backscattering/pairing involving channels-1 and -2. Within DEBC approach, they are readily recovered as a linear combination of the operators  $V_{a,(1,2)}$  and  $V_{b,(1,2)}$ , given by

$$\begin{aligned} V_{a,(1,2)} &= \Gamma_1 \Gamma_2 e^{-i\sqrt{\pi}[\theta_1(0) - \theta_2(0)]} \\ V_{b,(1,2)} &= \Gamma_1 \Gamma_b e^{-i\sqrt{\pi}[\theta_1(0) + \theta_2(0)]} \quad , \end{aligned} \quad (72)$$

plus their Hermitean conjugates. The corresponding scaling dimensions are accordingly given by

$$\begin{aligned} d_{a,(1,2)} &= \{[[\mathbf{M}_N]^T \mathbf{K}_N^{-1} \mathbf{M}_N]_{1,1}\}^{-1} - \{[[\mathbf{M}_N]^T \mathbf{K}_N^{-1} \mathbf{M}_N]_{1,2}\}^{-1} = \frac{N}{2K_\rho^{-1} + (N-2)K_\sigma^{-1}} \leq K_\rho \\ d_{b,(1,2)} &= \{[[\mathbf{M}_N]^T \mathbf{K}_N^{-1} \mathbf{M}_N]_{1,1}\}^{-1} + \{[[\mathbf{M}_N]^T \mathbf{K}_N^{-1} \mathbf{M}_N]_{1,2}\}^{-1} = K_\sigma \quad . \end{aligned} \quad (73)$$

Both  $d_{a,(1,2)}$  and  $d_{b,(1,2)}$  are  $< 1$ , implying that boundary operators encoding normal inter-channel backscattering and pairing both correspond to relevant boundary interactions. Accordingly, we conclude that the  $N_a = 2$  fixed point is unstable and, by means of an obvious extension of the argument, that any fixed point with  $N_a \geq 3$  is unstable, as well. In conclusion, we see that, also for  $N > 2$ , the only stable fixed points in the phase diagram of the  $N$ -wire junction are the  $N$ -ones with  $N_a = 1$ . As those are all equivalent to each other, there must be intermediate FCFP's separating the corresponding phases.

FCFP's have been argued to potentially host ‘‘decoherence-frustrated’’ phases with reduced decoherence effects in the boundary quantum degrees of freedom [32, 33, 24]. In our case, FCFP's are expected to emerge at the bifurcations between RG trajectories leading to any one of the stable  $N_a = 1$  fixed points. While we are not able to provide an exact conformal boundary field theory description of the FCFP's, we can still access them in the  $\epsilon$ -expansion framework. Indeed, they emerge as nontrivial zeroes of the  $\beta$ -functions at the right-hand side of Eqs. (65), with the corresponding boundary couplings satisfying the equations

$$\bar{t}_a \{ \epsilon - \mathcal{F}[v] \sum_{b \neq a} \bar{t}_b^2 \} = 0 \quad . \quad (74)$$

By inspection, we see that there is only a solution with all the  $\bar{t}_a^* \neq 0$  (FCFP $_N$ ), corresponding to

$$\bar{t}_1^* = \dots = \bar{t}_N^* = t_*(N) = \sqrt{\frac{\epsilon}{(N-1)\mathcal{F}[v]}} \quad . \quad (75)$$

Next (assuming  $N \geq 3$ ), it is possible to have nontrivial solutions in which one  $\bar{t}_a^* = 0$ , all the others being  $\neq 0$  (FCFP $_{N-1}$ ). These are given by

$$\begin{aligned} \bar{t}_a^* &= 0 \\ \bar{t}_b^* &= t_*(N-1) = \sqrt{\frac{\epsilon}{(N-2)\mathcal{F}[v]}} \quad , \quad (b \neq a) \quad . \end{aligned} \quad (76)$$

Going ahead (assuming  $N \geq 4$ ), we find  $N(N-1)/2$  FCFP's in which two  $\bar{t}_a^* = 0$ , with all the others being  $\neq 0$ , etc. Remarkably, Eqs. (74) do not exhibit solutions with just one  $\bar{t}_a^* \neq 0$  and all

the others being = 0, which gives us one more insight about the possible topology of the boundary phase diagram of the junction. To do so, we first of all note that, if all the  $N$  bare couplings are equal to each other, then the symmetry among them is not broken along the RG flow generated by Eqs. (65). In this case, we therefore expect the junction to flow towards the FCFP $_N$ . At variance, a slight breaking of the symmetry between the couplings does, in fact, take the system out of the FCFP $_N$ . To show this, let us assume that, in the vicinities of the FCFP $_N$ , the couplings are set so that  $\bar{t}_{1,L} = t_*(N) - \rho$ , while  $\bar{t}_{a,L} = t_*(N) + \sigma$  for  $a = 2, \dots, N$ , with  $0 < \rho \ll 1$  and  $0 < \sigma \ll 1$ . On linearizing Eqs. (65), one obtains

$$\begin{aligned} \frac{d\rho(l)}{dl} &= 2\epsilon\sigma(l) \\ \frac{d\sigma(l)}{dl} &= \frac{2\epsilon}{N-1} \rho(l) - 2\epsilon\sigma(l) \quad . \end{aligned} \quad (77)$$

Once integrated, setting  $\lambda_1 = -\epsilon + \epsilon\sqrt{1 + \frac{4}{N-1}}$ ,  $\lambda_2 = -\epsilon - \epsilon\sqrt{1 + \frac{4}{N-1}}$ , one finds

$$\begin{aligned} \rho(l) &= e^{\lambda_1 l} \left\{ \frac{1 + \sqrt{1 + \frac{4}{N-1}}}{2\sqrt{1 + \frac{4}{N-1}}} \rho(0) + \frac{1}{\sqrt{1 + \frac{4}{N-1}}} \sigma(0) \right\} + e^{\lambda_2 l} \left\{ \frac{-1 + \sqrt{1 + \frac{4}{N-1}}}{2\sqrt{1 + \frac{4}{N-1}}} \rho(0) - \frac{1}{\sqrt{1 + \frac{4}{N-1}}} \sigma(0) \right\} \\ \sigma(l) &= \frac{\lambda_1 e^{\lambda_1 l}}{2\epsilon} \left\{ \frac{1 + \sqrt{1 + \frac{4}{N-1}}}{2\sqrt{1 + \frac{4}{N-1}}} \rho(0) + \frac{1}{\sqrt{1 + \frac{4}{N-1}}} \sigma(0) \right\} + \frac{\lambda_2 e^{\lambda_2 l}}{2\epsilon} \left\{ \frac{-1 + \sqrt{1 + \frac{4}{N-1}}}{2\sqrt{1 + \frac{4}{N-1}}} \rho(0) - \frac{1}{\sqrt{1 + \frac{4}{N-1}}} \sigma(0) \right\} \quad . \end{aligned} \quad (78)$$

From Eqs. (78) one infers that the RG trajectories flow towards the FCFP $_{N-1}$  fixed point, obtained by decreasing  $\bar{t}_1$  and symmetrically increasing all the other couplings. Conversely, if both  $\rho(0)$  and  $\sigma(0)$  are  $< 0$ , then a direct flow to an  $N_a = 1$  fixed point is recovered. Now, the above analysis can be straightforwardly iterated, eventually generalizing to the  $N$ -wire junction the RG flow diagram derived in Ref. [18]. In Fig.3, we draw a sketch of the minimal flow diagram for the junction. We see that, for  $1/2 < K < 1$ , the RG trajectories flow away from the disconnected fixed point, either towards one of the  $N_a = 1$  fixed points, or towards some FCFP, depending on the symmetry between the initial values of the boundary couplings. Eventually, reducing the symmetry between the boundary couplings implies a flow between different FCFP's, till, when all the symmetries are removed, the system flows towards one of the maximally stable  $N_a = 1$  fixed points.

We now compute the  $g$ -function at the various fixed points of the  $N$ -wire junction, eventually arguing that the corresponding results are consistent with the expected topology of the phase diagram only provided one properly accounts for the real fermionic modes, which is at the heart of our approach.

## 5.2. Impurity entropy at the fixed points of a junction between $N$ quantum wires and a topological superconductor

To begin with, let us consider the disconnected fixed point, corresponding to type  $N$  CIBC's at both boundaries in each channel. As a general remark we note that, in the junction we consider

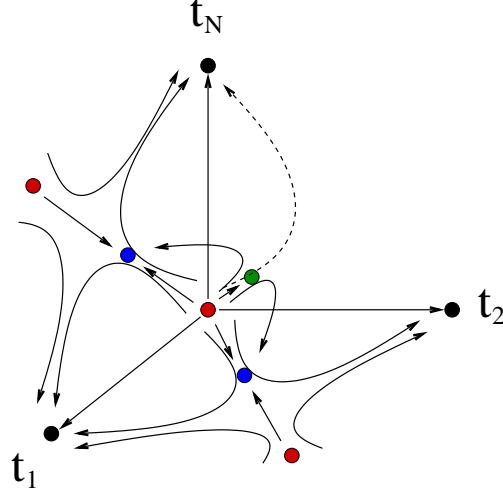


Figure 3: Sketch of the typical renormalization group flow diagram of a junction of  $N$  interacting quantum wires with a topological superconductor drawn for  $U > 0$  and  $K_\sigma < 1$  (see text). In this range of parameters, we see that the disconnected fixed point, as well as the fixed points with  $N_a > 1$ , are unstable against turning on a nonzero boundary interaction. In the presence of a symmetry between two, or more than two, boundary couplings, the renormalization group trajectories flow towards FCFP's (drawn in green and blue). Eventually, when one boundary coupling takes over all the others, the system flows towards one of the  $N_a = 1$  fixed points.

here, we have  $2MM$ 's (one at each boundary), as well as  $N$  KF's, for a total of  $2 + N$  real fermionic modes. Consistent with the discussion of section 2, if  $N$  is odd, we introduce the auxiliary wire, with Luttinger parameters  $\bar{u}, \bar{K}$ , providing an extra Klein factor  $\bar{\Gamma}$ , so to make the total number of real fermionic zero mode operators even. From Eqs. (A.8,A.13,A.14) and taking into account the degeneracy factor associated with zero-mode real fermionic operators, for  $N$  even, we eventually find for the partition function at the disconnected fixed point the result

$$\mathcal{Z}_{\text{Disc}} = 2^{1+\frac{N}{2}} [\eta(q_c)]^{-1} [\eta(q_r)]^{-(N-1)} \mathcal{Z}_{\text{Disc},e,0} \quad , \quad (79)$$

with  $q_{c,r} = e^{-\frac{u_{c,r}\beta\pi}{\ell}}$ , and

$$\mathcal{Z}_{\text{Disc},e,0} = \sum_{\{m_{1,\phi}, \dots, m_{N,\phi}\} \in \mathbf{Z}} \exp \left\{ -\frac{\pi\beta}{2\ell} \vec{m}_\phi^T \mathbf{B}_{N,e} \vec{m}_\phi \right\} \quad , \quad (80)$$

$\vec{m}_\phi^T = (m_{1,\phi}, \dots, m_{N,\phi})$ , and the matrix  $\mathbf{B}_{N,e}$  given by

$$\mathbf{B}_{N,e} = [\mathbf{M}_N]^T \begin{bmatrix} \frac{u_\rho}{K_\rho} & 0 & \dots & 0 \\ 0 & \frac{u_\sigma}{K_\sigma} & \dots & 0 \\ \vdots & \vdots & \ddots & \vdots \\ 0 & 0 & \dots & \frac{u_\sigma}{K_\sigma} \end{bmatrix} \mathbf{M}_N \quad . \quad (81)$$

At variance, for  $N$  odd, one obtains

$$\mathcal{Z}_{\text{Disc}} = 2^{1+\frac{N+1}{2}} [\eta(\bar{q})]^{-1} [\eta(q_c)]^{-1} [\eta(q_r)]^{-(N-1)} \mathcal{Z}_{\text{Disc},o,0} \quad , \quad (82)$$

with  $\bar{q} = e^{-\frac{i\beta\pi}{\ell}}$ , and

$$\mathcal{Z}_{\text{Disc},o,0} = \sum_{\{m_{1,\phi}, \dots, m_{N,\phi}, m_{N+1,\phi}\} \in \mathbf{Z}} \exp \left\{ -\frac{\pi\beta}{2\ell} \vec{m}_\phi^T \mathbf{B}_{N,o} \vec{m}_\phi \right\}, \quad (83)$$

and the matrix  $\mathbf{B}_{N,o}$  constructed from  $\mathbf{B}_{N,e}$  by adding one row and one column with all the elements = 0 except  $[\mathbf{B}_{N,o}]_{N+1,N+1} = \frac{i}{K}$ . To extract the  $g$ -function, we have to consider the partition function in the  $\ell \rightarrow \infty$  limit at fixed  $\beta$ , which can be readily done by employing the Poisson summation formula in the form presented in Eq. (C.10). As a result, we obtain

$$\begin{aligned} \mathcal{Z}_{\text{Disc}} &\xrightarrow{\ell \rightarrow \infty} 2^{1+\frac{N}{2}} e^{\frac{\pi\ell}{6\beta u\rho} + \frac{\pi\ell(N-1)}{6\beta u\sigma}} [K_\rho K_\sigma^{(N-1)}]^{1/2}, \quad (\text{N even}) \\ \mathcal{Z}_{\text{Disc}} &\xrightarrow{\ell \rightarrow \infty} 2^{1+\frac{N+1}{2}} e^{\frac{\pi\ell}{6\beta u\rho} + \frac{\pi\ell(N-1)}{6\beta u\sigma} + \frac{\pi\ell}{6\beta iu}} [\bar{K} K_\rho K_\sigma^{(N-1)}]^{1/2}, \quad (\text{N odd}), \end{aligned} \quad (84)$$

from which we eventually obtain for  $g_{\text{Disc}}$  the result

$$\begin{aligned} g_{\text{Disc}} &= 2^{\frac{N+2}{4}} [K_\rho K_\sigma^{(N-1)}]^{1/4}, \quad (\text{N even}) \\ g_{\text{Disc}} &= 2^{\frac{N+3}{4}} [\bar{K} K_\rho K_\sigma^{(N-1)}]^{1/4}, \quad (\text{N odd}). \end{aligned} \quad (85)$$

To generalize Eqs. (85) to a fixed point with type A CIBC's in the first  $N_a$  channels and type  $N$  in the remaining  $N_n$  ones, we refer to Eq. (A.15) of Appendix A for the spectrum of the zero-mode operators. Accordingly, for  $N$  even, we obtain that the zero-mode contribution to the total partition function is given by

$$\mathcal{Z}_{(N_a, N_n), e, 0} = \sum_{\{m_{a,\theta}, m_{b,\phi}\} \in \mathbf{Z}} \exp \left\{ -\frac{\pi\beta}{2\ell} \left[ \vec{m}_\theta^T \tilde{\mathbf{B}}_{N,e} \vec{m}_\theta + \vec{m}_\phi^T \mathbf{B}_{N,e} \vec{m}_\phi \right] \right\}, \quad (86)$$

with  $\vec{m}_\theta^T = (m_{1,\theta}, \dots, m_{N_a,\theta}, 0, \dots, 0)$ ,  $\vec{m}_\phi^T = (0, \dots, 0, m_{N_a+1,\phi}, \dots, m_{N,\phi})$ , and the matrix  $\tilde{\mathbf{B}}_{N,e}$  obtained from  $\mathbf{B}_{N,e}$  in Eq. (81) by substituting  $K_{c,r}^{-1}$  with  $K_{c,r}$ , respectively. Similarly, for  $N$  odd, one obtains

$$\mathcal{Z}_{(N_a, N_n), o, 0} = \sum_{\{m_{a,\theta}, m_{b,\phi}\} \in \mathbf{Z}} \exp \left\{ -\frac{\pi\beta}{2\ell} \left[ \vec{m}_\theta^T \tilde{\mathbf{B}}_{N,o} \vec{m}_\theta + \vec{m}_\phi^T \mathbf{B}_{N,o} \vec{m}_\phi \right] \right\}, \quad (87)$$

with  $\tilde{\mathbf{B}}_{N,o}$  constructed from  $\mathbf{B}_{N,o}$  by means of the same criterion used to build  $\tilde{\mathbf{B}}_{N,e}$  from  $\mathbf{B}_{N,e}$ . Postponing, for the time being, the calculation of the degeneracy factors due to the zero-mode real fermion operators,  $\delta_{e,o}[N_a, N_n]$ , we now employ the approach of Appendix C to compute the  $g$ -function from the results of Eqs. (86,87). Taking into account that the contribution to the total partition function due to the oscillator modes does not depend on the specific CIBC's in the various channels, we obtain

$$\begin{aligned} \mathcal{Z}_{N_a, N_n} &\xrightarrow{\ell \rightarrow \infty} \delta_e[N_a, N_n] e^{\frac{\pi\ell}{6\beta u\rho} + \frac{\pi\ell(N-1)}{6\beta u\sigma}} [K_\sigma^{(N-N_a-1)} K_\rho^{-1} K^2]^{1/2} \left[ 1 + \frac{(N_n-1)KU}{\pi u} \right]^{-1/2}, \quad (\text{N even}) \quad (88) \\ \mathcal{Z}_{N_a, N_n} &\xrightarrow{\ell \rightarrow \infty} \delta_o[N_a, N_n] e^{\frac{\pi\ell}{6\beta u\rho} + \frac{\pi\ell(N-1)}{6\beta u\sigma} + \frac{\pi\ell}{6\beta iu}} [\bar{K} K_\sigma^{(N-N_a-1)} K_\rho^{-1} K^2]^{1/2} \left[ 1 + \frac{(N_n-1)KU}{\pi u} \right]^{-1/2}, \quad (\text{N odd}). \end{aligned}$$

In [Appendix B](#) we discuss in detail the calculation of  $\delta_{e,o}[N_a, N_n]$ . Here, we just quote the final result for the  $g$ -function, which is

$$\begin{aligned} g_{N_a, N_n} &= 2^{\frac{3N_a + N_n - 2}{4}} [K_\sigma^{(N_n - N_a - 1)} K_\rho^{-1} K^2]^{\frac{1}{4}} \left[ 1 + \frac{(N_n - 1)KU}{\pi u} \right]^{-\frac{1}{4}}, \quad (\text{N even}) \\ g_{N_a, N_n} &= 2^{\frac{3N_a + N_n - 1}{2}} [\bar{K} K_\sigma^{(N_n - N_a - 1)} K_\rho^{-1} K^2]^{\frac{1}{4}} \left[ 1 + \frac{(N_n - 1)KU}{\pi u} \right]^{-\frac{1}{4}}, \quad (\text{N odd}) \end{aligned} \quad (89)$$

On normalizing  $g_{N_a, N_n}$  to  $g_{\text{Disc}}$ , we obtain the ratio

$$\rho_{N_a, N_n} = \frac{g_{N_a, N_n}}{g_{\text{Disc}}} = \left[ \frac{2^{\frac{N_a}{2} - 1}}{K_\rho^{\frac{1}{2}} K_\sigma^{\frac{N_a}{2}}} \right] \left\{ \frac{K^{\frac{1}{2}}}{\left[ 1 + \frac{(N_n - 1)KU}{\pi u} \right]^{\frac{1}{4}}} \right\}, \quad (90)$$

which gives back the result of Eq. (13) for  $N_a = N_n = 1$  and the results of Eq. (15) for  $N_a = 2, N_n = 0$ . Besides the consistency check, a first important result is that one obtains

$$\rho_{1, N-1} = \sqrt{\frac{K}{2K_\sigma K_\rho}} \left[ 1 + \frac{(N-2)KU}{\pi u} \right]^{-\frac{1}{4}} = \frac{1}{\sqrt{2K}} \left\{ 1 - \frac{(N-1) \left( \frac{KU}{\pi u} \right)^2}{\left[ 1 + \frac{(N-2)KU}{\pi u} \right]} \right\}^{\frac{1}{4}} < 1, \quad (91)$$

as well as

$$\frac{\rho_{N_a+1, N_n-1}}{\rho_{N_a, N_n}} = \sqrt{\frac{2}{K_\sigma}} \left[ \frac{1 + \frac{(N_n-1)KU}{\pi u}}{1 + \frac{(N_n-2)KU}{\pi u}} \right]^{\frac{1}{4}}, \quad (92)$$

which is  $< 1$  for  $K_\sigma < 1$ . Thus, the systematic calculation of the  $g$ -function at fixed points with given CIBC's ultimately confirms the phase diagram emerging from the perturbative RG approach combined with DEBC method. There are  $N$  equivalent stable fixed points, corresponding to  $N_a = 1, N_n = N - 1$ . These are separated by FCFP's that are expected to lie along specific symmetry line in the boundary parameter space [18]. To compute the  $g$ -function at the FCFP's, we employ the  $\epsilon$ -expansion method discussed in Ref. [18]. Specifically, we assume that  $d_b = 1 - \epsilon$ , with  $0 < \epsilon \ll 1$  and eventually find that the FCFP's are all located at values of the boundary parameters  $t_* \propto (\mathcal{F}(2 - K_\sigma^{-1}))^{-\frac{1}{2}}$ , with the function  $\mathcal{F}$  defined in Eq. (B.41) of Ref. [18] and reviewed here, in [Appendix D](#). In general, letting  $M (\leq N)$  be the number of finite couplings  $t_{*,M}$  at a FCFP, we find  $t_{*,M} = \sqrt{\frac{\epsilon}{(M-1)\mathcal{F}(v)}}$ . To proceed with the calculation of the corresponding value of the  $g$ -function,  $g_{\text{FCFP},M}$ , we go through exactly the same derivation of appendix G of Ref. [18]. As a result, to leading order in the  $t_{*,M}$ , we find

$$g_{\text{FCFP},M} = g_{\text{Disc}} \{1 - 2\pi^2 M t_{*,M}^4\} = g_{\text{Disc}} \left\{ 1 - \frac{2\pi^2 M \epsilon^2}{(M-1)\mathcal{F}(v)} \right\}. \quad (93)$$

A remarkable consequence of Eq. (93) is that, since, given two integers  $M, M'$  both  $\leq N$ , we find  $\frac{M}{M-1} \geq \frac{M'}{M'-1}$ , provided  $M \leq M'$ ,  $g_{\text{FCFP},M}/g_{\text{FCFP},M'}$  is  $> 1$  ( $< 1$ ) if  $M > M'$  ( $M < M'$ ), that is, if an RG trajectory takes place between two FCFP's, it must take the system towards the fixed point with the lower value of  $M$ , consistently with the result of Ref. [18] in the case  $N = 3, U = 0$ .

## 6. Conclusions

We discuss the method to consistently compute the  $g$ -function at the boundary fixed points of the phase diagram of junctions between interacting quantum wires and/or topological superconductors, involving real fermionic modes in the corresponding boundary Hamiltonian (localized Majorana modes and/or Klein factors). We show that, in doing the calculation, one has to treat *all* of the real fermionic degrees of freedom on the same footing, which is apparently a version of the Majorana-Klein hybridization phenomenon, which requires KF's to be considered as actual “physical” degrees of freedom in exactly the same way as MM's, when describing junctions between interacting quantum wires and topological superconductors [28]. Incidentally, in our procedure for computing  $g$ , we also introduced a means to avoid ambiguities in counting the degrees of freedom associated with an odd total number of real fermions, by introducing an auxiliary wire, fully disconnected from the junction. The additional wire has the effect of providing an additional KF, which makes the total number of real fermionic modes always even. While affecting the value of  $g$  at a specific fixed points, our procedure eventually gives back the right value of the *ratio* between  $g$  computed at two different points.

By comparing the results of perturbative RG approach and DEBC-method with the explicit calculation of the  $g$ -function and the implications of the  $g$ -theorem, we have mapped out a remarkable correspondence between the  $N = 2$  junction and the non- $\mathbf{Z}_3$ -symmetric Y3J, for suitably chosen values of the system parameters. In particular, we have employed the correspondence to recover informations about the phase diagram of the former system from known results about the phase diagram of the latter, and vice versa. Concerning the  $N = 2$  junction, we have shown that the condition  $K_\sigma > 1$  is enough to reverse its phase diagram with respect to the result of Ref. [18] for  $K_\sigma < 1$ . Increasing  $K_\sigma$  to values  $> 1$ , we proved that the FCFP corresponds to the true stable phase of the system and is identified with the  $M$ -FCFP of the Y3J and, eventually, that, for large enough values of  $K_\sigma$ , the  $N = 2$  junction undergoes a phase transition to a phase with perfect healing of the junction between wires-1 and -2, with the MM decoupled from the two wires. Conversely, for the Y3J, we demonstrated the emergence of a “planar” FCFP's (that is, with one of the boundary coupling strengths set to 0), which is a novel feature, so far not discussed for such systems. In addition, we were able to infer the phase diagram of the  $N = 2$ -junction at zero inter-wire interaction and for  $K > 1$  in each wire, a regime which was not discussed in Ref. [18].

Despite being effective in deriving a number of results on the phase diagram of both systems, the correspondence between the  $N = 2$  junction and the non- $\mathbf{Z}_3$ -symmetric Y3J still presents a number of “critical” issues, which will have to be further analyzed, possibly with the help of a numerical approach to the problem, such as the one employed in Ref. [53]. In particular, issues related to our work that deserve to be further analyzed are:

- The failure of the  $\epsilon$ -expansion method to provide quantitative results about the FCFP, when applied to the Y3J in the  $\mathbf{Z}_3$ -symmetric limit. As we show in [Appendix D.2](#), the perturbative  $\beta$ -function for the boundary running coupling in the Y3J contain terms that are all  $\propto \epsilon$ , which makes the perturbative RG approach not reliable for extracting informations about the FCFP, at variance to what happens in the  $N = 2$ -junction [18]. (Yet, it must be stressed that, while not applicable in general, the  $\epsilon$ -expansion method works fine for the Y3J, as well, in some range of values of the system's parameters, such as the one considered in section 4.1, leading to Eqs. (33,34) .)

- The nature of the FCFP that our correspondence predicts in the  $N = 2$  junction with no inter-wire interaction,  $1 < K < 2$  in each wire, and for symmetric boundary couplings. In particular, it would be extremely interesting to figure out whether there is still just one FCFP and whether it is continuously connected to the one we found in Ref. [18] for  $1/2 < K < 1$ , or if there is more than one FCFP's, possibly of some intrinsically different nature;

- Whether the fact that the correspondence extends to the  $g$ -function, despite the fact that the physical nature of the real modes in the Y3J and in the  $N = 2$  junction are fundamentally different, is just an accident, or can apply, possibly in some different form, in similar systems.

Apart from the ones listed above, from our results, there are a number of issues that we left over and should be properly addressed, such as the relation between the validity of the  $g$ -theorem in the presence of real fermionic modes and the conservation of the total fermion parity, the explicit calculation of the  $g$ -functions at FCFP's where the  $\epsilon$ -expansion method fails, or the extension of our derivation to systems such as the ‘‘Majorana-Kondo devices’’, which at the same time encompass Majorana and (topological) Kondo physics [29]. These topics are outside of the range of this work and we plan to address them in forthcoming publications.

## Acknowledgements

We thank P. Sodano for valuable discussions. The research of I.A. is supported by NSERC Discovery Grant 04033-2016 and the Canadian Institute for Advanced Research.

## Appendix A. Lattice Hamiltonian, boundary conditions and mode expansion of the bosonic fields

In this appendix, we concisely review the bosonization procedure for the interacting lattice fermionic Hamiltonian for the junction between  $N$  QW's and a TS. Following the bosonization procedure, we present the mode expansion for the bosonic fields entering the corresponding TLL Hamiltonian at given type  $N$ , or type  $A$ , boundary conditions at  $x = 0$  and at  $x = \ell$ .

The lattice model Hamiltonian for the  $N$ -wire junction is given by  $H_{N,\text{Fer}} = H_{0,\text{Fer},N} + H_{I,\text{Fer},N} + H_{b,\text{Fer},N}$ , with

$$\begin{aligned}
H_{0,\text{Fer},N} &= \sum_{a=1}^N \left\{ -J \sum_{j=1}^{\ell-2} \{ c_{j,a}^\dagger c_{j+1,a} + c_{j+1,a}^\dagger c_{j,a} \} - \mu \sum_{j=1}^{\ell-1} c_{j,a}^\dagger c_{j,a} \right\} \\
H_{I,\text{Fer},N} &= V \sum_{a=1}^N \sum_{j=1}^{\ell-2} \left( c_{j,a}^\dagger c_{j,a} - \frac{1}{2} \right) \left( c_{j+1,a}^\dagger c_{j+1,a} - \frac{1}{2} \right) + U \sum_{a \neq b=1}^N \sum_{j=1}^{\ell-1} \left( c_{j,a}^\dagger c_{j,a} - \frac{1}{2} \right) \left( c_{j,b}^\dagger c_{j,b} - \frac{1}{2} \right) \\
H_{b,\text{Fer},N} &= - \sum_{a=1}^N t_a \gamma_L \{ c_{a,1} - c_{a,1}^\dagger \} - i \sum_{a=1}^N t_a \gamma_R \{ c_{a,\ell-1} + c_{a,\ell-1}^\dagger \} \equiv H_{b,\text{Fer},N}^{(1)} + H_{b,\text{Fer},N}^{(\ell-1)} \quad , \quad (\text{A.1})
\end{aligned}$$

with  $\gamma_L, \gamma_R$  being the localized MM's at the junctions between the QW's and the TS and the  $t_a$ 's being all real and positive, as a possible phase can be always reabsorbed into an appropriate redefinition of the lattice fields. In the absence of interaction, retaining only low-energy,

long-wavelength fermionic modes allows for expanding the lattice fermion operators as  $c_{j,a} \sim \{e^{ik_f j} \psi_{R,a}(x) + e^{-ik_f j} \psi_{L,a}(x)\}$ , with the Fermi momentum  $\pm k_f = \arccos\left(-\frac{\mu}{2J}\right)$ . Bosonizing the chiral fermionic fields requires introducing  $N$  pairs of canonically conjugate fields  $\{\phi_{R,a}(x), \phi_{L,a}(x)\}$  ( $a = 1, \dots, N$ ). In the noninteracting limit, they can be expressed in terms of  $N$  pairs of chiral bosonic fields as

$$\begin{aligned}\psi_{R,a}(x) &= \Gamma_a e^{i\sqrt{4\pi}\phi_{R,a}(x)} \\ \psi_{L,a}(x) &= \Gamma_a e^{i\sqrt{4\pi}\phi_{L,a}(x)}\end{aligned}\quad . \quad (\text{A.2})$$

with the chiral bosonic fields satisfying the algebra

$$\begin{aligned}[\phi_{R,a}(x), \phi_{R,a}(x')] &= -[\phi_{L,a}(x), \phi_{L,a}(x')] = \frac{i}{4}\epsilon(x-x') \\ [\phi_{R,a}(x), \phi_{L,a}(x')] &= -[\phi_{L,a}(x'), \phi_{R,a}(x)] = \frac{i}{4}\end{aligned}\quad , \quad (\text{A.3})$$

with all the other commutators equal to 0, and the  $N$  KF's defined so that  $\{\Gamma_a, \Gamma_{a'}\} = 2\delta_{a,a'}$ , and, if  $H_{b,\text{Fer},N}$  contains localized MM's  $\gamma_1, \dots, \gamma_M$ , requiring that  $\{\gamma_j, \Gamma_a\} = 0, \forall a, j$ . In the interacting case, Eqs. (A.2) are replaced by

$$\begin{aligned}\psi_{R,a}(x) &= \Gamma_a e^{i\sqrt{\pi}[\phi_a(x) + \theta_a(x)]} \\ \psi_{L,a}(x) &= \Gamma_a e^{i\sqrt{\pi}[\phi_a(x) - \theta_a(x)]}\end{aligned}\quad . \quad (\text{A.4})$$

with the (canonically conjugate) fields  $\{\phi_a(x), \theta_a(x)\}$  described by the bulk Hamiltonian  $H_{N,B} = H_{N,B,0} + H_{N,B,\text{Inter}}$  and

$$\begin{aligned}H_{N,B,0} &= \frac{u}{2} \int_0^\ell dx \sum_{a=1}^N [K(\partial_x \phi_a(x))^2 + K^{-1}(\partial_x \theta_a(x))^2] \\ H_{N,B,\text{Inter}} &= \sum_{a \neq b=1}^N \frac{U}{2\pi} \int_0^\ell dx [(\partial_x \theta_a(x))(\partial_x \theta_b(x))]\end{aligned}\quad , \quad (\text{A.5})$$

with the Luttinger parameter  $K$  and the plasmon velocity  $u$  determined by the intra-wire interaction  $V$  and by the Fermi velocity in the wires,  $v_f$ . By means of an appropriate orthogonal transformation,  $H_{N,B}$  can be separated into independent terms by rotating to the basis of the center-of-mass fields  $\Phi(x), \Theta(x)$  and the relative fields  $\varphi_1(x), \dots, \varphi_{N-1}(x)$  and  $\vartheta_1(x), \dots, \vartheta_{N-1}(x)$ , defined as

$$\begin{bmatrix} \Phi(x) \\ \varphi_1(x) \\ \vdots \\ \varphi_{N-1}(x) \end{bmatrix} = \mathbf{M}_N \begin{bmatrix} \phi_1(x) \\ \phi_2(x) \\ \vdots \\ \phi_N(x) \end{bmatrix}, \quad \begin{bmatrix} \Theta(x) \\ \vartheta_1(x) \\ \vdots \\ \vartheta_{N-1}(x) \end{bmatrix} = \mathbf{M}_N \begin{bmatrix} \theta_1(x) \\ \theta_2(x) \\ \vdots \\ \theta_N(x) \end{bmatrix}, \quad (\text{A.6})$$

with the matrix  $\mathbf{M}_N$  only depending on  $N$  and given by

$$\mathbf{M}_N = \begin{bmatrix} \frac{1}{\sqrt{N}} & \frac{1}{\sqrt{N}} & \frac{1}{\sqrt{N}} & \cdots & \frac{1}{\sqrt{N}} \\ \frac{1}{\sqrt{2}} & -\frac{1}{\sqrt{2}} & 0 & \cdots & 0 \\ \frac{1}{\sqrt{6}} & \frac{1}{\sqrt{6}} & -\frac{2}{\sqrt{6}} & \cdots & 0 \\ \cdots & \cdots & \cdots & \cdots & \cdots \\ \frac{1}{\sqrt{N(N-1)}} & \frac{1}{\sqrt{N(N-1)}} & \frac{1}{\sqrt{N(N-1)}} & \cdots & -\frac{(N-1)}{\sqrt{N(N-1)}} \end{bmatrix}. \quad (\text{A.7})$$

In terms of the rotated fields, one obtains

$$H_{N,B} = \frac{u_\rho}{2} \int_0^\ell dx [K_\rho (\partial_x \Phi(x))^2 + K_\rho^{-1} (\partial_x \Theta(x))^2] + \frac{u_\sigma}{2} \int_0^\ell dx \sum_{a=1}^{N-1} [K_\sigma (\partial_x \varphi_a(x))^2 + K_\sigma^{-1} (\partial_x \vartheta_a(x))^2] , \quad (\text{A.8})$$

with

$$\begin{aligned} u_\rho K_\rho &= uK \quad , \quad \frac{u_\rho}{K_\rho} = u \left( K^{-1} + \frac{(N-1)U}{\pi u} \right) \\ u_\sigma K_\sigma &= uK \quad , \quad \frac{u_\sigma}{K_\sigma} = u \left( K^{-1} - \frac{U}{\pi u} \right) . \end{aligned} \quad (\text{A.9})$$

Eqs. (A.9) yield  $(u_\rho, K_\rho) = (u_N, K_N)$  and  $(u_\sigma, K_\sigma) = (u_0, K_0)$ , with  $K_n = K / \sqrt{1 + \frac{(n-1)UK}{\pi u}}$  and  $u_n = u \sqrt{1 + \frac{(n-1)UK}{\pi u}}$ . Note that, in particular, Eqs. (A.9) are consistently defined only as long as  $\frac{KU}{\pi u} < 1$ , which is our over-all assumption in this work. Also, for a repulsive inter-wire interaction ( $U > 0$ ), by definition one always has  $K_\rho < 1$ . As stated in section 3.1,  $H_{N,B}$ , for  $N = 2$ , corresponds to the bulk Hamiltonian of Ref. [18], with equal Luttinger parameters in the two wires,  $K_1 = K_2 = K, u_1 = u_2 = u$ . Following the notation of Ref. [18], we use  $N$  to denote open boundary conditions at both boundaries in a single bosonic channel corresponding to a disconnected wire, which implies pure normal reflection at both boundaries. This implies open boundary conditions for the lattice fermions [20] or, in terms of the bosonic fields, pinning of  $\theta_a(x)$  at both boundaries, as  $\theta_a(0) = \sqrt{\pi} n_{0,a}, \theta_a(\ell) = \sqrt{\pi} n_{\ell,a}, n_{0,a}, n_{\ell,a} \in \mathbf{Z}$ .

As a simple, paradigmatic, example we consider a single field  $\phi(x)$  which, together with its dual field  $\theta(x)$ , is described by the TLL Hamiltonian

$$H = \frac{u}{2} \int_0^\ell dx [K (\partial_x \phi(x))^2 + K^{-1} (\partial_x \theta(x))^2] . \quad (\text{A.10})$$

Imposing Neumann boundary conditions on  $\phi(x)$  at both boundaries implies the mode expansions

$$\begin{aligned} \phi(x) &= \phi_0 + \sum_{n=1}^{\infty} \left\{ \frac{1}{\sqrt{K\pi n}} \cos \left[ \frac{\pi n x}{\ell} \right] [\alpha_n + \alpha_n^\dagger] \right\} \\ \theta(x) &= \theta_0 + \frac{p_\phi x}{\ell} + i \sum_{n=1}^{\infty} \left\{ \sqrt{\frac{K}{\pi n}} \sin \left[ \frac{\pi n x}{\ell} \right] [\alpha_n - \alpha_n^\dagger] \right\} , \end{aligned} \quad (\text{A.11})$$

with the oscillator modes satisfying the algebra  $[\alpha_n, \alpha_{n'}^\dagger] = n \delta_{n,n'}$  and the spectrum of the zero-mode operators given by  $p_\phi = \sqrt{\pi} m_\phi$ , with  $m_\phi$  relative integer. A mode expansion complementary to the one in Eqs. (A.11) is recovered when imposing type A boundary conditions on  $\phi(x)$  at both boundaries, and, accordingly, type N boundary conditions on  $\theta(x)$ . In this case, one obtains

$$\begin{aligned} \phi(x) &= \phi_0 + \frac{p_\theta x}{\ell} + i \sum_{n=1}^{\infty} \left\{ \frac{1}{\sqrt{K\pi n}} \sin \left[ \frac{\pi n x}{\ell} \right] [\alpha_n - \alpha_n^\dagger] \right\} \\ \theta(x) &= \theta_0 + \sum_{n=1}^{\infty} \left\{ \sqrt{\frac{K}{\pi n}} \cos \left[ \frac{\pi n x}{\ell} \right] [\alpha_n + \alpha_n^\dagger] \right\} , \end{aligned} \quad (\text{A.12})$$

with the eigenvalues of  $p_\theta$  equal to  $\sqrt{\pi}m_\theta$ , and  $m_\theta$  relative integer.

For the  $N$ -wire junction, when all the wires satisfy type  $N$  boundary conditions at both boundaries, one obtains the mode expansion

$$\begin{aligned}
\Phi(x) &= \Phi_0 + \sum_{n=1}^{\infty} \left\{ \frac{1}{\sqrt{K_\rho \pi n}} \cos \left[ \frac{\pi n x}{\ell} \right] [\alpha_{c,n} + \alpha_{c,n}^\dagger] \right\} \\
\varphi_a(x) &= \varphi_{a,0} + \sum_{n=1}^{\infty} \left\{ \frac{1}{\sqrt{K_\sigma \pi n}} \cos \left[ \frac{\pi n x}{\ell} \right] [\alpha_{a,n} + \alpha_{a,n}^\dagger] \right\} \\
\Theta(x) &= \Theta_0 + \frac{p_\Phi x}{\ell} + i \sum_{n=1}^{\infty} \left\{ \sqrt{\frac{K_\rho}{\pi n}} \sin \left[ \frac{\pi n x}{\ell} \right] [\alpha_{c,n} - \alpha_{c,n}^\dagger] \right\} \\
\vartheta_a(x) &= \vartheta_{a,0} + \frac{p_{a,\varphi} x}{\ell} + i \sum_{n=1}^{\infty} \left\{ \sqrt{\frac{K_\sigma}{\pi n}} \sin \left[ \frac{\pi n x}{\ell} \right] [\alpha_{a,n} - \alpha_{a,n}^\dagger] \right\} , \tag{A.13}
\end{aligned}$$

with the oscillator modes satisfying the algebra  $[\alpha_{b,n}, \alpha_{b',n'}^\dagger] = n\delta_{b,b'}\delta_{n,n'}$ , and the spectrum of the zero-mode operators given by

$$\begin{bmatrix} p_\Phi \\ p_{1,\varphi} \\ \vdots \\ p_{N-1,\varphi} \end{bmatrix} = \mathbf{M}_N \begin{bmatrix} \sqrt{\pi}m_{1,\phi} \\ \sqrt{\pi}m_{2,\phi} \\ \vdots \\ \sqrt{\pi}m_{N,\phi} \end{bmatrix} , \tag{A.14}$$

with  $m_{1,\phi}, \dots, m_{N,\phi}$  relative integers. In the general case in which one has type  $A$  CIBC's at both boundaries in the first  $N_a$  channels and type  $N$  CIBC's in the remaining  $N_n$  ones, Eqs. (A.14) generalize to

$$\begin{bmatrix} p_\Theta \\ p_{1,\vartheta} \\ \vdots \\ p_{N-1,\vartheta} \end{bmatrix} = \mathbf{M}_N \begin{bmatrix} \sqrt{\pi}m_{1,\theta} \\ \vdots \\ \sqrt{\pi}m_{N_a,\theta} \\ \vdots \\ 0 \end{bmatrix} , \quad \begin{bmatrix} p_\Phi \\ p_{1,\varphi} \\ \vdots \\ p_{N-1,\varphi} \end{bmatrix} = \mathbf{M}_N \begin{bmatrix} 0 \\ \vdots \\ \sqrt{\pi}m_{N_a+1,\phi} \\ \vdots \\ \sqrt{\pi}m_{N,\phi} \end{bmatrix} , \tag{A.15}$$

for the eigenvalues of the zero-mode operators of the  $(\Phi, \varphi_1, \dots, \varphi_{N-1})$  and of the  $(\Theta, \vartheta_1, \dots, \vartheta_{N-1})$ -fields respectively, with  $m_{1,\theta}, \dots, m_{N_a,\theta}$  and  $m_{N_a+1,\phi}, \dots, m_{N,\phi}$  relative integers.

## Appendix B. Stabilization of fixed points with $N_a > 1$

In order to rigorously define the algorithm we use in the main text to count the degrees of freedom associated with real fermionic zero-mode operators at a fixed points with type  $A$  CIBC's in the first  $N_a$  channels, type  $N$  CIBC's in the remaining  $N_n$  channels, we now concisely review the approach employed in Ref. [18] to artificially stabilize the  $N_a = 2, N_n = 0$  fixed point in the  $N = 2$  junction and eventually extend it to the  $N$ -wire junction, with a generic  $N$ . As a reference

model Hamiltonian, we consider  $H_{N,\text{Fer}}$  in Eq. (A.1) taken in the noninteracting limit. To recover type  $N$  CIBC's in the last  $N_n = N - N_a$  channels, we set  $t_{N_a+1} = \dots = t_N = 0$ . Next, we rewrite the complex fermion lattice operators in the first  $N_a$  channels in terms of real fermion lattice operators  $\{\xi_{j,a}, \eta_{j,a}\}$  as

$$\begin{aligned} c_{j,a} &= \frac{1}{2} \{\xi_{j,a} + i\eta_{j,a}\} \\ c_{j,a}^\dagger &= \frac{1}{2} \{\xi_{j,a} - i\eta_{j,a}\} \quad , \end{aligned} \quad (\text{B.1})$$

with  $a = 1, \dots, N_a$ . In terms of the real fermion lattice operators, the boundary Hamiltonian  $H_{b,\text{Fer},N}$  can be rewritten as

$$H_{b,\text{Fer},N} = -2i \sum_{a=1}^{N_a} t_a \{\gamma_L \eta_{1,a} + \gamma_R \xi_{\ell-1,a}\} \quad . \quad (\text{B.2})$$

Now, we note that, besides  $H_{b,\text{Fer},N}$ , the operators  $\{\eta_{1,a}, \xi_{\ell-1,a}\}$  enter  $H_{0,\text{Fer},N}$  in the term  $H'$ , given by

$$H' = \sum_{a=1}^{N_a} \left\{ -\frac{iJ}{2} [\xi_{2,a} \eta_{1,a} + \xi_{\ell-1,a} \eta_{\ell-2,a}] - \frac{i\mu}{2} [\xi_{1,a} \eta_{1,a} + \xi_{\ell-1,a} \eta_{\ell-1,a}] - \frac{iJ}{2} [\xi_{1,a} \eta_{2,a} + \xi_{\ell-2,a} \eta_{\ell-1,a}] \right\} \quad . \quad (\text{B.3})$$

The key point, now, is to regard Eq. (B.3) as a special case of the generic Hamiltonian  $\tilde{H}'$ , defined as

$$\tilde{H}' = \sum_{a=1}^{N_a} \left\{ -\frac{iJ_{A,a}}{2} [\xi_{2,a} \eta_{1,a} + \xi_{\ell-1,a} \eta_{\ell-2,a}] - \frac{i\mu_a}{2} [\xi_{1,a} \eta_{1,a} + \xi_{\ell-1,a} \eta_{\ell-1,a}] - \frac{iJ_{B,a}}{2} [\xi_{1,a} \eta_{2,a} + \xi_{\ell-2,a} \eta_{\ell-1,a}] \right\}, \quad (\text{B.4})$$

with  $J_{A,a} = J_{B,a} = J$  and  $\mu_a = \mu$ . To stabilize a fixed point with type  $A$  CIBC's in the first  $N_a$  channels, we therefore fine-tune the parameters of  $\tilde{H}'$  as

$$\begin{aligned} J_{A,1} &= \dots = J_{A,N_a} = 0 \\ \mu_1 &= \dots = \mu_{N_a} = 0 \\ J_{B,1} &= \dots = J_{B,N_a} = J \quad . \end{aligned} \quad (\text{B.5})$$

As a result, QW's from 1 to  $N_a$  are separately coupled to a Majorana mode at their endpoints, respectively given by  $\xi_{1,a}$  and by  $\eta_{\ell-1,a}$ , which makes them all renormalize to  $A$  boundary conditions at both boundaries. As highlighted in section 2, this leaves one unpaired real fermion zero-mode operator for each one of the first  $N_a$  QW's. In addition, there are  $N_n$  KF's from the remaining decoupled  $N_n$  QW's plus, if  $N$  is odd, the auxiliary KF  $\bar{\Gamma}$ . To fully account for all the degrees of freedom one has eventually to consider the two MM's at the endpoints of the TS's and the  $2N_a$  real fermion operators  $\{\eta_{1,a}, \xi_{\ell-1,a}\}$ , with  $a = 1, \dots, N_a$ . They are coupled to each other via  $H_{b,\text{Fer},N}$  in Eq. (B.2), which implies additional  $2N_a - 2$  real fermion zero-mode operators. Taking all this into account, we eventually provide the results for  $\delta_e[N_a, N_n]$  and  $\delta_o[N_a, N_n]$  as

$$\begin{aligned}\delta_e[N_a, N_n] &= 2^{\frac{3N_a}{2} + \frac{N_n-2}{2}} \\ \delta_e[N_a, N_n] &= 2^{\frac{3N_a}{2} + \frac{N_n-1}{2}} \quad ,\end{aligned}\tag{B.6}$$

which are the formulas we use when computing the  $g$ -function in section 5.2.

In employing the method we develop here for the derivation of section 3.2 for the Y3J, we note that, when considering the two boundary Hamiltonian for this specific system, due to the fact that only three real fermion modes actually enter the boundary interaction (the three KF's from the three QW's), one recovers a sort of ‘‘special case’’, corresponding to  $N = 2$  and, formally,  $\gamma_L = \gamma_R = \hat{\gamma}$ . In this case,  $H_{b,\text{Fer},N}$  in Eq.(B.2) reduces to

$$\hat{H}_{b,\text{Fer},2} = -2i \sum_{a=1}^2 t_a \{ \hat{\gamma} [\eta_{1,a} + \xi_{\ell-1,a}] \} \quad ,\tag{B.7}$$

which has three zero-energy real fermion eigenmodes, differently from the case of two distinct MM's at the two boundaries

Before concluding this appendix, we concisely review how to use the construction detailed above to derive the set of allowed boundary operators at the  $A \otimes A$  fixed point of the  $N = 2$  junction. To do so, we resort to the one-boundary version of the system, with the corresponding boundary Hamiltonian,  $H_{b,F,2}^{(1)}$ , simply given by  $H_{b,\text{Fer},N=2}$  in Eq. (B.2), with the coupling to  $\gamma_R$  dropped off. Accordingly, we simplify Eq. (B.4), by also assuming that the couplings are the same in each channel, to

$$\tilde{H}' \rightarrow -\frac{iJ_A}{2} [\xi_{2,1}\eta_{1,1} + \xi_{2,2}\eta_{1,2}] - \frac{i\mu}{2} [\xi_{1,1}\eta_{1,1} + \xi_{1,2}\eta_{1,2}] - \frac{iJ_B}{2} [\xi_{1,1}\eta_{2,1} + \xi_{1,2}\eta_{1,2}] \quad ,\tag{B.8}$$

and, to stabilize the  $A \otimes A$  fixed point, we set  $J_A = \mu = 0$ . This makes  $H_{b,F,2}^{(1)}$  fully decouple from the bulk of the system. In particular, on rewriting it as

$$H_{b,F,2}^{(1)} = -2it\gamma_R\gamma \quad ,\tag{B.9}$$

with  $t = \sqrt{t_1^2 + t_2^2}$  and  $\gamma = \frac{t_1}{t}\eta_{1,1} + \frac{t_2}{t}\eta_{1,2}$ , we recover a real-fermionic zero-mode operator,  $\tilde{\gamma} = -\frac{t_2}{t}\eta_{1,1} + \frac{t_1}{t}\eta_{1,2}$ , which is fully decoupled from the system, as long as  $J_A = \mu = 0$ . Turning on  $J_A$  and  $\mu$ , the corresponding contribution to  $\tilde{H}'$ ,  $\delta\tilde{H}'$ , can be written as

$$\delta\tilde{H}' = -\frac{i}{2t} \{ [t_1(J_A\xi_{2,1} + \mu\xi_{1,1}) + t_2(J_A\xi_{2,2} + \mu\xi_{1,2})]\gamma + [-t_2(J_A\xi_{2,1} + \mu\xi_{1,1}) + t_1(J_A\xi_{2,2} + \mu\xi_{1,2})]\tilde{\gamma} \} .\tag{B.10}$$

At large values of  $t$ ,  $\gamma$  is locked together with  $\gamma_L$  so, in analogy to what happens with the residual coupling to the MM at the  $A \otimes N$  fixed point, the term  $\propto \gamma$  in  $\delta\tilde{H}'$  only contributes to second-order in the corresponding boundary couplings (see Ref. [18] for a detailed discussion about this point). To this order, it gives rise to the boundary operators arising from fermion bilinears at the  $A \otimes A$  fixed point: the inter-channel normal boundary backscattering and the inter-channel boundary pairing operator, the intra-channel normal backscattering operator in both channels. At variance,  $\tilde{\gamma}$  is decoupled from other real fermionic modes. Accordingly, the term in  $\delta\tilde{H}'$  that is  $\propto \tilde{\gamma}$  does act as an effective residual coupling to the MM, eventually leading to the boundary operators  $\tilde{V}_{1,\text{Res}}, \tilde{V}_{2,\text{Res}}$  of section 3.1.

## Appendix C. Duality and Poisson summation formula

As illustrated in the main text, at a given fixed point, the  $g$ -function corresponding to type  $A$  boundary conditions can be extracted from the partition function  $\mathcal{Z}_{AA} = \sum_n \exp\left[-\frac{x_{AA}^n \beta u}{\ell}\right]$ , by sending  $\ell \rightarrow \infty$  at fixed  $\beta$ . To recast  $\mathcal{Z}_{AA}$  in a form suitable for taking such a limit, one has to make a combined use of the duality properties of the Dedekind function, as well as of Poisson's summation formula (PSF), which we review in this appendix.

Given a complex number  $\tau = \tau_x + i\tau_y$ , with  $\tau_y > 0$ , and setting  $q = e^{\pi i \tau}$ , the Dedekind function  $\eta(q)$  is defined as  $\eta(q) = e^{\frac{\pi i}{24}} \prod_{n=1}^{\infty} [1 - q^n]$ .  $\eta(q)$  is known to exhibit the duality property (which is relevant to our derivation)  $\eta(q) = \frac{1}{\sqrt{-i\tau}} \eta(\tilde{q})$ , with  $\tilde{q} = e^{-\frac{2\pi i}{\tau}}$ . In fact, once one sets  $\tau = \frac{i\beta\pi}{u\ell}$ , one obtains the needed change of variable in the  $\eta$ -function.

Moving to PSF, for a single-variable function  $f(x)$ , it is defined starting from the quantity  $F$ , given by

$$F = \sum_{n \in \mathbf{Z}} f(n) \quad . \quad (\text{C.1})$$

Defining the Fourier transform of  $f(x)$ ,  $\hat{f}(p)$ , as

$$\hat{f}(p) = \int_{-\infty}^{\infty} dx e^{-ipx} f(x) \quad , \quad (\text{C.2})$$

PSF states the identity

$$F = \sum_{n \in \mathbf{Z}} f(n) = \sum_{m \in \mathbf{Z}} \hat{f}(m) \quad . \quad (\text{C.3})$$

PSF can be readily extended to a sum over a generic  $d$ -dimensional Bravais lattice  $\Lambda$ . Indeed, given a function of  $d$  variables,  $f(x_1, \dots, x_d)$ , we set

$$F = \sum_{\mathbf{R} \in \Lambda} f(\mathbf{R}) \quad . \quad (\text{C.4})$$

Assuming that,  $\forall \mathbf{R} \in \Lambda, \exists (n_1, \dots, n_d)$  such that  $\mathbf{R} = \sum_{i=1}^d n_i \mathbf{R}_i$ , we therefore obtain

$$F = \sum_{n_1, \dots, n_d \in \mathbf{Z}} f\left(\sum_{i=1}^d n_i \mathbf{R}_i\right) \quad . \quad (\text{C.5})$$

Let us define a  $d \times d$ -matrix  $\mathbf{A}$  such that,  $\forall x_1, \dots, x_d \in \mathbf{R}^d$ , one gets

$$\sum_{i=1}^d x_i \mathbf{R}_i = \mathbf{A} \cdot \begin{bmatrix} x_1 \\ \vdots \\ x_d \end{bmatrix} \quad . \quad (\text{C.6})$$

We note that we obtain

$$\frac{1}{(2\pi)^{\frac{d}{2}}} \int_{-\infty}^{\infty} dx_1 \dots dx_d e^{-i[p_1 x_1 + \dots + p_d x_d]} f\left(\mathbf{A} \cdot \begin{bmatrix} x_1 \\ \vdots \\ x_d \end{bmatrix}\right) = [\det\mathbf{A}]^{-1} \hat{f}\left(\mathbf{A}^{-1} \cdot \begin{bmatrix} p_1 \\ \vdots \\ p_d \end{bmatrix}\right) , \quad (\text{C.7})$$

with  $\hat{f}(p_1, \dots, p_d)$  being the multidimensional Fourier transform of  $f(x_1, \dots, x_d)$ . On explicitly performing the integral, we eventually get

$$F = \frac{1}{\det\mathbf{A}} \sum_{\mathbf{K} \in \Lambda^*} \hat{f}(\mathbf{K}) , \quad (\text{C.8})$$

with  $\Lambda^*$  being the dual lattice of  $\Lambda$ . Now, in the specific problem we consider, we typically obtain

$$f(x_1, \dots, x_d) = \exp\left[-\frac{\pi\beta u}{2K\ell}(x_1^2 + \dots + x_d^2)\right] \Rightarrow \hat{f}(p_1, \dots, p_d) = \left(\frac{2\ell K}{\beta u}\right)^{\frac{d}{2}} \exp\left[-\frac{\ell K}{2\pi\beta u}(p_1^2 + \dots + p_d^2)\right]. \quad (\text{C.9})$$

Eq. (C.9) eventually implies

$$\sum_{\mathbf{R} \in \Lambda} \exp\left[-\frac{\pi\beta u}{2K\ell}|\mathbf{R}|^2\right] = \frac{1}{\det\mathbf{A}} \left(\frac{2\ell K}{\beta u}\right)^{\frac{d}{2}} \sum_{\mathbf{K} \in \Lambda^*} \exp\left[-\frac{\ell K}{2\pi\beta u}|\mathbf{K}|^2\right] . \quad (\text{C.10})$$

Finally, using the duality of the Dedekind function, we get

$$\eta\left(e^{-\frac{\pi\beta u}{\ell}}\right) = \sqrt{\left(\frac{2\ell}{\beta u}\right)} \eta\left(e^{-\frac{4\pi\ell}{\beta u}}\right) , \quad (\text{C.11})$$

which eventually implies

$$\eta^{-d}\left(e^{-\frac{\pi\beta u}{\ell}}\right) \sum_{\mathbf{R} \in \Lambda} \exp\left[-\frac{\pi\beta u}{2K\ell}|\mathbf{R}|^2\right] = \frac{K^{\frac{d}{2}}}{\det\mathbf{A}} \eta^{-d}\left(e^{-\frac{4\pi\ell}{\beta u}}\right) \sum_{\mathbf{K} \in \Lambda^*} \exp\left[-\frac{\ell K}{2\pi\beta u}|\mathbf{K}|^2\right] . \quad (\text{C.12})$$

Eq. (C.12) is the key equation we use to compute the  $g$ -function at the various fixed points of the systems we study in our paper.

## Appendix D. Review of the $\epsilon$ -expansion approach to junction of quantum wires

In this appendix, we review the  $\epsilon$ -expansion approach to the RG equations and to the calculation of the  $g$ -function at the FCFP's in a junction between  $N$  interacting quantum wires and a topological superconductor and in the Y3J. In the former case, we revisit and generalize the derivation discussed in Ref. [18]. In the latter case, we highlight the peculiarities of the  $\epsilon$ -expansion applied to the Y3J, estimate the  $g$ -function at the FCFP of such a system [2] and eventually discuss the analogies with the  $N$ -wire junction.

*Appendix D.1. Renormalization group equations for a junction between  $N$  quantum wires and a topological superconductor*

To encompass FCFP's, the  $\beta$ -functions for the boundary couplings of a junction between  $N$  quantum wires and a topological superconductor must include nonlinear terms in the boundary couplings themselves. This requires employing an adapted version of Cardy's method to derive nonlinear contributions to the  $\beta$ -function in perturbed conformal field theories from two-point OPE's [54], to terms involving up to three-point OPE's in the boundary interaction operators [36, 18]. The starting point is the full partition function  $\mathcal{Z}$  written as a power series of the boundary action  $S_b$  as

$$\mathcal{Z} = \mathcal{Z}_0 \sum_{n=0}^{\infty} \frac{(-1)^n}{n!} \langle \mathbf{T}_\tau S_b^n \rangle_0 \quad , \quad (\text{D.1})$$

with  $S_b = \int_{-\frac{\beta}{2}}^{\frac{\beta}{2}} d\tau H_b(\tau)$ ,  $H_b(\tau)$  being the boundary Hamiltonian in imaginary time  $\tau$ ,  $\mathbf{T}_\tau$  being the imaginary time-ordering operator,  $\mathcal{Z}_0$  being the partition function computed at the reference point corresponding to the absence of boundary interactions (that is, the disconnected fixed point), and  $\langle \dots \rangle_0$  denoting averages computed at the reference fixed point. In addition, to regularize diverging contributions arising at short imaginary-time distances, one introduces a hard-core short imaginary time cutoff  $\tau_0$  by requiring  $|\tau_i - \tau_j| \geq \tau_0$  for all  $i \neq j$ . To derive the RG equations, we increase  $\tau_0$  to  $\tau_0 + \delta\tau$  (which corresponds to reducing the cut-off  $D_0$  in energy domain) and derive how the  $\bar{t}_a$ 's correspondingly change. Using as boundary Hamiltonian  $H_{b,B,N}^{(1)}$  in Eq. (60), we see that, to second order in the  $\bar{t}_a$ 's, only terms not involving  $\gamma_L$  can be generated which, clearly, do not contribute any renormalization to the boundary couplings. Therefore, to find the leading nonlinear correction to  $\beta$ -functions, one has to go to third order in the  $\bar{t}_a$ 's. In doing so, one has to systematically subtract terms equal to  $H_b(\tau)$  times a free-energy correction arising to second order in the boundary couplings. Considering that a boundary operator product factorizes into a product of real fermion operators (MM's and/or KF's) and a product of bosonic vertex operators, we therefore begin by reviewing the following rules for the fermionic OPE's [18]:

$$\begin{aligned} \mathbf{T}_\tau[\gamma_L(\tau_1)\gamma_L(\tau_2)\gamma_L(\tau_3)] &= \epsilon(\tau_1, \tau_2, \tau_3)\gamma_L \\ \mathbf{T}_\tau[\Gamma_a(\tau_1)\Gamma_a(\tau_2)\Gamma_a(\tau_3)] &= \epsilon(\tau_1, \tau_2, \tau_3)\Gamma_a \\ \mathbf{T}_\tau[\Gamma_a(\tau_1)\Gamma_a(\tau_2)\Gamma_b(\tau_3)] &= \epsilon(\tau_1, \tau_2)\Gamma_b \quad , \end{aligned} \quad (\text{D.2})$$

with  $a \neq b$  and  $\epsilon(\tau_1, \tau_2, \tau_3)$ ,  $\epsilon(\tau_1, \tau_2)$  being fully antisymmetric functions of their arguments. Moreover, we also need the rules for the OPE's between bosonic vertex operators, which we here review in the large-system size, zero-temperature limit, and which are given by

$$\begin{aligned} \mathbf{T}_\tau[e^{i\sqrt{\pi}\phi_a(\tau_1)}e^{i\sqrt{\pi}\phi_a(\tau_2)}e^{-i\sqrt{\pi}\phi_a(\tau_3)}] &\rightarrow_{\tau_1 \sim \tau_2 \sim \tau_3} \left| \frac{\tau_1 - \tau_2}{(\tau_1 - \tau_3)(\tau_2 - \tau_3)} \right|^{2d_b} e^{i\sqrt{\pi}\phi_a(\tau_3)} \\ \mathbf{T}_\tau[e^{i\sqrt{\pi}\phi_a(\tau_1)}e^{-i\sqrt{\pi}\phi_a(\tau_2)}e^{i\sqrt{\pi}\phi_b(\tau_3)}] &\rightarrow_{\tau_1 \sim \tau_2 \sim \tau_3} \left| \frac{\tau_1 - \tau_3}{\tau_2 - \tau_3} \right|^{\frac{1}{Nk_p} - \frac{1}{Nk_\sigma}} \left| \frac{1}{\tau_1 - \tau_2} \right|^{2d_b} e^{i\sqrt{\pi}\phi_b(\tau_3)} \quad , \end{aligned} \quad (\text{D.3})$$

with  $a \neq b$ , et cetera. Following the derivation of Ref. [18], we also make the assumption that the coupling to the Majorana mode is a slightly relevant operator, that is, that we have  $1 - (2d_b)^{-1} = \epsilon$ , with  $0 < \epsilon \ll 1$ . Now, to leading order in  $\epsilon$ , we set  $d_b^{-1} = 2$  in the integrals involving the OPE's at the right hand side of Eq. (D.3). Accordingly, due to the remarkable identity

$$\left| \frac{\tau_1 - \tau_2}{(\tau_1 - \tau_3)(\tau_2 - \tau_3)} \right|^2 + \left| \frac{\tau_1 - \tau_3}{(\tau_1 - \tau_2)(\tau_2 - \tau_3)} \right|^2 + \left| \frac{\tau_2 - \tau_3}{(\tau_1 - \tau_3)(\tau_1 - \tau_2)} \right|^2 = \frac{1}{|\tau_1 - \tau_2|^2} + \frac{1}{|\tau_1 - \tau_3|^2} + \frac{1}{|\tau_2 - \tau_3|^2} \quad , \quad (\text{D.4})$$

after subtracting the free energy correction times  $H_b$ , as discussed above, we see that, to leading order in  $\epsilon$ , no renormalization of the  $t_a$ 's arises that is  $\propto t_a^3$ . Instead, a nonzero renormalization of the boundary coupling arises from corrections to the boundary action that can be derived by a straightforward generalization of the analysis done in Ref. [18] for  $N = 2$ . In particular, the relevant correction turns out to be given by

$$\delta S_b^{(3)} = 2i \sum_{a=1}^N \int d\tau_1 \frac{t_a}{\tau_0^\epsilon} \gamma_L(\tau_1) \Gamma_a(\tau_1) \cos[\sqrt{\pi} \phi_a(\tau_1)] \frac{1}{2} \sum_{b \neq a=1}^N \frac{t_b^2}{\tau_0^{2\epsilon}} \int d\tau_2 d\tau_3 \times \left\{ \left| \frac{\tau_1 - \tau_2}{\tau_1 - \tau_3} \right|^\nu + \left| \frac{\tau_1 - \tau_3}{\tau_1 - \tau_2} \right|^\nu \epsilon(\tau_1 - \tau_2) \epsilon(\tau_1 - \tau_3) - 1 \right\} \frac{1}{|\tau_1 - \tau_2|^2} \prod_{i < j=1}^N \theta(|\tau_i - \tau_j| - \tau_0) \quad , \quad (\text{D.5})$$

with  $\nu = \frac{1}{NK_\rho} - \frac{1}{NK_\sigma}$  and the cutoff function explicitly denoted. At this point, by analogy with Ref. [18], one differentiates Eq. (D.5), obtaining the nonlinear corrections to the  $\beta$ -functions for the running couplings. As a result, one gets

$$\frac{d\bar{t}_a}{d \ln(\tau/\tau_0)} = \frac{d\bar{t}_a}{d \ln\left(\frac{D_0}{D}\right)} = \epsilon \bar{t}_a - \mathcal{F}(\nu) \bar{t}_a \sum_{b \neq a=1}^N \bar{t}_b^2 \quad , \quad (\text{D.6})$$

with

$$\mathcal{F}(\nu) = 6 - 2 \int_1^\infty dx \left[ \frac{(x+1)^\nu + (x+1)^{-\nu}}{x^2} - \frac{x^\nu + x^{-\nu}}{(x+1)^2} + \left( \frac{x+1}{x} \right)^\nu + \left( \frac{x+1}{x} \right)^{-\nu} - 2 \right] \quad , \quad (\text{D.7})$$

that is, Eq. (65) of the main text.

#### Appendix D.2. Renormalization group equations for the running coupling strengths at a Y-junction of three spinless interacting quantum wires

We now extend the  $\epsilon$ -approach to derive the RG equations for the Y3J with  $1 < K < 3$  and, in general, boundary couplings all different from each other. To do so, we start from the boundary Euclidean action  $S_b$ , which is now given by

$$\begin{aligned}
S_b = & -\frac{\bar{t}_{2,1}}{\tau_0^\epsilon} \int d\tau \Gamma_1(\tau)\Gamma_2(\tau)[e^{-i\sqrt{\pi}\phi_{1,2}(\tau)} - e^{i\sqrt{\pi}\phi_{1,2}(\tau)}] - \frac{\bar{t}_{3,2}}{\tau_0^\epsilon} \int d\tau \Gamma_2(\tau)\Gamma_3(\tau)[e^{-i\sqrt{\pi}\phi_{2,3}(\tau)} - e^{i\sqrt{\pi}\phi_{2,3}(\tau)}] \\
& - \frac{\bar{t}_{1,3}}{\tau_0^\epsilon} \int d\tau \Gamma_3(\tau)\Gamma_1(\tau)[e^{-i\sqrt{\pi}\phi_{3,1}(\tau)} - e^{i\sqrt{\pi}\phi_{3,1}(\tau)}] \quad , \quad (D.8)
\end{aligned}$$

with  $\phi_{a,b}(\tau) = \phi_a(0, \tau) - \phi_b(0, \tau)$ ,  $\epsilon = 1 - \frac{1}{K}$  and  $\bar{t}_{a+1,a}$  denoting the dimensionless coupling strengths. To implement the  $\epsilon$ -expansion, we assume  $K > 1$  and  $0 < 1 - K^{-1} \ll 1$ . The key ingredients of our derivation are the OPE's between the operators entering  $S_b$ , which are given by

$$\begin{aligned}
\langle \mathbf{T}_\tau \Gamma_a(\tau_1)\Gamma_b(\tau_2) \rangle &= \delta_{a,b}\epsilon(\tau_1 - \tau_2) \\
\langle \mathbf{T}_\tau e^{\pm i\sqrt{\pi}\phi_a(\tau_1)} e^{\mp i\sqrt{\pi}\phi_b(\tau_2)} \rangle &= \frac{\delta_{a,b}}{|\tau_1 - \tau_2|^{\frac{1}{K}}} \quad . \quad (D.9)
\end{aligned}$$

In principle, nonzero contributions to the  $\beta$ -function may arise to  $\mathcal{O}(\bar{t}_a\bar{t}_b)$ . To check whether this is the case, we consider the OPE

$$\begin{aligned}
& \sum_{a,b=1,2,3} \bar{t}_{a+1,a}\bar{t}_{b+1,b} \mathbf{T}_\tau \{ \Gamma_a(\tau_1)\Gamma_{a+1}(\tau_1)[e^{-i\sqrt{\pi}\phi_{a,a+1}(\tau_1)} - e^{i\sqrt{\pi}\phi_{a,a+1}(\tau_1)}] \Gamma_b(\tau_2)\Gamma_{b+1}(\tau_2)[e^{-i\sqrt{\pi}\phi_{b,b+1}(\tau_2)} - e^{i\sqrt{\pi}\phi_{b,b+1}(\tau_2)}] \} \\
& =_{\tau_1 \sim \tau_2} -2\{\bar{t}_{2,1}^2 + \bar{t}_{3,2}^2 + \bar{t}_{1,3}^2\} |\tau_1 - \tau_2|^{-\frac{2}{K}} \theta(|\tau_1 - \tau_2| - \tau_0) - \epsilon(\tau_1 - \tau_2) \times \\
& \sum_{a \neq b=1,2,3} \bar{t}_{a+1,a}\bar{t}_{b+1,b} \mathbf{T}_\tau \{ \Gamma_a(\tau_1)\Gamma_b(\tau_2)[e^{-i\sqrt{\pi}[\phi_a(\tau_1) - \phi_b(\tau_2)]} + e^{i\sqrt{\pi}[\phi_a(\tau_1) - \phi_b(\tau_2)]}] \} |\tau_1 - \tau_2|^{-\frac{1}{K}} \theta(|\tau_1 - \tau_2| - \tau_0), \quad (D.10)
\end{aligned}$$

with  $3 + 1 \equiv 1$ . The term on the right-hand side of Eq. (D.10) merely renormalizes the total free energy. Therefore, to find nonlinear contributions to the  $\beta$ -functions for the boundary couplings, we need to go to third order in the  $\bar{t}_{a+1,a}$ 's. This requires considering the three-point OPE's between operators entering  $S_b$ . In doing this, we find three different contributions, which we separately discuss in the following

- **Term number 1:**

Taking into account the symmetries effective under integrating over the imaginary times and taking the  $\beta \rightarrow \infty$ -limit, one obtains a correction to the boundary action,  $\delta S_b^{(1)}$ , given by

$$\begin{aligned}
\delta S_b^{(1)} = & \frac{\bar{t}_{2,1}(\bar{t}_{3,2}^2 + \bar{t}_{1,3}^2)}{2} \int d\tau_1 d\tau_2 d\tau_3 \epsilon(\tau_1 - \tau_3)\epsilon(\tau_2 - \tau_3) \prod_{i<j=1}^3 \theta(|\tau_i - \tau_j| - \tau_0) \Gamma_1(\tau_3)\Gamma_2(\tau_3) \times \\
& \left\{ \frac{|\tau_1 - \tau_3|^{\frac{1}{K}}}{|\tau_1 - \tau_2|^{\frac{2}{K}}|\tau_2 - \tau_3|^{\frac{1}{K}}} + \frac{|\tau_2 - \tau_3|^{\frac{1}{K}}}{|\tau_1 - \tau_2|^{\frac{2}{K}}|\tau_1 - \tau_3|^{\frac{1}{K}}} \right\} [e^{-i\sqrt{\pi}\phi_{1,2}(\tau_3)} - e^{i\sqrt{\pi}\phi_{1,2}(\tau_3)}] + \\
& \frac{\bar{t}_{3,2}(\bar{t}_{1,3}^2 + \bar{t}_{2,1}^2)}{2} \int d\tau_1 d\tau_2 d\tau_3 \epsilon(\tau_1 - \tau_3)\epsilon(\tau_2 - \tau_3) \prod_{i<j=1}^3 \theta(|\tau_i - \tau_j| - \tau_0) \Gamma_2(\tau_3)\Gamma_3(\tau_3) \times \\
& \left\{ \frac{|\tau_1 - \tau_3|^{\frac{1}{K}}}{|\tau_1 - \tau_2|^{\frac{2}{K}}|\tau_2 - \tau_3|^{\frac{1}{K}}} + \frac{|\tau_2 - \tau_3|^{\frac{1}{K}}}{|\tau_1 - \tau_2|^{\frac{2}{K}}|\tau_1 - \tau_3|^{\frac{1}{K}}} \right\} [e^{-i\sqrt{\pi}\phi_{2,3}(\tau_3)} - e^{i\sqrt{\pi}\phi_{2,3}(\tau_3)}] +
\end{aligned}$$

$$\frac{\bar{t}_{1,3}(\bar{t}_{2,1}^2 + \bar{t}_{3,2}^2)}{2} \int d\tau_1 d\tau_2 d\tau_3 \epsilon(\tau_1 - \tau_3)\epsilon(\tau_2 - \tau_3) \prod_{i<j=1}^3 \theta(|\tau_i - \tau_j| - \tau_0) \Gamma_3(\tau_3)\Gamma_1(\tau_3) \times$$

$$\left\{ \frac{|\tau_1 - \tau_3|^{\frac{1}{k}}}{|\tau_1 - \tau_2|^{\frac{2}{k}}|\tau_2 - \tau_3|^{\frac{1}{k}}} + \frac{|\tau_2 - \tau_3|^{\frac{1}{k}}}{|\tau_1 - \tau_2|^{\frac{2}{k}}|\tau_1 - \tau_3|^{\frac{1}{k}}} \right\} [e^{-i\sqrt{\pi}\phi_{3,1}(\tau_3)} - e^{i\sqrt{\pi}\phi_{3,1}(\tau_3)}], \quad (\text{D.11})$$

minus a term given by the product of  $S_b$  times the free energy correction to  $O(\bar{t}_a^2)$ . Performing the subtraction and using shifted integration variables, we eventually find

$$\delta S_b^{(1)} = \int dw_1 dw_2 \theta(|w_1| - \tau_0) \theta(|w_2| - \tau_0) \theta(|w_1 - w_2| - \tau_0) \times$$

$$\left\{ \frac{\epsilon(w_1)\epsilon(w_2)}{|w_1 - w_2|^{\frac{2}{k}}} \left[ \left| \frac{w_1}{w_2} \right|^{\frac{1}{k}} + \left| \frac{w_2}{w_1} \right|^{\frac{1}{k}} \right] - \frac{2}{|w_1 - w_2|^{\frac{2}{k}}} \right\} \times$$

$$\sum_{a=1}^3 \frac{\bar{t}_{a+1,a}(\bar{t}_{a+2,a+1}^2 + \bar{t}_{a,a+2}^2)}{2} \int d\tau_3 \Gamma_a(\tau_3)\Gamma_{a+1}(\tau_3) [e^{-i\sqrt{\pi}\phi_{a,a+1}(\tau_3)} - e^{i\sqrt{\pi}\phi_{a,a+1}(\tau_3)}], \quad (\text{D.12})$$

with  $w_{1,2} = \tau_{1,2} - \tau_3$ . On differentiating  $\delta S_b^{(1)}$  with respect to  $\tau_0$ , we obtain

$$\frac{\partial \delta S_b^{(1)}}{\partial \tau_0} = \frac{1}{\tau_0^{\frac{2}{k}-1}} \mathcal{A} \left[ \frac{1}{K} \right] \sum_{a=1}^3 \bar{t}_{a+1,a}(\bar{t}_{a+2,a+1}^2 + \bar{t}_{a,a+2}^2) \int d\tau_3 \Gamma_a(\tau_3)\Gamma_{a+1}(\tau_3) [e^{-i\sqrt{\pi}\phi_{a,a+1}(\tau_3)} - e^{i\sqrt{\pi}\phi_{a,a+1}(\tau_3)}], \quad (\text{D.13})$$

with

$$\mathcal{A}[\nu] = -2 \int_{\frac{3}{2}}^{\infty} dz \left\{ \frac{1}{(z - \frac{1}{2})^{2\nu}} \left[ \frac{1}{(z + \frac{1}{2})^\nu} + \left( z + \frac{1}{2} \right)^\nu + 2 \right] - \frac{1}{(z + \frac{1}{2})^{2\nu}} \left[ \frac{1}{(z - \frac{1}{2})^\nu} + \left( z - \frac{1}{2} \right)^\nu - 2 \right] \right.$$

$$\left. + \left( \frac{z + \frac{1}{2}}{z - \frac{1}{2}} \right)^\nu + \left( \frac{z - \frac{1}{2}}{z + \frac{1}{2}} \right)^\nu - 2 \right\}. \quad (\text{D.14})$$

Apparently,  $\mathcal{A}[\nu]$  in Eq. (D.14) generalizes the  $\mathcal{F}$ -function of Ref. [18] to the Y3J. Assuming  $K^{-1} = 1 - \epsilon$  and expanding to leading order in  $\epsilon$ , one finds  $\mathcal{A}[\nu = 1 - \epsilon] \approx c\epsilon + O(\epsilon^2)$ , with the coefficient  $c \approx 16.45$ .

- **Term number 2:**

Already accounting for the symmetries that become effective under integrating over the imaginary times, this corresponds to

$$-\bar{t}_{2,1}\bar{t}_{3,2}\bar{t}_{1,3} \mathbf{T}_\tau \{ \Gamma_1(\tau_1)\Gamma_2(\tau_1)\Gamma_2(\tau_2)\Gamma_3(\tau_2)\Gamma_3(\tau_3)\Gamma_1(\tau_3) \} \times$$

$$\mathbf{T}_\tau \{ [e^{-i\sqrt{\pi}\phi_{1,2}(\tau_1)} - e^{i\sqrt{\pi}\phi_{1,2}(\tau_1)}][e^{-i\sqrt{\pi}\phi_{2,3}(\tau_2)} - e^{i\sqrt{\pi}\phi_{2,3}(\tau_2)}][e^{-i\sqrt{\pi}\phi_{3,1}(\tau_3)} - e^{i\sqrt{\pi}\phi_{3,1}(\tau_3)}] \}, \quad (\text{D.15})$$

and, clearly, it cannot contribute any further renormalization to the  $\bar{t}_a$ 's.

• **Term number 3:**

This corresponds to a correction to  $S_b$  given by

$$\begin{aligned}
\delta S_b^{(3)} &= \frac{1}{6} \sum_{a=1}^3 \bar{t}_{a+1,a}^3 \int_0^\beta d\tau_1 d\tau_2 d\tau_3 \mathbf{T}_\tau \{ \Gamma_a(\tau_1) \Gamma_{a+1}(\tau_1) \Gamma_a(\tau_2) \Gamma_{a+1}(\tau_2) \Gamma_a(\tau_3) \Gamma_{a+1}(\tau_3) \} \times \\
&\mathbf{T}_\tau \{ [e^{-i\sqrt{\pi}\phi_{a,a+1}(\tau_1)} - e^{i\sqrt{\pi}\phi_{a,a+1}(\tau_1)}] [e^{-i\sqrt{\pi}\phi_{a,a+1}(\tau_2)} - e^{i\sqrt{\pi}\phi_{a,a+1}(\tau_2)}] [e^{-i\sqrt{\pi}\phi_{a,a+1}(\tau_3)} - e^{i\sqrt{\pi}\phi_{a,a+1}(\tau_3)}] \} \times \\
&\theta(|\tau_1 - \tau_2| - \tau_0) \theta(|\tau_2 - \tau_3| - \tau_0) \theta(|\tau_2 - \tau_3| - \tau_0) = \\
&-\frac{1}{6} \sum_{a=1}^3 \bar{t}_{a+1,a}^3 \int_0^\beta d\tau_1 d\tau_2 d\tau_3 \Gamma_a(\tau_3) \Gamma_{a+1}(\tau_3) \times \\
&\mathbf{T}_\tau \{ [e^{-i\sqrt{\pi}\phi_{a,a+1}(\tau_1)} - e^{i\sqrt{\pi}\phi_{a,a+1}(\tau_1)}] [e^{-i\sqrt{\pi}\phi_{a,a+1}(\tau_2)} - e^{i\sqrt{\pi}\phi_{a,a+1}(\tau_2)}] [e^{-i\sqrt{\pi}\phi_{a,a+1}(\tau_3)} - e^{i\sqrt{\pi}\phi_{a,a+1}(\tau_3)}] \} \times \\
&\theta(|\tau_1 - \tau_2| - \tau_0) \theta(|\tau_2 - \tau_3| - \tau_0) \theta(|\tau_2 - \tau_3| - \tau_0) \quad , \tag{D.16}
\end{aligned}$$

again minus a term given by the product of  $S_b$  times the free energy correction to  $\mathcal{O}(\bar{t}_a^2)$ . As a result, taking into account the OPE

$$e^{ia\sqrt{\pi}\phi_{a,a+1}(\tau_1)} e^{ib\sqrt{\pi}\phi_{a,a+1}(\tau_2)} e^{ic\sqrt{\pi}\phi_{a,a+1}(\tau_3)} \approx_{\tau_1 \sim \tau_2 \sim \tau_3} |\tau_1 - \tau_2|^{\frac{2ab}{K}} |\tau_1 - \tau_3|^{\frac{2ac}{K}} |\tau_2 - \tau_3|^{\frac{2bc}{K}} \quad , \tag{D.17}$$

we obtain

$$\begin{aligned}
\delta S_b^{(3)} &= \sum_{a=1}^3 \frac{\bar{t}_{a+1,a}^3}{6} \int dw_1 dw_2 \times \tag{D.18} \\
&\left\{ \frac{|w_1 - w_2|^{\frac{2}{K}}}{|w_1|^{\frac{2}{K}} |w_2|^{\frac{2}{K}}} + \frac{|w_1|^{\frac{2}{K}}}{|w_1 - w_2|^{\frac{2}{K}} |w_2|^{\frac{2}{K}}} + \frac{|w_2|^{\frac{2}{K}}}{|w_1 - w_2|^{\frac{2}{K}} |w_1|^{\frac{2}{K}}} \theta(|w_1| - \tau_0) \theta(|w_2| - \tau_0) \theta(|w_1 - w_2| - \tau_0) \right. \\
&\left. - \frac{6}{|w_1 - w_2|^{\frac{2}{K}}} \theta(|w_1 - w_2| - \tau_0) \right\} \int_0^\beta d\tau_3 \sum_{a=1}^3 \Gamma_a(\tau_3) \Gamma_{a+1}(\tau_3) [e^{-i\sqrt{\pi}\phi_{a,a+1}(\tau_3)} - e^{i\sqrt{\pi}\phi_{a,a+1}(\tau_3)}] \quad .
\end{aligned}$$

On separately considering the contributions from positive- and negative- values of the integration variables, we may rewrite Eq. (D.18) as

$$\begin{aligned}
\delta S_b^{(3)} &= \sum_{a=1}^3 \frac{\bar{t}_{a+1,a}^3}{3} \int d\tau_3 \Gamma_a(\tau_3) \Gamma_{a+1}(\tau_3) [e^{-i\sqrt{\pi}\phi_{a,a+1}(\tau_3)} - e^{i\sqrt{\pi}\phi_{a,a+1}(\tau_3)}] \int_{\tau_0}^\infty dw_1 dw_2 \times \\
&\left\{ \frac{|w_1 - w_2|^{\frac{2}{K}}}{w_1^{\frac{2}{K}} w_2^{\frac{2}{K}}} + \frac{w_1^{\frac{2}{K}}}{|w_1 - w_2|^{\frac{2}{K}} w_2^{\frac{2}{K}}} + \frac{w_2^{\frac{2}{K}}}{|w_1 - w_2|^{\frac{2}{K}} w_1^{\frac{2}{K}}} - \frac{6}{|w_1 - w_2|^{\frac{2}{K}}} \right\} \theta(|w_1 - w_2| - \tau_0) \\
&\sum_{a=1}^3 \frac{\bar{t}_{a+1,a}^3}{3} \int d\tau_3 \Gamma_a(\tau_3) \Gamma_{a+1}(\tau_3) [e^{-i\sqrt{\pi}\phi_{a,a+1}(\tau_3)} - e^{i\sqrt{\pi}\phi_{a,a+1}(\tau_3)}] \int_{\tau_0}^\infty dw_1 dw_2 \times \\
&\left\{ \frac{|w_1 + w_2|^{\frac{2}{K}}}{w_1^{\frac{2}{K}} w_2^{\frac{2}{K}}} + \frac{w_1^{\frac{2}{K}}}{|w_1 + w_2|^{\frac{2}{K}} w_2^{\frac{2}{K}}} + \frac{w_2^{\frac{2}{K}}}{|w_1 + w_2|^{\frac{2}{K}} w_1^{\frac{2}{K}}} - \frac{6}{|w_1 + w_2|^{\frac{2}{K}}} \right\} \quad , \tag{D.19}
\end{aligned}$$

On differentiating  $\delta S_b^{(3)}$  with respect to  $\tau_0$ , we therefore get

$$\frac{\partial \delta S_b^{(3)}}{\partial \tau_0} = \frac{1}{\tau_0^{\frac{2}{K}-1}} \mathcal{B} \left[ \frac{1}{K} \right] \sum_{a=1}^3 \bar{t}_{a+1,a}^3 \int d\tau_3 \Gamma_a(\tau_3) \Gamma_{a+1}(\tau_3) [e^{-i\sqrt{\pi}\phi_{a,a+1}(\tau_3)} - e^{i\sqrt{\pi}\phi_{a,a+1}(\tau_3)}] \quad , \quad (\text{D.20})$$

with

$$\begin{aligned} \mathcal{B}[v] = & -\frac{2}{3} \int_{\frac{3}{2}}^{\infty} dz \left\{ \left( \frac{z-1/2}{z+1/2} \right)^{2v} + \left( \frac{z+1/2}{z-1/2} \right)^{2v} + \frac{1}{(z^2-1/4)^{2v}} - \frac{6}{(z-1/2)^{2v}} \right\} \\ & - \frac{2}{3} \int_{\frac{3}{2}}^{\infty} dz \left\{ \left( \frac{z+1/2}{z-1/2} \right)^{2v} + \left( \frac{z-1/2}{z+1/2} \right)^{2v} + \frac{1}{(z^2-1/4)^{2v}} - \frac{6}{(z+1/2)^{2v}} \right\} \\ & - \frac{2}{3} \int_{\frac{3}{2}}^{\infty} dz \left\{ \left( \frac{z+1/2}{z-1/2} \right)^{2v} + \left( \frac{z-1/2}{z+1/2} \right)^{2v} + \frac{1}{(z^2-1/4)^{2v}} - 6 \right\} \quad . \end{aligned} \quad (\text{D.21})$$

Setting  $K^{-1} = 1 - \epsilon$  and expanding to leading order in  $\epsilon$  one obtains  $\mathcal{B}[1 - \epsilon] \approx b\epsilon + \mathcal{O}(\epsilon^2)$ , with  $b \sim 26.32$ . Thus, eventually putting together the contributions from Term 1 and Term 3, we find that the perturbative RG equations for the running couplings are given by

$$\begin{aligned} \frac{d\bar{t}_{2,1}}{d \ln(\tau/\tau_0)} &= \epsilon \{ \bar{t}_{2,1} - \bar{t}_{2,1} [b(\bar{t}_{2,1})^2 + c((\bar{t}_{3,2})^2 + (\bar{t}_{1,3})^2)] \} \\ \frac{d\bar{t}_{3,2}}{d \ln(\tau/\tau_0)} &= \epsilon \{ \bar{t}_{3,2} - \bar{t}_{3,2} [b(\bar{t}_{3,2})^2 + c((\bar{t}_{1,3})^2 + (\bar{t}_{2,1})^2)] \} \\ \frac{d\bar{t}_{1,3}}{d \ln(\tau/\tau_0)} &= \epsilon \{ \bar{t}_{1,3} - \bar{t}_{1,3} [b(\bar{t}_{1,3})^2 + c((\bar{t}_{2,1})^2 + (\bar{t}_{3,2})^2)] \} \end{aligned} \quad . \quad (\text{D.22})$$

From Eqs. (D.22), we find a FCFP at  $\bar{t}_{2,1} = \bar{t}_{3,2} = \bar{t}_{1,3} = t_* = 1/\sqrt{b+2c}$ , that is independent of  $\epsilon$ . Additional fixed points are found at  $\bar{t}_{2,1} = 0, \bar{t}_{3,2} = \bar{t}_{1,3} = 1/\sqrt{b+c}$ , plus permutations of the three indices. In the main text, however, we discuss the reliability of this result and use alternative methods, such as the DEBC-approach of the explicit calculation of the  $g$ -function in combination with the  $g$ -theorem, to make more accurate predictions about FCFP's in the phase diagram of the 3YJ.

For the purpose of discussing the relation between the  $N = 2$  junction and the Y3J, it is important to generalize Eqs. (D.22) to the case of unequal Luttinger parameters in the three wires. Specifically, we now assume that wire-1 and -2 are characterized by a Luttinger parameter  $K$ , while wire-3 is characterized by a Luttinger parameter  $K_3$  with, in general,  $K_3 \neq K$ . In this case, following the same procedure we followed above, yields the generalization of Eqs. (D.22) to

$$\begin{aligned}
\frac{d\bar{t}_{2,1}}{d\ln(\tau/\tau_0)} &= \left(1 - \frac{1}{K}\right)\bar{t}_{2,1} - \mathcal{B}\left[\frac{1}{K}\right](\bar{t}_{2,1})^3 - C\left[\frac{1}{K}, \frac{1}{K_3}\right]\bar{t}_{2,1}((\bar{t}_{3,2})^2 + (\bar{t}_{1,3})^2) \equiv \hat{\beta}_1[\bar{t}_{2,1}, \bar{t}_{3,2}, \bar{t}_{1,3}] \\
\frac{d\bar{t}_{3,2}}{d\ln(\tau/\tau_0)} &= \left(1 - \frac{1}{2K} - \frac{1}{2K_3}\right)\bar{t}_{3,2} - \mathcal{B}\left[\frac{1}{2K} + \frac{1}{2K_3}\right](\bar{t}_{3,2})^3 - C\left[\frac{1}{K}, \frac{1}{K_3}\right]\bar{t}_{3,2}(\bar{t}_{1,3})^2 - C\left[\frac{1}{K}, \frac{1}{K}\right]\bar{t}_{3,2}(\bar{t}_{2,1})^2 \\
&\equiv \hat{\beta}_2[\bar{t}_{2,1}, \bar{t}_{3,2}, \bar{t}_{1,3}] \\
\frac{d\bar{t}_{1,3}}{d\ln(\tau/\tau_0)} &= \left(1 - \frac{1}{2K} - \frac{1}{2K_3}\right)\bar{t}_{1,3} - \mathcal{B}\left[\frac{1}{2K} + \frac{1}{2K_3}\right](\bar{t}_{1,3})^3 - C\left[\frac{1}{K}, \frac{1}{K_3}\right]\bar{t}_{1,3}(\bar{t}_{3,2})^2 - C\left[\frac{1}{K}, \frac{1}{K}\right]\bar{t}_{1,3}(\bar{t}_{2,1})^2 \\
&\equiv \hat{\beta}_3[\bar{t}_{2,1}, \bar{t}_{3,2}, \bar{t}_{1,3}], \tag{D.23}
\end{aligned}$$

with the function  $\mathcal{B}[\nu]$  defined in Eq. (D.21) and  $C[\nu_1, \nu_2]$  generalizing  $\mathcal{A}[\nu]$  in Eq. (D.14) so

$$\begin{aligned}
C[\nu_1, \nu_2] &= -2 \int_{\frac{3}{2}}^{\infty} dz \left\{ \frac{1}{\left(z - \frac{1}{2}\right)^{\nu_1 + \nu_2}} \left[ \frac{1}{\left(z + \frac{1}{2}\right)^{\nu_2}} + \left(z + \frac{1}{2}\right)^{\nu_2} + 2 \right] - \frac{1}{\left(z + \frac{1}{2}\right)^{\nu_1 + \nu_2}} \left[ \frac{1}{\left(z - \frac{1}{2}\right)^{\nu_2}} + \left(z - \frac{1}{2}\right)^{\nu_2} - 2 \right] \right. \\
&\quad \left. + \left(\frac{z + \frac{1}{2}}{z - \frac{1}{2}}\right)^{\nu_2} + \left(\frac{z - \frac{1}{2}}{z + \frac{1}{2}}\right)^{\nu_2} - 2 \right\}, \tag{D.24}
\end{aligned}$$

which implies  $\mathcal{A}[\nu] = C[\nu, \nu]$ , as well as  $\mathcal{F}[\nu] = C[2 - \nu, \nu]$ .

## References

- [1] C. Chamon, M. Oshikawa, and I. Affleck, Phys. Rev. Lett. **91**, 206403 (2003).
- [2] M. Oshikawa, C. Chamon, and I. Affleck, Journal of Statistical Mechanics: Theory and Experiment **2006**, P02008 (2006).
- [3] S. Lal, S. Rao, and D. Sen, Phys. Rev. B **66**, 165327 (2002).
- [4] S. Chen, B. Trauzettel, and R. Egger, Phys. Rev. Lett. **89**, 226404 (2002).
- [5] X. Barnabé-Thériault, A. Sedeki, V. Meden, and K. Schönhammer, Phys. Rev. Lett. **94**, 136405 (2005).
- [6] B. Bellazzini and M. Mintchev, Journal of Physics A: Mathematical and General **39**, 11101 (2006).
- [7] C.-Y. Hou and C. Chamon, Phys. Rev. B **77**, 155422 (2008).
- [8] Z. Shi and I. Affleck, Phys. Rev. B **94**, 035106 (2016).
- [9] D. Giuliano and A. Nava, Phys. Rev. B **92**, 125138 (2015).
- [10] S. Mardanya and A. Agarwal, Phys. Rev. B **92**, 045432 (2015).
- [11] S.-i. Tomonaga, Progress of Theoretical Physics **13**, 482 (1955).
- [12] J. M. Luttinger, Journal of Mathematical Physics **4**, 1154 (1963).
- [13] F. D. M. Haldane, Journal of Physics C: Solid State Physics **14**, 2585 (1981).
- [14] F. D. M. Haldane, Phys. Rev. Lett. **47**, 1840 (1981).
- [15] C. L. Kane and M. P. A. Fisher, Phys. Rev. B **46**, 15233 (1992).
- [16] A. Y. Kitaev, Physics-Uspekhi **44**, 131 (2001).
- [17] L. Fidkowski, J. Alicea, N. H. Lindner, R. M. Lutchyn, and M. P. A. Fisher, Phys. Rev. B **85**, 245121 (2012).
- [18] I. Affleck and D. Giuliano, Journal of Statistical Mechanics: Theory and Experiment **2013**, P06011 (2013).
- [19] D. I. Pikulin, Y. Komijani, and I. Affleck, Phys. Rev. B **93**, 205430 (2016).
- [20] S. Eggert and I. Affleck, Phys. Rev. B **46**, 10866 (1992).
- [21] D. Giuliano, D. Rossini, P. Sodano, and A. Trombettoni, Phys. Rev. B **87**, 035104 (2013).
- [22] A. M. Tsvelik, Phys. Rev. Lett. **110**, 147202 (2013).
- [23] D. Giuliano and P. Sodano, EPL (Europhysics Letters) **103**, 57006 (2013).
- [24] D. Giuliano and P. Sodano, New Journal of Physics **10**, 093023 (2008).
- [25] D. Giuliano and P. Sodano, Nuclear Physics B **811**, 395 (2009).

- [26] D. Giuliano and P. Sodano, EPL (Europhysics Letters) **88**, 17012 (2009).
- [27] A. Cirillo, M. Mancini, D. Giuliano, and P. Sodano, Nuclear Physics B **852**, 235 (2011).
- [28] B. Béri and N. R. Cooper, Phys. Rev. Lett. **109**, 156803 (2012).
- [29] E. Eriksson, A. Nava, C. Mora, and R. Egger, Phys. Rev. B **90**, 245417 (2014).
- [30] A. Altland, B. Béri, R. Egger, and A. M. Tsvelik, Journal of Physics A: Mathematical and Theoretical **47**, 265001 (2014).
- [31] A. Altland, B. Béri, R. Egger, and A. M. Tsvelik, Phys. Rev. Lett. **113**, 076401 (2014).
- [32] A. H. Castro Neto, E. Novais, L. Borda, G. Zaránd, and I. Affleck, Phys. Rev. Lett. **91**, 096401 (2003).
- [33] E. Novais, A. H. Castro Neto, L. Borda, I. Affleck, and G. Zarand, Phys. Rev. B **72**, 014417 (2005).
- [34] C. L. Kane and M. P. A. Fisher, Phys. Rev. Lett. **68**, 1220 (1992).
- [35] I. Affleck and A. W. W. Ludwig, Phys. Rev. Lett. **67**, 161 (1991).
- [36] I. Affleck and A. W. W. Ludwig, Phys. Rev. B **48**, 7297 (1993).
- [37] P. Calabrese and J. Cardy, Journal of Statistical Mechanics: Theory and Experiment **2004**, P06002 (2004).
- [38] D. Friedan and A. Konechny, Phys. Rev. Lett. **93**, 030402 (2004).
- [39] D. Friedan, A. Konechny, and C. Schmidt-Colinet, Phys. Rev. Lett. **109**, 140401 (2012).
- [40] D. Friedan and A. Konechny, Adv. Theor. Math. Phys. **13**, 1847 (2009).
- [41] M. Oshikawa and I. Affleck, Nuclear Physics B **495**, 533 (1997).
- [42] C.-Y. Hou, A. Rahmani, A. E. Feiguin, and C. Chamon, Phys. Rev. B **86**, 075451 (2012).
- [43] Y. Oreg, G. Refael, and F. von Oppen, Phys. Rev. Lett. **105**, 177002 (2010).
- [44] R. M. Lutchyn, J. D. Sau, and S. Das Sarma, Phys. Rev. Lett. **105**, 077001 (2010).
- [45] J. von Delft and H. Schoeller, Annalen der Physik **7**, 225 (1998).
- [46] T. Lee, International Journal of Modern Physics A **31**, 1650154 (2016).
- [47] D. Chevallier, D. Sticlet, P. Simon, and C. Bena, Phys. Rev. B **85**, 235307 (2012).
- [48] D. Chevallier, P. Simon, and C. Bena, Phys. Rev. B **88**, 165401 (2013).
- [49] I. Affleck and D. Giuliano, Journal of Statistical Physics **157**, 666 (2014).
- [50] B. Béri, Phys. Rev. Lett. **110**, 216803 (2013).
- [51] A. Altland and R. Egger, Phys. Rev. Lett. **110**, 196401 (2013).
- [52] J. Lee and F. Wilczek, Phys. Rev. Lett. **111**, 226402 (2013).
- [53] A. Rahmani, C.-Y. Hou, A. Feiguin, M. Oshikawa, C. Chamon, and I. Affleck, Phys. Rev. B **85**, 045120 (2012).
- [54] J. Cardy, Scaling and Renormalization in Statistical Physics, Cambridge Lecture Notes in Physics (Cambridge University Press, 1996).